

Resonance-aware parton-shower matching for off-shell top–antitop production with semi-leptonic decays at electron–positron colliders

Ansgar Denner,^a Daniele Lombardi,^b Mathieu Pellen,^c Giovanni Pelliccioli^d

^a*Institut für Theoretische Physik und Astrophysik, Universität Würzburg,
Emil-Hilb-Weg 22, 97074 Würzburg, Germany*

^b*Dipartimento di Fisica, Università di Torino, and INFN, Sezione di Torino Via Pietro Giuria, 1 I-10125,
Torino, Italy*

^c*Universität Freiburg, Physikalisches Institut, D-79104 Freiburg, Germany*

^d*Dipartimento di Fisica, Università di Milano–Bicocca and INFN, Sezione di Milano–Bicocca, Piazza della
Scienza 3, 20126 Milano, Italy*

E-mail: ansgar.denner@uni-wuerzburg.de, daniele.lombardi@unito.it,
mathieu.pellen@physik.uni-freiburg.de, giovanni.pelliccioli@unimib.it

ABSTRACT: We present full off-shell NLO corrections in QCD obtained with the MoCANLO code matched to parton shower. A resonance-aware matching procedure has been devised for the MC@NLO method tuned to the Catani–Seymour dipole subtraction. Specifically, we consider the off-shell production of a top–antitop pair in the semi-leptonic decay channel in electron–positron collisions and match it to the final-state QCD parton shower of PYTHIA8. Distortions of resonances’ line shapes are avoided by providing the details of the resonance-cascade chain on an event-by-event basis to the parton shower and by adapting the matching accordingly through the introduction of dedicated counterterms.

KEYWORDS: QCD, NLO, parton-shower matching, top quark

Contents

1	Introduction	1
2	NLO matching to parton shower in MoCANLO	3
2.1	Theory background	4
2.1.1	The MC@NLO method in a nutshell	4
2.1.2	The PYTHIA8 final-state Simple Shower	7
2.2	Catani–Seymour-based MC@NLO matching	8
2.2.1	Construction of the parton-shower counterterms	8
2.2.2	Correction of the IR limits	12
2.2.3	Kinematic mapping for shower dipoles with massless emitter–spectator pairs	13
2.3	Treatment of top resonances	16
2.3.1	Kinematic mappings for shower decay dipoles	19
2.3.2	Kinematic mappings for shower production dipoles	24
2.3.3	Decay phase space of a massive emitter/spectator particle	29
2.3.4	Selection of resonance histories	31
3	Details of the calculation	37
3.1	Technical aspects of the event generation	37
3.2	Input parameters and kinematic selections	39
3.2.1	Physical input parameters	39
3.2.2	Matching and PYTHIA8 settings	40
3.2.3	Event selection	41
4	Results	42
4.1	Matching and shower effects	43
4.2	Hadron-level events	46
5	Conclusions	46

1 Introduction

Despite its many experimental confirmations and remarkable predictive power, the Standard Model of particle physics is far from a complete theory, since many unsolved issues and unanswered questions persist. This underscores the need for the particle-physics community to advance further by developing new tests and searches that could shed light on still poorly-understood mechanisms of nature. In line with the new research paradigm that has established itself in the last decades, such progress also translates into a continuous increase of accuracy of experimental measurements at particle colliders, primarily at the Large Hadron Collider. At the end of its Run 3 and, more importantly, with the upcoming high-luminosity stage, unprecedented accuracy levels will be achieved. Moreover, complementary insights may come from new generations of colliders: In the last few years many options have been considered, especially among lepton colliders, resulting in proposals such as the International Linear Collider (ILC) [1–3], the FCC-ee [4], or the Compact Linear Collider (CLIC) [5].

Since a main road to possibly unveil new-physics effects is the comparison of measurements with theory predictions, it is obvious that upgrades on the experimental side must be followed by similar improvements of the theoretical simulations. Significant steps forward have been made to increase the accuracy of fixed-order predictions by computing higher and higher orders in the perturbative expansion, both in the strong and in the electroweak (EW) coupling. Next-to-leading-order (NLO) calculations obtained in full generality also for processes with a high multiplicity of the final state have become standard, and next-to-next-to-leading-order (NNLO) results represent the new precision frontier. Actually, for simple processes, even higher perturbative contributions have already become available.

Nonetheless, it is well known that realistic predictions can not just rely on fixed-order calculations. No matter how many perturbative orders can be computed, fixed-order predictions are doomed to fail in those phase-space regions that are sensitive to infrared (IR) physics, owing to the appearance of large logarithmic terms that spoil the convergence of the perturbative series. Physical results can only be obtained upon resumming these terms to all orders. This renders the matching to parton shower (PS) unavoidable. Even in their first implementations, where only leading-logarithmic (LL) accuracy could be addressed, PSs boasted many strengths compared to analytic methods to perform the resummation, since they could account for a vast class of logarithmic contributions in a process-independent way. Moreover, the matching to PS allows the embedding of fixed-order calculations into fully-fledged Monte Carlo generators, which can model hadronisation and multi-particle interactions. Each PS code is based on specific approximations and precise choices that enter the construction of the soft/collinear cascade of emissions evolving the collision process from the hard to the non-perturbative scale. Each of these choices comes with advantages and disadvantages, which explains and, to some extent, justifies the proliferation of PS event generators. Among the most widespread tools, one finds PYTHIA [6, 7], HERWIG [8, 9], and SHERPA [10, 11]. PYTHIA itself includes two more showers on top of the default one (named *Simple Shower* [6]): DIRE [12] (no more supported as of PYTHIA8.316) and VINCIA [13–15].

For many years, the matching of NLO predictions to PSs was considered a solved problem. Both the additive matching of MC@NLO [8, 16–19] and the multiplicative one of POWHEG [20–22] have been implemented in various public codes and tested for many processes. Moreover, new schemes have been proposed more recently, like KrkNLO [23, 24] and MAcNLOPS [25], being a mixture of additive and multiplicative matching. This is why a lot of effort has been recently invested in promoting this matching to NNLO results [26–30]. Nonetheless, now that new generations of showers are beginning to appear [31–36], where next-to-leading-logarithmic (NLL) accuracy, or even higher, is under better control, the NLO-matching problem has received renewed attention from a different perspective. A proper matching must preserve not only the perturbative accuracy of fixed-order predictions, but also the higher logarithmic accuracy of the PS. In view of these new challenges, it is a worthwhile endeavour to revisit available matching approaches, or even to explore new solutions.

In this work we consider the MC@NLO method to match NLO QCD predictions obtained with MoCANLO [37], a Monte Carlo integrator that is well-suited for calculations of NLO corrections for multi-particle processes. One of its key features is a refined integration based on *adaptive-multichannel* [38–40], which also allows one to target Born-like and real contributions with dedicated integration channels. Indeed, especially for processes with a non-trivial resonance structure, not all kinematic topologies that are relevant for the integration of the real amplitude can be easily expressed in terms of a corresponding underlying-Born topology, i.e. a topology obtained from the real one by removing the additional emission. Even though this problem can be circumvented in POWHEG by splitting the real contribution into a *singular*, *remnant*, and *regular* part, a separate integration of the real amplitude is achieved much more naturally in MC@NLO, making it better suited for MoCANLO-multichannel integration. However, by choosing MC@NLO, one also in-

herits the problem of the large fraction of negative weights that affect the method [18]. This is a consequence of the introduction of PS counterterms required to remove double counting and preserve fixed-order accuracy. The problem is largely ameliorated in POWHEG, where no PS counterterm is needed, since the first shower emission is generated according to a Sudakov exponential constructed with the exact tree-level real amplitude. While this approach renders POWHEG more efficient, it inevitably makes it more complicated to preserve the accuracy of the PS beyond LL. To address this issue, the handling of IR divergences in POWHEG should be re-examined thoroughly.

The POWHEG method [20, 21] is implemented in the POWHEG-BOX framework [22], where the NLO subtraction is carried out using the Frixione–Kunszt–Signer (FKS) approach [41]. This scheme has different advantages, like for instance keeping the number of IR-singular regions relatively low and considerably simplifying the definition of the Sudakov exponential in terms of positive-definite quantities. By contrast, in Catani–Seymour (CS) subtraction [42–44], where counterterms are defined over the entire phase space, constructing the POWHEG Sudakov exponential is less straightforward. Indeed, this subtraction scheme has been used in combination with POWHEG only for simple processes, such as Drell–Yan production [45]. In MC@NLO, both FKS and CS subtractions are instead fully legitimate and have been implemented in various computer programs and used in different calculations. Even if an implementation of the FKS approach for final-state radiation within MoCANLO was also discussed in Ref. [46], most of MoCANLO’s results have been obtained using CS subtraction. The latter is also employed in this work, where we present an implementation of MC@NLO based on CS subtraction. This is mostly due to the choice of matching our predictions to the PYTHIA8 Simple Shower. Since for final-state radiation the latter is essentially a *dipole shower*, where each emission involves an emitter and a spectator, this makes it easier to embed PS counterterms into a CS framework, where the subtraction of singularities is also performed in terms of dipoles.

As a first application of our implementation, we consider off-shell top–antitop-quark production with semileptonic decays at NLO in QCD at a lepton collider. Even though the simpler initial state as compared to proton colliders offers a clearer testing environment, preserving off-shell effects in the matching poses additional challenges. Indeed, the PS must be instructed to keep the resonances’ line shapes untouched during the event evolution in order to avoid unphysical effects. In POWHEG, this problem was faced with a careful reorganisation of the NLO subtraction procedure [47, 48], which found numerous applications in a variety of processes [49–52]. In MC@NLO, the situation is more delicate, as described in Ref. [53], since dedicated PS counterterms must be defined for a complete subtraction of double counting as soon as PYTHIA8 tries to preserve the invariant masses of the resonances. In this work, we have approached the issue again and offered a possible solution.

This manuscript is structured as follows: We provide details of our resonance-aware implementation of MC@NLO for MoCANLO in Section 2. Some technical aspects of our event generator together with the complete specification of the setup used for our runs are given in Section 3. We continue presenting some numerical results in Section 4. Finally, in Section 5 we draw our conclusions.

2 NLO matching to parton shower in MoCANLO

In this section, we illustrate our strategy to match a lepton-collider event at NLO in QCD computed using the MoCANLO code to the final-state QCD PS of PYTHIA8. The in-house generator MoCANLO [37] has already proven suitable for the evaluation of processes with high-multiplicity final states and non-trivial resonance structures [54–57]. Its efficiency mostly relies on an elaborated multichannel sampling [38–40]. In order to benefit from this feature when matching NLO computations to PSs, we make use of the MC@NLO method, which allows the separate integration of contributions with and without real radiation.

To set up the stage, we begin in Section 2.1.1 with a short recap of the MC@NLO method. Some features of the final-state Simple Shower of PYTHIA8 that are relevant for NLO matching are recalled in Section 2.1.2. We then specialise the discussion in Section 2.2 to the case where MC@NLO is used to match an NLO calculation based on CS subtraction [42–44], as needed for MoCANLO.

In order for the PS not to alter the invariant mass of resonances, information on the resonance-cascade chain must be provided to PYTHIA8 for each event. Even when restricting to the QCD shower, the appearance of top resonances in the NLO process necessitates a special handling of the shower splitting kinematics, for which no direct analogue exists in the CS mappings used in NLO subtraction. Since our goal is to provide results for the production of a top–antitop pair, we also illustrate how we adapted the MC@NLO method in the presence of top resonances starting from Section 2.3.

2.1 Theory background

2.1.1 The MC@NLO method in a nutshell

We refer to *NLO matching* as a prescription to consistently combine NLO predictions with PSs. If an event obtained with an NLO generator is naively evolved by the shower, the latter introduces terms of the same perturbative order as the ones accounted for by the fixed-order calculation. Any double counting of such terms spoils the formal accuracy of the NLO result. The MC@NLO method solves this issue by subtracting back from the NLO calculation these spurious terms that are added by the shower. This is done with dedicated subtraction terms, which are sometimes referred to in the literature as *parton-shower counterterms* \mathcal{C}_{PS} .

To fix the notation, we recall that the NLO-accurate differential cross section $d\sigma_{\text{NLO}}$ can be decomposed in the following contributions:

$$d\sigma_{\text{NLO}} = d\Phi_{\text{B}} \mathcal{B}(\Phi_{\text{B}}) + d\Phi_{\text{B}} \mathcal{V}(\Phi_{\text{B}}) + d\Phi_{\text{B}} \sum_r \mathcal{I}_{\text{dip}}^{(r)}(\Phi_{\text{B}}) + d\Phi_{\text{R}} \left(\mathcal{R}(\Phi_{\text{R}}) - \sum_r \mathcal{C}_{\text{dip}}^{(r)}(\Phi_{\text{R}}) \right), \quad (2.1)$$

where Φ_{B} and Φ_{R} refer to the Born and real phase spaces, respectively. With \mathcal{B} , \mathcal{V} , \mathcal{R} we denote the Born, virtual, and real terms, while $\mathcal{I}_{\text{dip}}^{(r)}$ and $\mathcal{C}_{\text{dip}}^{(r)}$ refer to the integrated and subtraction dipoles. The index r is used to label the IR-singular regions. Depending on the subtraction scheme, r must be identified with a pair of emitter–emissus¹ particles (in FKS) or a triplet of emitter, emissus, and spectator particles (in CS). Note that in Eq. (2.1) the subtraction dipoles are defined on a real kinematics where the Born and the radiation phase space are factorised in a way that depends on the singular region r .

Starting from Eq. (2.1), the MC@NLO method distinguishes between the standard (\mathcal{S}) and hard (\mathcal{H}) contributions, which read

$$d\sigma_{\mathcal{S}} = d\Phi_{\text{B}} \mathcal{B}(\Phi_{\text{B}}) + d\Phi_{\text{B}} \mathcal{V}(\Phi_{\text{B}}) + d\Phi_{\text{B}} \sum_r \mathcal{I}_{\text{dip}}^{(r)}(\Phi_{\text{B}}) - d\Phi_{\text{B}} \int \left(\sum_r d\Phi_{\text{rad}}^{(r)} \mathcal{C}_{\text{dip}}^{(r)}(\Phi_{\text{B}}, \Phi_{\text{rad}}^{(r)}) - \sum_{r'} d\Phi_{\text{rad}}^{(r')} \mathcal{C}_{\text{PS}}^{(r')}(\Phi_{\text{B}}, \Phi_{\text{rad}}^{(r')}) \right), \quad (2.2)$$

$$d\sigma_{\mathcal{H}} = d\Phi_{\text{R}} \mathcal{R}(\Phi_{\text{R}}) - d\Phi_{\text{R}} \sum_{r'} \mathcal{C}_{\text{PS}}^{(r')}(\Phi_{\text{R}}), \quad (2.3)$$

where we have denoted by $\Phi_{\text{rad}}^{(r)}$ or $\Phi_{\text{rad}}^{(r')}$ the radiation phase space. The separation into \mathcal{S} and \mathcal{H} contributions is based on the multiplicity of the final state of the event. Events with Born-like kinematics are part of the standard contribution, while the ones with real kinematics are contained

¹We denote the radiated particle by *emissus*.

in the hard one. Owing to this separation, in order for the event sample to have the correct distribution according to the NLO cross section, it is crucial that contributions of the fixed-order calculation defined on the Born phase space are integrated together in $d\sigma_S$. Indeed, if some of these contributions entered the weight of hard events, they would be cut according to the wrong kinematics.

In Eqs. (2.2) and (2.3) we have introduced the PS counterterms $\mathcal{C}_{\text{PS}}^{(r')}$, which also carry a dependence on an index r' . Note that in general $r' \neq r$, since r' runs over the sectors considered by the PS algorithm to generate radiation, which do not necessarily coincide with the singular regions of the subtraction scheme. From the definition of the \mathcal{S} and \mathcal{H} contributions, it is clear that in order for the two to be separately finite, the $\mathcal{C}_{\text{PS}}^{(r')}$ terms must act as local subtraction terms. Since $\mathcal{C}_{\text{PS}}^{(r')}$ are required to avoid double counting and are consequently extracted from the PS, the fact that $\mathcal{C}_{\text{PS}}^{(r')}$ can locally account for all IR singularities present at NLO is a non-trivial requirement, which in most of the cases is not fulfilled. We further discuss this problem in Sections 2.1.2 and 2.2.

As an additional remark, even if $\mathcal{C}_{\text{PS}}^{(r')}$ in the standard and the hard cross sections have the same analytic expressions, they are defined on different phase spaces (Born and real kinematics, respectively) on which cuts and observables are evaluated. As shown in the following, this definition is a crucial ingredient to prevent double counting. Nevertheless, this implies that, in the presence of cuts, the sum of the standard and hard cross sections does not reproduce the NLO one, not even at the integrated level., i.e. $\sigma_{\text{NLO}} \neq \sigma_S + \sigma_H$. The equality at fixed order can only be restored by enforcing the shower counterterms of the hard event to be cut on Born kinematics.

Given a generic observable \mathcal{O} , we define \mathcal{O}_n its explicit expression in terms of n final-state momenta. Therefore, $\mathcal{O}_n(\Phi_B)$ gives the value of a generic observable evaluated on a fully-differential Born kinematics with a final state of multiplicity n . For a standard event, the observable evaluates to $\mathcal{S}(\mathcal{O}_n)$, i.e.

$$\begin{aligned} \mathcal{S}(\mathcal{O}_n) &= \left\{ \left[\mathcal{B} + \mathcal{V} + \sum_r \mathcal{I}_{\text{dip}}^{(r)} \right] (\Phi_B) \right. \\ &\quad \left. - \int \left[\sum_r d\Phi_{\text{rad}}^{(r)} \mathcal{C}_{\text{dip}}^{(r)}(\Phi_B, \Phi_{\text{rad}}^{(r)}) - \sum_{r'} d\Phi_{\text{rad}}^{(r')} \mathcal{C}_{\text{PS}}^{(r')}(\Phi_B, \Phi_{\text{rad}}^{(r')}) \right] \right\} \cdot \mathcal{O}_n(\Phi_B) \\ &= \bar{\mathcal{B}}(\Phi_B) \cdot \mathcal{O}_n(\Phi_B), \end{aligned} \quad (2.4)$$

where we have denoted as $\bar{\mathcal{B}}$ the fully-differential weight of the standard event. Similarly, for a hard event the same observable receives the contribution $\mathcal{H}(\mathcal{O}_{n+1})$, resulting from:

$$\mathcal{H}(\mathcal{O}_{n+1}) = \left[\mathcal{R} - \sum_{r'} \mathcal{C}_{\text{PS}}^{(r')} \right] (\Phi_R) \cdot \mathcal{O}_{n+1}(\Phi_R), \quad (2.5)$$

where \mathcal{O} is now evaluated on an $n+1$ kinematics.

Once an event is interfaced to a PS, the latter fills up the available phase space with additional radiation. Only on a fully inclusive phase space, the shower unitarity guarantees that the value of the observable is not modified. In a fiducial phase space, the additional radiation recoils against the momenta of events distributed with fixed-order accuracy, causing some of those events to be moved inside or outside the fiducial region. Together with approximate higher-order corrections in the shower, this potentially leads to differences in the predictions when comparing fixed-order and PS-matched results, even for IR-safe observables.

To show how double counting is prevented (see also Ref. [58]), we define the action of a generic shower on an observable \mathcal{O}_n via the functional \mathbb{S} :

$$\mathbb{S}[\mathcal{O}_n] = \Delta^{\text{PS}}(t_i) \mathcal{O}_n(\Phi_B) + \sum_{r'} \frac{\mathcal{C}_{\text{PS}}^{(r')}(\Phi_R)}{\mathcal{B}(\Phi_B)} \Delta^{\text{PS}}(t) \mathcal{O}_{n+1}(\Phi_R). \quad (2.6)$$

This definition is motivated by unitarity and, as recalled below, it carries a probabilistic interpretation. It also provides a unique map from a given phase space to another one with final-state multiplicity increased by one, so that the right-hand side of Eq. (2.6) requires expressions for the generic observable \mathcal{O} in terms of both n and $n + 1$ kinematics. Accordingly, the real kinematics Φ_{R} generated by the shower is constructed from a Born kinematics through the emission of one additional radiation. This means that Φ_{R} must always be thought as factorised in terms of a Born and a radiation kinematics. The phase space of the radiation $\Phi_{\text{rad}}^{(r')}$ can be parametrised in terms of three radiation variables, which depend on the region r' where the radiation process occurs.

In the previous equation, we have introduced the PS Sudakov factor $\Delta^{\text{PS}}(t_i)$, which in standard LL parton showers is responsible for the resummation of all collinear radiation emitted from a *starting scale* t_i in a given evolution variable down to a cut-off scale t_0 . An evolution (or ordering) variable t is used by the shower to fill up the phase space with radiation. All emission is ordered in a decreasing value of t . The freedom in the specific choice of t is one of the ingredients that distinguishes different shower algorithms. In general, we can write $\Delta^{\text{PS}}(t_i)$ explicitly as

$$\begin{aligned} \Delta^{\text{PS}}(t_i) &= \exp\left\{-\sum_{r'} \int_{t_0}^{t_i} d\Phi_{\text{rad}}^{(r')} \frac{\mathcal{C}_{\text{PS}}^{(r')}(\Phi_{\text{B}}, \Phi_{\text{rad}}^{(r')})}{\mathcal{B}(\Phi_{\text{B}})}\right\} \\ &= 1 - \sum_r \int_{t_0}^{t_i} d\Phi_{\text{rad}}^{(r')} \frac{\mathcal{C}_{\text{PS}}^{(r')}(\Phi_{\text{B}}, \Phi_{\text{rad}}^{(r')})}{\mathcal{B}(\Phi_{\text{B}})} + \mathcal{O}(\alpha_s^2), \end{aligned} \quad (2.7)$$

where we have adopted a simplified notation for the integral over the radiation kinematics, highlighting only the integration boundaries in the shower ordering variable, for simplicity. Moreover, in the second line, we have reported the first-order expansion of the shower Sudakov exponential, since the shower kernel \mathcal{C}_{PS} is of $\mathcal{O}(\alpha_s)$. Owing to the positivity of the argument in the Sudakov exponent, the shower Sudakov $\Delta^{\text{PS}}(t_i)$ admits a probabilistic interpretation. It describes the probability for a parton not to radiate from t_i to t_0 . Therefore, the first term in Eq. (2.6) gives the probability that no resolved radiation (i.e. with $t > t_0$) is generated, so that the original kinematics is left untouched; the second term gives the probability that the shower generates exactly one additional radiation at the scale t , with no further emission from t to t_0 .

If we make use of Eq. (2.6) (noticing that \mathbb{S} only acts on the observable and not on its fully-differential weight) and the Sudakov expansion in Eq. (2.7) for $\Delta^{\text{PS}}(t_i)$, the weight of a standard event after the action of the shower reads:

$$\begin{aligned} \mathbb{S}[\mathcal{S}(\mathcal{O}_n)] &= \bar{\mathcal{B}}(\Phi_{\text{B}}) \cdot \mathbb{S}[\mathcal{O}_n] = \bar{\mathcal{B}}(\Phi_{\text{B}}) \mathcal{O}_n(\Phi_{\text{B}}) \\ &\quad - \sum_{r'} \int_{t_0}^{t_i} d\Phi_{\text{rad}}^{(r')} \mathcal{C}_{\text{PS}}^{(r')}(\Phi_{\text{B}}, \Phi_{\text{rad}}^{(r')}) \underbrace{\frac{\bar{\mathcal{B}}(\Phi_{\text{B}})}{\mathcal{B}(\Phi_{\text{B}})}}_{=1+\mathcal{O}(\alpha_s)} \mathcal{O}_n(\Phi_{\text{B}}) \\ &\quad + \sum_{r'} \mathcal{C}_{\text{PS}}^{(r')}(\Phi_{\text{R}}) \underbrace{\frac{\bar{\mathcal{B}}(\Phi_{\text{B}})}{\mathcal{B}(\Phi_{\text{B}})}}_{=1+\mathcal{O}(\alpha_s)} \Delta^{\text{PS}}(t) \mathcal{O}_{n+1}(\Phi_{\text{R}}) + \mathcal{O}(\alpha_s^2), \end{aligned} \quad (2.8)$$

where we have highlighted that, if we aim at preserving NLO accuracy [i.e. neglecting terms of $\mathcal{O}(\alpha_s^2)$], the ratio of the NLO weight $\bar{\mathcal{B}}$ over the Born weight \mathcal{B} can be approximated by one when it multiplies the shower counterterm [second and third lines of Eq. (2.8)]. We now see that the first-order expansion of the Sudakov exponent, giving the non-emission probability and therefore living on a Born kinematics, introduces a spurious $\mathcal{O}(\alpha_s)$ term that spoils the NLO accuracy of the event weight. This term is exactly compensated by a similar term of opposite sign in the standard-event definition in Eq. (2.4). The third line of Eq. (2.8) contains an additional $\mathcal{O}(\alpha_s)$ term that arises

when the shower generates one resolved radiation. This contribution introduces a double counting on the real kinematics that is accounted for by the shower counterterm entering the weight of the hard event,

$$\begin{aligned}\mathbb{S}[\mathcal{H}(\mathcal{O}_{n+1})] &= \left[\mathcal{R} - \sum_{r'} \mathcal{C}_{\text{PS}}^{(r')} \right] (\Phi_{\text{R}}) \cdot \mathbb{S}[\mathcal{O}_{n+1}] \\ &= \left[\mathcal{R} - \sum_{r'} \mathcal{C}_{\text{PS}}^{(r')} \right] (\Phi_{\text{R}}) \Delta^{\text{PS}}(t'_i) \mathcal{O}_{n+1}(\Phi_{\text{R}}) + \mathcal{O}(\alpha_s^2),\end{aligned}\quad (2.9)$$

where t'_i is the starting scale for the shower in the presence of an $n+1$ kinematics, which is different from the starting scale t_i entering Eq. (2.8). Even if $t'_i \neq t_i$, at our target accuracy we can use the expansion $\Delta^{\text{PS}}(t) = 1 + \mathcal{O}(\alpha_s)$ in the third line of Eq. (2.8) and similarly for $\Delta^{\text{PS}}(t'_i)$ in Eq. (2.9), so that the two terms cancel each other. This explains why it is crucial for the shower counterterms of the standard and hard events to be cut on different phase spaces. Note that in the last expression we have only considered the first PS iteration, giving the probability that the shower does not modify the real kinematics with additional radiation. This is the only relevant contribution at $\mathcal{O}(\alpha_s)$.

2.1.2 The PYTHIA8 final-state Simple Shower

The MC@NLO approach strongly relies on the specific PS used for the NLO matching. In particular, a detailed understanding of the shower algorithm is required in order to construct \mathcal{C}_{PS} . Since our aim is to match MOCANLO to PYTHIA8, we briefly recall some relevant aspects of this shower. A detailed overview of PYTHIA8 can be found for instance in Ref. [7]. In what follows, we focus on the Simple-Shower algorithm (default in PYTHIA8) for final-state QCD emissions.

As already mentioned, the evolution of an event is carried out in PYTHIA8 in an ordering variable t from a starting scale t_i to a cut-off scale t_0 , which are typically identified with the characteristic scale of the hard process and the hadronisation scale, respectively. The variable t is chosen to be a squared transverse-momentum-like quantity $p_{\text{T,PS}}^2$ (see Section 2.2). At each evolution step, additional radiation can potentially be emitted from all emitter-recoiler pairs that are colour connected within the large N_c limit. Each pair defines a *shower dipole* and is in one-to-one correspondence with the regions r' introduced in Eqs. (2.2) and (2.3). First, each pair is treated separately and allowed to generate a candidate emission at scale $p_{\text{T,PS}}^{2,(r')}$. Then, among all candidate emissions from all dipoles only the hardest one is kept, namely the one with $p_{\text{T,PS}}^2 = \max_{r'} p_{\text{T,PS}}^{2,(r')}$ for all r' . If an emission with $t = p_{\text{T,PS},1}^2$ has already been generated in a previous step, the ordering constraint applies to the selected emission, which must satisfy $p_{\text{T,PS}}^2 < p_{\text{T,PS},1}^2$. This algorithm for choosing an emitting dipole is known as *highest-bid mechanism* (see for instance Ref. [7] or Appendix B of Ref. [21]).

A value $p_{\text{T,PS}}^{2,(r')}$ for a candidate emission is obtained using the *veto algorithm* (see Ref. [7]) with a PS Sudakov factor like the one of Eq. (2.7). The radiation kinematics Φ_{rad} is then completed by two more variables: a uniformly distributed azimuthal angle ϕ_{PS} and an energy fraction variable z_{PS} (see Section 2.2). The latter is distributed according to the exponent of the Sudakov factor Δ^{PS} , whose functional form is derived from the collinear limits of the real amplitude, and therefore based on the well-known Dokshitzer-Gribov-Lipatov-Altarelli-Parisi (DGLAP) splitting functions [59–61]. We denote with P_{ij} the standard DGLAP kernels and with \tilde{P}_{ij} the PS ones, where the indices i and j refer to the emitter and emitted particles.

When the emitter particle is a quark splitting according to $q \rightarrow qg$, the emitter belongs to a unique dipole. Indeed, in the large N_c limit, since quarks carry only one colour index (being described by the fundamental representation of QCD), they admit a unique colour-connected recoiler.

In this case one has

$$\tilde{P}_{gg}(z_{\text{PS}}) = C_F \frac{1 + z_{\text{PS}}^2}{1 - z_{\text{PS}}}, \quad (2.10)$$

with C_F being the Casimir of the fundamental representation. Equation (2.10) exactly matches the usual DGLAP kernel P_{gg} .

When a gluon splits, the situation is more involved. A first approximation consists of dropping any information on spin correlation by considering the form of the DGLAP functions averaged over the azimuthal angle around the direction of the gluon's momentum. Moreover, a splitting gluon has two possible colour-connected recoilers, since it carries two colour indices (being part of the adjoint representation). These two recoilers define two possible dipoles between which the splitting gluon is shared. The correct DGLAP splitting kernels P_{gg} and P_{gq} are reconstructed only when the contributions from these two dipoles are summed together [62, 63]. For the splitting $g \rightarrow gg$, each dipole comes with a PS kernel that reads

$$\tilde{P}_{gg}(z_{\text{PS}}) = \frac{C_A}{2} \frac{1 + z_{\text{PS}}^3}{1 - z_{\text{PS}}}, \quad (2.11)$$

with C_A the Casimir of the adjoint representation. The additional factor of one half is instead a symmetry factor. Indeed, if we label the gluons from the splitting $g \rightarrow g_i g_j$, we notice that

$$\begin{aligned} \frac{1}{2} P_{gg}(z_{\text{PS}}) &= C_A \frac{(1 - z_{\text{PS}}(1 - z_{\text{PS}}))^2}{z_{\text{PS}}(1 - z_{\text{PS}})} = \frac{C_A}{2} \frac{1 + z_{\text{PS}}^3}{1 - z_{\text{PS}}} + \frac{C_A}{2} \frac{1 + (1 - z_{\text{PS}})^3}{z_{\text{PS}}} \\ &= \tilde{P}_{g_i g_j}(z_{\text{PS}}) + \tilde{P}_{g_j g_i}(1 - z_{\text{PS}}) \xrightarrow{g_i \leftrightarrow g_j} 2 \tilde{P}_{g_i g_j}(z_{\text{PS}}). \end{aligned} \quad (2.12)$$

In the last step we used the fact that observables do not distinguish between the gluons g_i and g_j , which provides an implicit symmetrisation $z_{\text{PS}} \leftrightarrow 1 - z_{\text{PS}}$.

Finally, for the splitting $g \rightarrow \bar{q}q$, the gluon is again allowed to split separately in the two dipoles. If only massless quarks are considered, both dipoles contribute with a kernel

$$\tilde{P}_{gq}(z_{\text{PS}}) = \frac{N_f T_F}{2} (1 - 2z_{\text{PS}}(1 - z_{\text{PS}})), \quad (2.13)$$

with N_f the number of active flavours and $T_F = 1/2$ the colour factor.

2.2 Catani–Seymour-based MC@NLO matching

As shown in Eq. (2.2), the subtraction dipoles $\mathcal{C}_{\text{dip}}^{(r)}$ enter the weight of a standard event and are defined on a factorised real phase space with fiducial cuts applied to the Born kinematics. On the other hand, the real contribution \mathcal{R} must be part of the hard event. Since the real and the subtraction-dipole contributions are integrated separately, the IR cancellation of singularities at NLO is spoiled, unless the PS counterterms act as local subtraction terms.

2.2.1 Construction of the parton-shower counterterms

We first observe that, since PYTHIA8 uses a dipole shower for the generation of final-state radiation, each region r' can be defined by a triplet of particles, namely an emitter, an emissus, and a recoiler. This is very close to the definition of singular regions r in the CS NLO subtraction. Therefore, for each region r' one can find a corresponding CS dipole in a given region r , but not vice versa. Indeed, while in CS subtraction for an emitter–emissus pair that gives rise to a QCD singular splitting all possible colour-charged spectators are taken into account, the PYTHIA8 shower only considers dipoles whose emitter and spectator are colour connected. This is consistent with the large N_c approximation. Consequently, only a subset S_{PS} of the set of CS dipoles S_{CS} has its PS

counterpart. If only dipoles formed by massless particles are involved, then $S_{\text{PS}} \subset S_{\text{CS}}$. However, this no longer holds in the presence of resonances, as discussed starting from Section 2.3.

We illustrate now that, in order to embed the PS counterterms $\mathcal{C}_{\text{PS}}^{(r')}$ in our NLO subtraction algorithm, these terms can not simply be written in the bare form extracted from the shower, but need to be carefully modified. For this reason we mark for the rest of this manuscript the bare PS counterterms with a tilde, i.e. $\tilde{\mathcal{C}}_{\text{PS}}^{(r')}$, to distinguish them from their modified versions $\mathcal{C}_{\text{PS}}^{(r')}$, which we introduce in this Section. To this end, we start extending the sum over $r' \in S_{\text{PS}}$ in Eqs. (2.2) and (2.3) to a sum over the larger set of singular regions $r \in S_{\text{CS}}$, and define $\tilde{\mathcal{C}}_{\text{PS}}^{(r)} = 0$ whenever $r \notin S_{\text{PS}}$. In the shower evolution, only a subset of singular regions is considered, since soft singularities are only partially captured by splitting kernels that are constructed from the collinear limits of the real amplitude. Therefore, the full IR structure of the latter can not be completely accounted for. To circumvent this issue, we adopt a solution originally proposed in Ref. [16] and define the PS counterterms as

$$\mathcal{C}_{\text{PS}}^{(r)}(\Phi_{\text{B}}, \Phi_{\text{rad}}^{(r)}) = \mathcal{G}(\Phi_{\text{rad}}^{(r)}) \tilde{\mathcal{C}}_{\text{PS}}^{(r)}(\Phi_{\text{B}}, \Phi_{\text{rad}}^{(r)}) + \left[1 - \mathcal{G}(\Phi_{\text{rad}}^{(r)})\right] \mathcal{C}_{\text{dip}}^{(r)}(\Phi_{\text{B}}, \Phi_{\text{rad}}^{(r)}), \quad (2.14)$$

where $\tilde{\mathcal{C}}_{\text{PS}}^{(r)}$ is the part of the bare counterterm matching the PS splitting kernel. The function $\mathcal{G}(\Phi_{\text{rad}}^{(r)})$ is a damping factor defined such that, when the singular limit of the region r is approached, $\mathcal{G}(\Phi_{\text{rad}}^{(r)}) \rightarrow 0$ and thus $\mathcal{C}_{\text{PS}}^{(r)} \rightarrow \mathcal{C}_{\text{dip}}^{(r)}$. In this limit, Eq. (2.14) guarantees that the local IR cancellation takes place. Moreover, if the form of $\mathcal{G}(\Phi_{\text{rad}}^{(r)})$ is properly chosen, no double-counting problem is introduced. Indeed, the PS counterterms are only altered close to the IR-singular regions that are not in the domain of the PS anyhow, since its evolution is cut at $t = t_0$. Our actual choice of $\mathcal{G}(\Phi_{\text{rad}}^{(r)})$ is discussed in Section 2.2.2. Note that if $r \notin S_{\text{PS}}$, then the first term on the right-hand side of Eq. (2.14) is absent.

We can write down explicitly the analytic form of $\tilde{\mathcal{C}}_{\text{PS}}$ that is needed to compensate for spurious terms introduced by the PS at $\mathcal{O}(\alpha_s)$ relative to the LO. For simplicity, we temporarily drop any dependence on the singular region r and consider the case where $r \in S_{\text{PS}}$. One should note that, in Eq. (2.14), $\tilde{\mathcal{C}}_{\text{PS}}$ has been defined on a real phase space factorised in terms of the Born kinematics Φ_{B} and the radiation variables Φ_{rad} , which are also used to evaluate the subtraction dipole \mathcal{C}_{dip} . Here, Φ_{rad} is the set of variables obtained from the CS mapping for a specific singular region. Nevertheless, by definition, $\tilde{\mathcal{C}}_{\text{PS}}$ depends explicitly on the PS radiation variables $\Phi_{\text{rad}}^{\text{PS}} = \{p_{\text{T,PS}}^2, z_{\text{PS}}, \phi_{\text{PS}}\}$, which we introduced in Section 2.1.2. Therefore, we can first write the contribution dI_{PS} of $\tilde{\mathcal{C}}_{\text{PS}}$ to the differential cross sections in Eqs. (2.2) and (2.3) [leaving aside for a moment the damping-function corrections in Eq. (2.14)] as

$$\begin{aligned} dI_{\text{PS}} &= d\Phi_{\text{B}} d\Phi_{\text{rad}}^{\text{PS}} \tilde{\mathcal{C}}_{\text{PS}}(\Phi_{\text{B}}, \Phi_{\text{rad}}^{\text{PS}}) \\ &= d\Phi_{\text{B}} \frac{1}{16\pi^2} \frac{d\phi_{\text{PS}}}{2\pi} dz_{\text{PS}} dp_{\text{T,PS}}^2 \frac{8\pi\alpha_s(\mu_{\text{R}})}{p_{\text{T,PS}}^2} \tilde{P}_{ij}(z_{\text{PS}}) |\mathcal{M}_{\text{B}}|^2, \end{aligned} \quad (2.15)$$

where we have used $d\Phi_{\text{rad}}^{\text{PS}} = J_{\text{PS}} d\phi_{\text{PS}} dz_{\text{PS}} dp_{\text{T,PS}}^2$, and $J_{\text{PS}} = 1/(32\pi^3)$ being a Jacobian factor arising from the factorisation of the real emission phase space. The splitting kernels \tilde{P}_{ij} are the ones that have been described in Section 2.1.2, with i and j the indices of the emitter and emitted particles in the understood region r .

Few remarks on Eq. (2.15) are in order. First of all, we notice that the coupling α_s is evaluated at the renormalisation scale μ_{R} . Since this scale is also the one used for the evaluation of the strong coupling in the real amplitude, this choice allows for a more efficient cancellation of singularities. Even though α_s in the PS is computed at the evolution scale $p_{\text{T,PS}}^2$ [64], the mismatch only introduces differences at the relative $\mathcal{O}(\alpha_s^2)$, which are beyond our target accuracy.

We also observe that, in Eq. (2.15), the dependence on the Born kinematics is fully contained in the Born amplitude \mathcal{M}_{B} . Since the PS is based on the large- N_c limit, this amplitude must be

evaluated at leading colour. On the other hand, only a full dependence on the colour structure guarantees to match the IR-singular structure of the real amplitude. This problem is handled using the prescription of Ref. [65], according to which $|\mathcal{M}_B|^2$ must be understood as a sum over the colour-planar configurations c (large N_c limit)

$$|\mathcal{M}_B|^2 = \sum_c |\mathcal{M}_B^{(c)}|^2, \quad (2.16)$$

where $|\mathcal{M}_B^{(c)}|^2$ is the full squared Born amplitude times a factor that depends on the colour flow c . The computation of this factor requires to access the amplitude in its colour-flow decomposition, for which we make use of RECOLA [66]. Even if at the integrated level only the sum of the terms $|\mathcal{M}_B^{(c)}|^2$ is needed, Eq. (2.16) becomes relevant at the even-generation level. Once an unweighted event is generated, it is also attached a colour configuration c with a probability proportional to the relative size of $|\mathcal{M}_B^{(c)}|^2/|\mathcal{M}_B|^2$.

We are left with the problem of correctly integrating $\tilde{\mathcal{C}}_{\text{PS}}$ as part of the standard and hard weights in Eqs. (2.2) and (2.3). Indeed, even if $\tilde{\mathcal{C}}_{\text{PS}}$ explicitly depend on $\Phi_{\text{rad}}^{\text{PS}}$, they cannot be integrated independently from $\mathcal{C}_{\text{dip}}^{(r)}$ or the real contribution, but in a *correlated* way, which guarantees that IR-singular limits are approached simultaneously by all terms. Only in this way a local cancellation of singularities can be achieved. This means first that the PS counterterms must be integrated over Φ_{rad} , i.e. the CS phase space for the radiation variables. Despite its dependence on the considered singular region, Φ_{rad} can always be parametrised in terms of three variables, so that one can write $d\Phi_{\text{rad}} = J_{\text{CS}} d\phi_{\text{CS}} dz_{\text{CS}} dy_{\text{CS}}$, with J_{CS} an appropriate Jacobian factor from the factorisation of the real phase space. Even if we are free to identify $\phi_{\text{CS}} = \phi_{\text{PS}}$, we have $z_{\text{CS}} \neq z_{\text{PS}}$ and in general a non-trivial relation connecting y_{CS} and the shower evolution variable $p_{\text{T,PS}}^2$. This requires to find the equations $p_{\text{T,PS}}^2 = p_{\text{T,PS}}^2(z_{\text{CS}}, y_{\text{CS}})$ and $z_{\text{PS}} = z_{\text{PS}}(z_{\text{CS}}, y_{\text{CS}})$, such that the integration of the PS counterterms can be recast as

$$dI_{\text{PS}} = d\Phi_B d\Phi_{\text{rad}}^{\text{PS}} \tilde{\mathcal{C}}_{\text{PS}}(\Phi_B, \Phi_{\text{rad}}^{\text{PS}}) = d\Phi_B d\Phi_{\text{rad}} c_J \left\| \frac{\partial \Phi_{\text{rad}}^{\text{PS}}}{\partial \Phi_{\text{rad}}} \right\| \tilde{\mathcal{C}}_{\text{PS}}(\Phi_B, \Phi_{\text{rad}}^{\text{PS}}(\Phi_{\text{rad}})), \quad (2.17)$$

where the Jacobian $J_{\text{var}}(z_{\text{CS}}, y_{\text{CS}})$ arising from the change of variables reads

$$J_{\text{var}}(z_{\text{CS}}, y_{\text{CS}}) = \left\| \frac{\partial \Phi_{\text{rad}}^{\text{PS}}}{\partial \Phi_{\text{rad}}} \right\| = \left\| \frac{\partial(z_{\text{PS}}, p_{\text{T,PS}}^2)}{\partial(z_{\text{CS}}, y_{\text{CS}})} \right\|, \quad (2.18)$$

and where $c_J = J_{\text{PS}}/J_{\text{CS}}$ accounts for the mismatch in the CS and PS Jacobians from the factorisation of the real phase space.

To better highlight the importance of a correlated integration, we examine the differential weight of a standard event in Eq. (2.2), and specifically the contribution originating from the difference of the subtraction dipoles and the PS counterterms. We write this difference as

$$dI_{\text{CS}} - dI_{\text{PS}} = d\Phi_B \sum_r \int d\Phi_{\text{rad}}^{(r)} \left(\mathcal{C}_{\text{dip}}^{(r)} - c_J J_{\text{var}}^{(r)} \tilde{\mathcal{C}}_{\text{PS}}^{(r)} \right), \quad (2.19)$$

where the explicit dependence on the singular region r in J_{var} has been highlighted. In order for the weight of an event not to diverge, the difference above must be finite. Even though the cancellation of singularities is always enforced in the proximity of the singular limits when Eq. (2.14) is employed, $\tilde{\mathcal{C}}_{\text{PS}}$ must mimic the correct subtraction term while approaching these limits to ensure the proper convergence of the numerical integration and to reduce the appearance of artificially large weights. If we restrict the discussion to one singular region r (whose dependence will be understood in what follows) defined by the pair of splitting particles i and j , then dI_{PS} reads as in Eq. (2.15). While this term fails in the description of the soft large-angle limits of the real amplitude, it correctly

reproduces its collinear/soft-collinear structure. To see this, we recall that in the CS subtraction approach, for a splitting pair i and j one must account for all dipoles sharing the same pair but with different colour-charged spectators k . It is by summing over all spectators k that soft large-angle configurations can be properly subtracted. For the time being, it is enough to consider the case where i , j , and k are massless. Therefore, we can write

$$dI_{\text{CS}} = d\Phi_{\text{B}} |\mathcal{M}_{\text{B}}|^2 \sum_k \underbrace{\frac{2\tilde{p}_i \cdot \tilde{p}_k}{16\pi^2} \frac{d\phi}{2\pi} dz_{\text{CS}} dy_{ij,k} (1 - y_{ij,k})}_{J_{\text{CS}} dz_{\text{CS}} dy_{ij,k} d\phi_{\text{PS}}} \underbrace{\frac{8\pi\alpha_s(\mu_{\text{R}})}{2p_i \cdot p_j} \left\langle \frac{\mathbf{T}_k \cdot \mathbf{T}_{ij}}{\mathbf{T}_{ij}^2} \mathbf{V}_{ij,k} \right\rangle}_{K_{\text{CS}}}, \quad (2.20)$$

with

$$J_{\text{CS}} = \frac{2\tilde{p}_i \cdot \tilde{p}_k (1 - y_{ij,k})}{16\pi^2 2\pi}, \quad (2.21)$$

where \mathbf{T}_{ij} and \mathbf{T}_k are matrices in colour space associated to the emitter and the spectator, and $\mathbf{V}_{ij,k}$ a matrix in the helicity space of the emitter.² For clarity, we have restored here the usual dependence on the triplet of indices for the variable y_{CS} , which now reads $y_{ij,k}$. We also recall that momenta marked with a tilde are the ones after the application of the CS mapping from a real phase space to the underlying-Born phase space where the radiated particle is removed.

When the collinear limit is approached, $y_{ij,k} \rightarrow 0$ for all k . We can use the definition of $y_{ij,k}$ to rewrite the denominator of the kernel K_{CS} as $p_i \cdot p_j = y_{ij,k} \tilde{p}_i \cdot \tilde{p}_k$, where the tilded momenta \tilde{p}_i and \tilde{p}_k are those of the emitter and spectator, respectively, in the underlying-Born phase space. The product $\tilde{p}_i \cdot \tilde{p}_k$ cancels an equal term in the measure J_{CS} , so that the residual dependence on the spectator in dI_{CS} is only through $y_{ij,k}$ and the expectation value of the matrix part of the kernel. As far as $y_{ij,k}$ is concerned, we immediately see that according to the CS parametrisation of the collinear limit [42]

$$y_{ij,k} \xrightarrow{k_{\perp}^2 \rightarrow 0} -\frac{k_{\perp}^2}{2z_{\text{CS}}(1-z_{\text{CS}})\tilde{p}_i \cdot \tilde{p}_k} \Rightarrow \frac{dy_{ij,k}}{y_{ij,k}} \xrightarrow{k_{\perp}^2 \rightarrow 0} \frac{dk_{\perp}^2}{k_{\perp}^2}, \quad (2.22)$$

so that any dependence on the spectator drops from the integration measure. In the previous equation, we recall that k_{\perp}^{μ} is a four vector that enters the CS parametrisation of the splitting in terms of light-cone coordinates (see also Section 2.2.3). Owing to the simplification in Eq. (2.22), the spectator sum can act directly on the kernel:

$$dI_{\text{CS}} \xrightarrow{k_{\perp}^2 \rightarrow 0} d\Phi_{\text{B}} |\mathcal{M}_{\text{B}}|^2 \frac{1}{16\pi^2} \frac{d\phi}{2\pi} dz_{\text{CS}} \frac{dk_{\perp}^2}{k_{\perp}^2} 8\pi\alpha_s(\mu_{\text{R}}) \underbrace{\sum_k \left\langle \frac{\mathbf{T}_k \cdot \mathbf{T}_{ij}}{\mathbf{T}_{ij}^2} \mathbf{V}_{ij,k} \right\rangle}_{\rightarrow P_{ij}(z_{\text{CS}})}. \quad (2.23)$$

If spin correlation is not involved in the splitting, i.e. if we exclude gluon splittings, or alternatively after azimuthal average, the shower splitting kernels \tilde{P}_{ij} and the DGLAP ones P_{ij} match. Under these assumptions, we found as expected that $dI_{\text{CS}} \rightarrow dI_{\text{PS}}$ when $y_{ij,k} \rightarrow 0$.

Even if obtaining the relations $p_{\text{T,PS}}^2 = p_{\text{T,PS}}^2(z_{\text{CS}}, y_{\text{CS}})$ and $z_{\text{PS}} = z_{\text{PS}}(z_{\text{CS}}, y_{\text{CS}})$ is a precondition to perform a correlated integration as discussed above, still it does not guarantee that the difference $dI_{\text{CS}} - dI_{\text{PS}}$ is finite for $y_{ij,k} \rightarrow 0$. Indeed, the two terms of the difference must approach the singular limit at the same rate. This requirement translates into the conditions:

$$p_{\text{T,PS}}^2(z_{\text{CS}}, y_{\text{CS}}) \xrightarrow{y_{\text{CS}} \rightarrow 0} 0, \quad (2.24)$$

$$z_{\text{PS}}(z_{\text{CS}}, y_{\text{CS}}) \xrightarrow{y_{\text{CS}} \rightarrow 0} z_{\text{CS}}. \quad (2.25)$$

²Note that, compared to the original Ref. [42], we have factored out from $\mathbf{V}_{ij,k}$ the term $8\pi\alpha_s(\mu_{\text{R}})$.

If Eq. (2.24) ensures a correct correlation in the collinear limit ($y_{\text{CS}} \rightarrow 0$), Eq. (2.25) is needed for the soft-collinear case, i.e. $(y_{\text{CS}}, z_{\text{CS}}) \rightarrow (0, 1)$. Clearly, this is enough to ensure a correlated integration in the soft limit, where anyhow the shower counterterms are not able to reproduce the singular structure of the real amplitude.

We close this section with a remark concerning the different ways the PS counterterms are incorporated in the integration of a standard and a hard event. When integrating $\tilde{\mathcal{C}}_{\text{PS}}^{(r')}$ within a standard event, one generates the phase-space kinematics for Φ_{B} , shared by all terms in Eq. (2.2), and a set of three random numbers (r^ϕ, r^z, r^y) that are used to sample the CS radiation variables, i.e. $\phi = 2\pi r^\phi$, $z_{\text{CS}} = f_z(r^z)$, and $y_{\text{CS}} = f_y(r^y)$. The functions f_z and f_y stand for a variable transformation used for importance sampling. In so doing, the physical ranges for z_{CS} and y_{CS} must be enforced:

$$z_- < z_{\text{CS}} < z_+, \quad y_- < y_{\text{CS}} < y_+. \quad (2.26)$$

Remembering that the Jacobian J_{var} accounts for the change of variables $(z_{\text{CS}}, y_{\text{CS}}) \rightarrow (z_{\text{PS}}, p_{\text{T,PS}}^2)$, $dI_{\text{PS}}^{\text{S}}$ for a standard event reads as in Eq. (2.17):

$$dI_{\text{PS}}^{\text{S}} = d\Phi_{\text{B}} d\Phi_{\text{rad}} c_J J_{\text{var}}(z_{\text{CS}}, y_{\text{CS}}) \tilde{\mathcal{C}}_{\text{PS}}(\Phi_{\text{B}}, \Phi_{\text{rad}}^{\text{PS}}(\Phi_{\text{rad}})). \quad (2.27)$$

Note that in practice the dependence of $dI_{\text{PS}}^{\text{S}}$ on J_{CS} cancels between $d\Phi_{\text{rad}}$ and c_J . Conversely, for a hard event one starts from the real phase space Φ_{R} and constructs a factorised kinematics $(\Phi_{\text{B}}, \Phi_{\text{rad}})$ differently for the different dipole regions. Since in this case $(z_{\text{CS}}, y_{\text{CS}})$ are obtained from Φ_{R} via the direct CS mapping, they automatically fulfil the physically-allowed kinematic ranges in Eq. (2.26). In this case $dI_{\text{PS}}^{\text{H}}$ is formally obtained as:

$$dI_{\text{PS}}^{\text{H}} = d\Phi_{\text{R}} c_J J_{\text{var}}(z_{\text{CS}}, y_{\text{CS}}) \tilde{\mathcal{C}}_{\text{PS}}(\Phi_{\text{B}}, \Phi_{\text{rad}}^{\text{PS}}(\Phi_{\text{rad}})). \quad (2.28)$$

Differently from Eq. (2.27), the knowledge of J_{CS} is required for $dI_{\text{PS}}^{\text{H}}$.

2.2.2 Correction of the IR limits

As already discussed above, Eqs. (2.2) and (2.3) assume that the PS counterterms $\tilde{\mathcal{C}}_{\text{PS}}^{(r)}$ can act as local counterterms in order for the standard and hard events to have finite weights. But there are many cases where this does not work. Indeed, there are regions of phase space that are simply not covered by the PS, due to either the nature of the evolution variable (see for instance the *dead zones* in HERWIG [16]) or to kinematic restrictions of the shower itself [see the transverse-momentum cut-off in Eq. (2.47)]. Moreover, the splitting kernels used by the shower might fail in reproducing the singular limits of the real amplitude. In the PYTHIA8 Simple-Shower algorithm, for instance, the analytic form of the kernels neither catches its soft large-angle behaviour nor accounts for spin-correlation effects.

For all these reasons, close to the singular limits one is forced to adjust the behaviour of the PS counterterms with the correct local subtraction contribution to restore a proper IR cancellation of singularities [see Eq. (2.14)]. Nevertheless, this should be done carefully: modifying the PS counterterms introduces a mismatch between the PS behaviour for the generation of the first radiation and what is actually subtracted by $\mathcal{C}_{\text{PS}}^{(r)}$. If the shower generation of the first radiation is not correctly subtracted as prescribed by the MC@NLO method, one introduces a double counting at α_s relative to the LO that spoils the NLO accuracy of the fixed-order result. Modifications of the PS counterterms must be restricted to regions where PS predictions are anyway not sensitive [67]: close enough to the singular limits perturbation theory breaks down, and hadronisation models typically step in the PS evolution. Therefore, changing the form of the PS counterterms in this regime has no consequences on the perturbative accuracy of the predictions and just ensures the numerical stability of the integration.

It is clear that a crucial role is played by the damping function \mathcal{G} of Eq. (2.14), which controls the way the CS subtraction terms take over the PS kernels inside the counterterm $\mathcal{C}_{\text{PS}}^{(r)}$. Since in terms of CS radiation variables both the soft and collinear regimes are approached when at least $y_{\text{CS}} \rightarrow 0$, one might devise a damping function \mathcal{G} with an explicit dependence on y_{CS} . To limit the modification of the PS kernels, the damping function can be switched on only for sufficiently small values of y_{CS} below a chosen threshold y_0 . This is very close in spirit to the approach used in FKS-based MC@NLO matching of Refs. [16, 67]. Nonetheless, this might still be problematic in our framework and lead to double-counting issues that are difficult to keep under control. Indeed, choosing an optimal value y_0 can be tricky if we want to restrict changes of the PS kernels to small values of the ordering variable $p_{\text{T,PS}}^2$. Since the connection between y_{CS} and $p_{\text{T,PS}}^2$ depends on the dipole, using a constant value of y_0 might result in switching on the damping function \mathcal{G} for too high values of $p_{\text{T,PS}}^2$.

To have a more direct connection between the damping function and the PS ordering variable, we use instead a $p_{\text{T,PS}}$ -based definition of \mathcal{G} , which reads

$$\mathcal{G}(p_{\text{T,PS}}^2) = \begin{cases} 1 & p_{\text{T,PS}}^2 \geq t_0 \\ \frac{\left(\frac{p_{\text{T,PS}}^2}{t_0}\right)^{2\alpha}}{\left(\frac{p_{\text{T,PS}}^2}{t_0}\right)^{2\alpha} + \left(1 - \frac{p_{\text{T,PS}}^2}{t_0}\right)^{2\alpha}} & p_{\text{T,PS}}^2 < t_0 \end{cases}, \quad (2.29)$$

where the definition of the cut-off scale t_0 might depend on the dipole itself [as in the case of massive emitter/recoiler discussed later in Section 2.3.2, see for instance Eq. (2.115)]. We remark that this solution is very close to how MC@NLO is implemented in HERWIG [9].

Note that with this specific realisation of \mathcal{G} , the CS subtraction terms correcting the IR behaviour of the PS counterterms are smoothly switched on only when $\tilde{\mathcal{C}}_{\text{PS}}^{(r)}$ in Eq. (2.14) are already vanishing. Indeed, by definition they do not have support for values $p_{\text{T,PS}}^2 < t_0$ below the hadronisation scale [see also Eq. (2.47)]. Additionally, further tuning on this behaviour is offered by the technical parameter α , which controls how fast the interpolating functional form of \mathcal{G} grows from zero to one: for larger values of α , \mathcal{G} becomes closer and closer to a step function with turning point $t_0/2$.

Since the damping function also multiplies those CS dipoles that do not have a PS counterpart (more precisely by a factor $1 - \mathcal{G}$, in order to restore the correct IR subtraction where the PS counterterms are doomed to fail), a value for $p_{\text{T,PS}}^2$ can still be computed once the relation $p_{\text{T,PS}}^2 = p_{\text{T,PS}}^2(z_{\text{CS}}, y_{\text{CS}})$ has been determined. In these cases, we use the relation for dipoles with a massless emitter and a massless spectator, which is obtained in the next section [see Eq. (2.42)].

2.2.3 Kinematic mapping for shower dipoles with massless emitter–spectator pairs

At the end of Section 2.2.1 we have emphasised the importance of integrating the PS counterterms in a correlated way, which requires to find a change of variables $p_{\text{T,PS}}^2(z_{\text{CS}}, y_{\text{CS}})$ and $z_{\text{PS}}(z_{\text{CS}}, y_{\text{CS}})$ that satisfies Eqs. (2.24) and (2.25). Since we are considering a CS singular region r with a non-vanishing PS counterterm [see Eq. (2.14)], the emitter, emissor, and spectator particles are the same in the CS mapping for subtraction and in the splitting used in the PS evolution. Moreover, all of the three particles are massless. We now study how the kinematics of the $2 \rightarrow 3$ splitting is treated in the two cases.

The CS mapping expresses the four-momenta of the emitter p_i^μ , the spectator p_k^μ , and the emissor p_j^μ in terms of the pre-branching momenta \tilde{p}_i^μ and \tilde{p}_k^μ [42]:

$$\begin{aligned} p_i^\mu &= z_{\text{CS}} \tilde{p}_i^\mu + y_{\text{CS}} (1 - z_{\text{CS}}) \tilde{p}_k^\mu + k_\perp^\mu, \\ p_j^\mu &= (1 - z_{\text{CS}}) \tilde{p}_i^\mu + y_{\text{CS}} z_{\text{CS}} \tilde{p}_k^\mu - k_\perp^\mu, \\ p_k^\mu &= (1 - y_{\text{CS}}) \tilde{p}_k^\mu. \end{aligned} \quad (2.30)$$

We recall that, in terms of the post-branching momenta p_i^μ , p_j^μ , and p_k^μ , the CS variables read

$$y_{\text{CS}} = \frac{p_i \cdot p_j}{p_i \cdot p_j + p_i \cdot p_k + p_j \cdot p_k}, \quad z_{\text{CS}} = \frac{p_i \cdot p_k}{p_i \cdot p_k + p_j \cdot p_k}. \quad (2.31)$$

Moreover, we can parametrise the momenta \tilde{p}_i^μ and \tilde{p}_k^μ in the dipole rest frame as

$$\tilde{p}_i^\mu = \frac{m_{\text{dip}}}{2}(1, 0, 0, 1), \quad \tilde{p}_k^\mu = \frac{m_{\text{dip}}}{2}(1, 0, 0, -1), \quad (2.32)$$

with m_{dip} the dipole invariant mass, i.e. $m_{\text{dip}}^2 = (\tilde{p}_i + \tilde{p}_k)^2$.

On the other hand, for an emitter with four-momentum \bar{p}_i and a spectator with four-momentum \bar{p}_k , PYTHIA8 constructs the splitting as follows [6]. The two momenta are first boosted in the rest frame of the dipole formed by the two particles. The boosted momenta \bar{p}'_i and \bar{p}'_k can be identified with the CS pre-branching momenta, parametrised as in Eq. (2.32). Therefore, we can set $\bar{p}'_i = \tilde{p}_i$ and $\bar{p}'_k = \tilde{p}_k$. Before the splitting, both particles are on shell i.e. $\tilde{p}_i^2 = 0$ and $\tilde{p}_k^2 = 0$. In order for the splitting to take place, the emitter has to acquire a non-zero virtuality. In practise, the emitter momentum \tilde{p}_i is replaced by a new momentum p_a , with $p_a^2 = (m_{\text{rad}}^*)^2 \neq 0$. The virtual particle with momentum p_a is the so-called *radiator*, in the shower language. For later convenience, we also introduce the virtuality of the splitting Q^2 , which for dipoles with a massless emitter and a massless spectator reads $Q^2 = (m_{\text{rad}}^*)^2$. Momentum conservation is enforced by adapting the recoiler momentum \tilde{p}_k to p_k , while preserving its invariant mass, i.e. $\tilde{p}_k^2 = p_k^2$. In the dipole rest frame, if the new momenta p_k and p_a are chosen to be aligned along the z axis ($p_{a,z} = -p_{k,z}$), we can write

$$m_{\text{dip}} = E_a + E_k, \quad E_a^2 = Q^2 + p_{a,z}^2, \quad E_k^2 = p_{k,z}^2 = p_{a,z}^2, \quad (2.33)$$

which leads to

$$E_a = \frac{m_{\text{dip}}^2 + Q^2}{2 m_{\text{dip}}}, \quad E_k = \frac{m_{\text{dip}}^2 - Q^2}{2 m_{\text{dip}}} = p_{a,z}. \quad (2.34)$$

We consider the shower kinematics of the splitting pair i and j after the branching:

$$\begin{aligned} p_{a,z} &= p_{i,z} + p_{j,z}, & E_i &= z_{\text{PS}} E_a, & E_j &= (1 - z_{\text{PS}}) E_a, \\ E_i^2 &= p_{i,z}^2 + p_{\perp,ij}^2, & E_j^2 &= p_{j,z}^2 + p_{\perp,ij}^2. \end{aligned} \quad (2.35)$$

In the previous equation, the PS variable z_{PS} has been introduced. In the PYTHIA8 Simple Shower it is defined as the energy sharing of the radiator daughters in the dipole rest frame. Moreover, $p_{\perp,ij}$ corresponds to the relative transverse momentum of the splitting pair. If we subtract the last two conditions in Eq. (2.35) and use the first three, we obtain:

$$(p_{i,z} - p_{j,z}) = \frac{(-1 + 2 z_{\text{PS}}) E_a^2}{p_{a,z}}. \quad (2.36)$$

Together with the first equation of Eq. (2.35), this yields

$$p_{i,z} = \frac{2 z_{\text{PS}} E_a^2 - Q^2}{2 p_{a,z}}, \quad p_{j,z} = \frac{2(1 - z_{\text{PS}}) E_a^2 - Q^2}{2 p_{a,z}}, \quad (2.37)$$

where we used $p_{a,z}^2 = E_a^2 - Q^2$. We can read from Eqs. (2.30) and (2.32) equivalent expressions for $p_{i,z}$ and $p_{j,z}$ in the CS parametrisation. Equating them with the ones in Eq. (2.37) allows us to write

$$\begin{aligned} \frac{2 z_{\text{PS}} E_a^2 - Q^2}{2 p_{a,z}} &= \frac{m_{\text{dip}}}{2} (z_{\text{CS}} - y_{\text{CS}} + y_{\text{CS}} z_{\text{CS}}), \\ \frac{2(1 - z_{\text{PS}}) E_a^2 - Q^2}{2 p_{a,z}} &= \frac{m_{\text{dip}}}{2} (1 - z_{\text{CS}} - y_{\text{CS}} z_{\text{CS}}). \end{aligned} \quad (2.38)$$

If we add up the two equations, the explicit dependence on z_{PS} and z_{CS} drops out and we obtain a direct relation between the radiator virtuality of the shower Q^2 and the CS variable y_{CS} ,³

$$Q^2 = m_{\text{dip}}^2 y_{\text{CS}}. \quad (2.39)$$

From either equality in Eq. (2.38), one can write an expression for z_{PS} in terms of y_{CS} , z_{CS} , and Q^2 , and finally determine $z_{\text{PS}} = z_{\text{PS}}(z_{\text{CS}}, y_{\text{CS}})$ as

$$z_{\text{PS}} = \frac{z_{\text{CS}} + y_{\text{CS}} - y_{\text{CS}} z_{\text{CS}}}{1 + y_{\text{CS}}}. \quad (2.40)$$

Now we have to find a similar relation for the shower ordering variable. Indeed, the current version of the PYTHIA8 shower does not use the virtuality Q^2 [for which we already have a simple relation $Q^2 = Q^2(z_{\text{CS}}, y_{\text{CS}})$ in Eq. (2.39)] as an evolution variable, but a transverse-momentum variable $p_{\text{T,PS}}^2$ [6]. This variable is introduced starting from the description of the splitting process $a \rightarrow i + j$ in light-cone coordinates, where the radiator reads $p_a = (p_a^+, p_a^-, \vec{p}_{a,\perp})$, with $p_a^\pm = E_a \pm p_{a,z}$. Clearly, if p_a is aligned to the z axis, $\vec{p}_{a,\perp} = \vec{0}$ and $\vec{p}_{i,\perp} = -\vec{p}_{j,\perp}$. We also introduce the light-cone energy fraction z_{LC} as $p_i^+ = z_{\text{LC}} p_a^+$ and $p_j^+ = (1 - z_{\text{LC}}) p_a^+$. By using the on-shell conditions $0 = p_i^+ p_i^- - \vec{p}_{i,\perp}^2$ and $0 = p_j^+ p_j^- - \vec{p}_{j,\perp}^2$ as well as the relation $Q^2 = p_a^2 = p_a^+ p_a^-$, we can derive expressions for p_a^- , p_i^- , and p_j^- . Enforcing momentum conservation for the second light-cone direction, i.e. $p_a^- = p_i^- + p_j^-$, leads to

$$\frac{Q^2}{p_a^+} = \frac{\vec{p}_{i,\perp}^2}{p_i^+} + \frac{\vec{p}_{j,\perp}^2}{p_j^+} = \frac{\vec{p}_{i,\perp}^2}{z_{\text{LC}} p_a^+} + \frac{\vec{p}_{i,\perp}^2}{(1 - z_{\text{LC}}) p_a^+} \Rightarrow p_{i,\perp}^2 = z_{\text{LC}} (1 - z_{\text{LC}}) Q^2. \quad (2.41)$$

Starting from the expression above for $p_{i,\perp}^2$, $p_{\text{T,PS}}^2$ is obtained by setting $z_{\text{LC}} \rightarrow z_{\text{PS}}$. This replacement gives nicer Lorentz-invariance properties to the evolution variable (in the dipole rest frame, energies can be easily related to invariant masses, as commented in Ref. [6]). Therefore, $p_{\text{T,PS}}^2$ and Q^2 are related via the equality

$$Q^2 = \frac{p_{\text{T,PS}}^2}{z_{\text{PS}} (1 - z_{\text{PS}})}, \quad (2.42)$$

which finally allows us to write an expression for $p_{\text{T,PS}}^2 = p_{\text{T,PS}}^2(z_{\text{CS}}, y_{\text{CS}})$:

$$p_{\text{T,PS}}^2 = z_{\text{PS}} (1 - z_{\text{PS}}) Q^2 = m_{\text{dip}}^2 y_{\text{CS}} \frac{(z_{\text{CS}} + y_{\text{CS}} - z_{\text{CS}} y_{\text{CS}}) (1 - z_{\text{CS}} + y_{\text{CS}} z_{\text{CS}})}{(1 + y_{\text{CS}})^2}. \quad (2.43)$$

We notice that the relations found for z_{PS} and $p_{\text{T,PS}}^2$ in terms of z_{CS} and y_{CS} are consistent with the ones reported in Ref. [68]. We also see that Eqs. (2.24) and (2.25) are satisfied by Eqs. (2.40) and (2.43). From the Eqs. (2.40) and (2.43), we can compute the Jacobian factor for the change of variables in Eq. (2.18):

$$J_{\text{var}}(z_{\text{CS}}, y_{\text{CS}}) = m_{\text{dip}}^2 \left| \frac{(1 - y_{\text{CS}})(1 - z_{\text{CS}} + y_{\text{CS}} z_{\text{CS}})(y_{\text{CS}} + z_{\text{CS}} - y_{\text{CS}} z_{\text{CS}})}{(1 + y_{\text{CS}})^3} \right|. \quad (2.44)$$

In the singular limits, the Jacobian factor behaves as

$$\lim_{y_{\text{CS}} \rightarrow 0} J_{\text{var}}(z_{\text{CS}}, y_{\text{CS}}) = m_{\text{dip}}^2 z_{\text{CS}} (1 - z_{\text{CS}}) \quad (\text{collinear limit}), \quad (2.45)$$

$$\lim_{(y_{\text{CS}}, z_{\text{CS}}) \rightarrow (0,1)} J_{\text{var}}(z_{\text{CS}}, y_{\text{CS}}) = 0 \quad (\text{soft limit}). \quad (2.46)$$

Since the CS integration ranges in Eq. (2.26) for a dipole with a massless emitter and a massless spectator read $0 < z_{\text{CS}} < 1$ and $0 < y_{\text{CS}} < 1$, the construction of \mathcal{C}_{PS} only requires additionally

³Equivalently, Eq. (2.39) could be read off from the definition of y_{CS} in Eq. (2.31) using the conservation of the dipole mass in PYTHIA8 and the vanishing masses of the emitter and spectator.

the ranges of the PS variables. For the ordering variable, the range is defined by a starting scale t_i for the shower evolution and by a cut-off t_0 . The latter is set by default to the small value $t_0 = 0.25 \text{ GeV}^2$. Below this scale, hadronisation takes over the shower evolution. As far as t_i is concerned, PYTHIA8 sets it by default to a quarter of the dipole invariant mass squared m_{dip}^2 . Only if an external scale t_{ext} is provided (for instance when interfacing the shower to an external Monte Carlo program), then the minimum between $m_{\text{dip}}^2/4$ and t_{ext} is chosen, i.e.

$$t_0 \leq p_{\text{T,PS}}^2 \leq \min \left\{ t_{\text{ext}}, \frac{m_{\text{dip}}^2}{4} \right\}. \quad (2.47)$$

Once a branching with $p_{\text{T,PS}}^2$ within the above interval has been generated, a trial value for z_{PS} is obtained initially by requiring that the virtuality of the splitting is lower than the dipole invariant mass, i.e. $Q^2 = \frac{p_{\text{T,PS}}^2}{z_{\text{PS}}(1-z_{\text{PS}})} < m_{\text{dip}}^2$. This restricts z_{PS} within the interval

$$\frac{1}{2} \left(1 - \sqrt{1 - \frac{4p_{\text{T,PS}}^2}{m_{\text{dip}}^2}} \right) \leq z_{\text{PS}} \leq \frac{1}{2} \left(1 + \sqrt{1 - \frac{4p_{\text{T,PS}}^2}{m_{\text{dip}}^2}} \right). \quad (2.48)$$

Nonetheless, a stricter range for z_{PS} arises when looking at the kinematics of the splitting. Indeed, given a pair $(z_{\text{PS}}, p_{\text{T,PS}}^2)$, together with an azimuthal angular variable ϕ_{PS} , the kinematics of the daughter particles can be fully reconstructed in the dipole rest frame, with the radiator aligned to the z axis,

$$\begin{aligned} p_i^\mu &= \left(\sqrt{p_{\perp,ij}^2 + p_{i,z}^2 + m_i^2}, p_{\perp,ij} \cos \phi_{\text{PS}}, p_{\perp,ij} \sin \phi_{\text{PS}}, p_{i,z} \right), \\ p_j^\mu &= \left(\sqrt{p_{\perp,ij}^2 + p_{j,z}^2 + m_j^2}, -p_{\perp,ij} \cos \phi_{\text{PS}}, -p_{\perp,ij} \sin \phi_{\text{PS}}, -p_{i,z} \right), \end{aligned} \quad (2.49)$$

where in our case $m_i = m_j = 0$. An explicit expression for $p_{\perp,ij}^2$ is easily obtained as:

$$p_{\perp,ij}^2 = E_i^2 - p_{i,z}^2 = z_{\text{PS}}^2 E_a^2 - p_{i,z}^2 = \frac{[z_{\text{PS}}(1-z_{\text{PS}})m_{\text{dip}}^2 + p_{\text{T,PS}}^2]^2 - m_{\text{dip}}^2 p_{\text{T,PS}}^2}{[z_{\text{PS}}(1-z_{\text{PS}})m_{\text{dip}}^2 - p_{\text{T,PS}}^2]^2} p_{\text{T,PS}}^2. \quad (2.50)$$

Enforcing the condition $p_{\perp,ij}^2 > 0$ gives

$$\frac{p_{\text{T,PS}}}{m_{\text{dip}}} \leq z_{\text{PS}} \leq 1 - \frac{p_{\text{T,PS}}}{m_{\text{dip}}}, \quad (2.51)$$

which is again consistent with Eq. (2.10) of Ref. [68]. At this point the kinematics of the radiator daughters and the recoiler can be completed by undoing the rotation used to align the radiator–recoiler system to the z axis, and boosting back to the laboratory frame.

2.3 Treatment of top resonances

If an event, of which only the kinematics and the colour configuration of the final-state particles are specified, is passed to PYTHIA8, the shower cannot preserve the invariant mass of possible intermediate resonances, since this information is not provided. When considering QCD showers, a top-quark resonance is highly distorted by additional QCD radiation, unless the shower is instructed to preserve its invariant mass. This can be done at the level of the Les Houches Event (LHE) record [69] providing the details of the resonance-cascade decay (or *resonance history*), which specifies the intermediate resonances the final-state particles originate from.

To preserve the invariant mass of a specified resonance, PYTHIA8 splits the shower evolution in two separate contributions: the shower of the production stage, where the resonance itself, if

charged, can radiate, and the shower of the decay stage, where radiation from its decay products is accounted for. In the Simple-Shower algorithm, *interleaved resonance decays* [70] (see also Ref. [71]) are switched off by default. Then, the two showers are evolved independently from different starting scales to the common shower cut-off scale. The starting scale of the production shower depends on the invariant mass of the dipole the resonance belongs to [as in Eq. (2.47)], while the one of the decay shower is half of the resonance invariant mass. This is substantially different from the case where interleaved resonance decays are included. In this latter case, shower branchings from the production stage compete at each evolution step with the possibility for the resonance to decay. For the rest of this work, we consider the first situation, i.e. the default Simple-Shower behaviour. In order to illustrate the underlying philosophy, we examine how PYTHIA8 would treat an event that is doubly resonant in the top quark, i.e. $e^+e^- \rightarrow \bar{t}^*(\rightarrow \bar{b}W^{+,*})t^*(\rightarrow bW^{-,*})$. This case is general enough to cover all features that have to be included in our construction to fix the matching in the presence of events that are either doubly or singly resonant in the top quark. Indeed, the strategy outlined in Section 2.2 provides a correct matching only for non-resonant events, i.e. when no resonant top histories contribute. By combining all ingredients (as illustrated in Section 2.3.4), our framework becomes sufficiently general to treat the full off-shell process $e^+e^- \rightarrow \bar{b}b + 4f$, where $4f$ stands for the leptonic and/or hadronic decay products of the two W bosons.

The soft-gluon-radiation pattern from the off-shell $\bar{t}t$ pair is treated in PYTHIA8 according to Ref. [72]. We start considering an amplitude \mathcal{M}_{n+1} for the emission of a gluon from off-shell top quarks. In the soft-gluon limit, this amplitude can be written in terms of a Born amplitude \mathcal{M}_n and a soft-gluon current J^μ ,

$$\mathcal{M}_{n+1,a} \sim g_s \mathcal{M}_{n,b} T_{ba}^\lambda (J \cdot \epsilon_\lambda), \quad (2.52)$$

where T^λ is the colour generator associated to the gluon with polarisation vector ϵ_λ^μ , a and b are colour indices in the fundamental representation of SU(3), and g_s is related to α_s via $\alpha_s = g_s^2/(4\pi)$. The product of propagators in \mathcal{M}_{n+1} , arising from the radiation off the top-quark line of momentum p , can be rewritten using partial fractioning as,

$$\frac{1}{[(p+k)^2 - M_t^2]} \frac{1}{(p^2 - M_t^2)} = \frac{1}{(2pk)(p^2 - M_t^2)} - \frac{1}{(2pk)[(p+k)^2 - M_t^2]}, \quad (2.53)$$

where k is the momentum of the radiated gluon and where we have set $M_t^2 = m_t^2 - im_t\Gamma_t$, with m_t and Γ_t the top-quark mass and width, respectively. In doing so, if p_t and $p_{\bar{t}}$ are the top/antitop-quark momenta, and q_b and $q_{\bar{b}}$ the two bottom/antibottom ones, the current J^μ in Eq. (2.52) for the soft-gluon emission can be described as a sum of three contributions,

$$J^\mu = J_{\bar{t}t}^\mu - J_{\bar{t}b}^\mu + J_{\bar{t}\bar{b}}^\mu, \quad (2.54)$$

with [72]

$$\begin{aligned} J_{\bar{t}t}^\mu &= \left(\frac{p_t^\mu}{p_{\bar{t}} \cdot k} - \frac{p_{\bar{t}}^\mu}{p_t \cdot k} \right), \\ J_{\bar{t}b}^\mu &= \left(\frac{q_b^\mu}{q_b \cdot k} - \frac{p_t^\mu}{p_t \cdot k} \right) \frac{p_t^2 - M_t^2}{(p_t + k)^2 - M_t^2}, \\ J_{\bar{t}\bar{b}}^\mu &= \left(\frac{q_{\bar{b}}^\mu}{q_{\bar{b}} \cdot k} - \frac{p_{\bar{t}}^\mu}{p_{\bar{t}} \cdot k} \right) \frac{p_{\bar{t}}^2 - M_t^2}{(p_{\bar{t}} + k)^2 - M_t^2}, \end{aligned} \quad (2.55)$$

where the terms in parenthesis originate from universal tree-level eikonal factorisation with one or two massive emitters. The three currents in Eq. (2.54) can be interpreted as follows. The part of the matrix element containing $J_{\bar{t}t}^\mu$ is the soft-gluon matrix element for on-shell $\bar{t}t$ production,

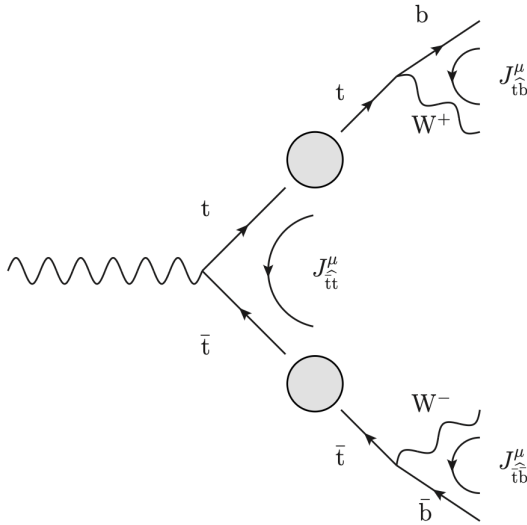


Figure 1. Selection of dipoles done by PYTHIA8 to describe the soft-gluon-radiation pattern from an off-shell $\bar{t}t$ pair. The two blobs separate the squared current $J_{\bar{t}t}^2$, describing gluon radiation from the top/antitop-quark production, and the two squared currents J_{tb}^2 and $J_{\bar{t}\bar{b}}^2$, for radiation from the top/antitop-quark decays.

while those including J_{tb}^μ and $J_{\bar{t}\bar{b}}^\mu$ are the soft-gluon matrix elements for the decays of on-shell t and \bar{t} quarks, respectively (up to the propagator ratios, which account for the off-shellness of the resonances). Since interference contributions are neglected, taking the square of the amplitude in the soft-gluon approximation in Eq. (2.52) allows for the description of the radiation pattern in terms of three building blocks, shown pictorially in Figure 1: a squared current $J_{\bar{t}t}^2$, accounting for corrections to the top/antitop production, and two squared currents J_{tb}^2 and $J_{\bar{t}\bar{b}}^2$, for corrections to their decays.

This approximate description is the one used by PYTHIA8 to model the additional gluon radiation from intermediate top/antitop-quark resonances. This is done preserving their invariant masses $p_t^2/p_{\bar{t}}^2$ on an event-by-event basis. The squared-current term $J_{\bar{t}t}^2$ is obtained in PYTHIA8 with a PS that treats the top/antitop quarks as stable particles with masses $p_t^2/p_{\bar{t}}^2$. The squared currents J_{tb}^2 and $J_{\bar{t}\bar{b}}^2$ correspond to two separate showers, which makes it possible to preserve the top virtualities by definition (the invariant mass of a dipole is always preserved by the Simple-Shower splitting process).

Radiation from the production When the PS includes radiation off top-quark lines, the first gluon emission from $J_{\bar{t}t}^2$ must also be subtracted back in the context of NLO matching. In MC@NLO this must be done introducing an appropriate set of new PS counterterms to prevent double counting. Indeed, a full off-shell NLO calculation already includes real-radiation contributions from off-shell top quarks.

In CS subtraction, dipoles are only constructed using external on-shell particles as emitter, emissus, and spectator. Moreover, the emission of an internal top propagator does not lead to any IR singularity of the real amplitude. This means that these new PS counterterms $\mathcal{C}_{\text{PS}}^{(r')}$ correspond to regions r' not in the set S_{CS} , i.e. $r' \notin S_{\text{CS}}$. The squared current $J_{\bar{t}t}^2$ of our example covers radiation of top propagators in doubly-resonant top topologies. In this case, two new dipoles are needed, one with a top-quark emitter and an antitop-quark spectator ($\widehat{t\bar{t}}$ dipole) and one where the roles are reversed ($\widehat{\bar{t}t}$ dipole).

For singly-resonant topologies, the colour line of the only top/antitop quark present in the event must connect the top/antitop quark itself and an s -channel antibottom/bottom quark. This dipole also corresponds to a region $r' \notin S_{\text{CS}}$, and therefore must be accounted for by two new counter-terms: one with a top/antitop-quark emitter and an antibottom/bottom-quark spectator ($\widehat{\text{tb}}/\widehat{\text{tb}}$ dipoles) and one with a bottom/antibottom-quark emitter and an antitop/top-quark spectator ($\widehat{\text{bt}}/\widehat{\text{bt}}$ dipoles). Note that the last dipole does correspond to a singular region with potentially soft and collinear radiation from a bottom/antibottom quark. In a non-resonance-aware construction as the one presented in Section 2.2, a PS counterterm is used where the bottom/antibottom-quark emitter recoils against the external colour-connected antibottom/bottom quark. However, in the presence of a singly-resonant topology, this is not how the kinematics of the splitting is constructed in PYTHIA8, where the bottom/antibottom-quark emitter recoils against the colour-connected antitop/top quark directly, affecting the kinematics of all its decay products (and not only of its antibottom/bottom quark). Details on the construction of these PS counterterms relevant for the production stage of off-shell top quarks are discussed in Section 2.3.2.

Radiation from the decay An additional issue arises when considering radiation from the decay products of the top quark. As discussed in Refs. [72, 73], the probability of radiating a gluon off the decay, normalised to the LO cross section, is proportional to the sum of two terms (see also Ref. [74] for its treatment in PYTHIA8):

$$\frac{E_g^2}{E_g^2 + \Gamma_t^2} (J_{\text{tb}}^2 + J_{\widehat{\text{tb}}}^2) + \frac{\Gamma_t^2}{E_g^2 + \Gamma_t^2} J_{\widehat{\text{bb}}}^2. \quad (2.56)$$

The first contribution of Eq. (2.56) results from the sum of the two squared currents J_{tb}^2 and $J_{\widehat{\text{tb}}}^2$, introduced above. This term rules the emission pattern whenever the time scale $\tau_g \sim 1/E_g$ for the emission of a soft gluon of energy E_g is much smaller than the top-quark life time $\tau_t \sim 1/\Gamma_t$, meaning that $\tau_t \gg \tau_g$. Indeed, when τ_t is long enough, from the gluon perspective the two bottom quarks are produced at different times and radiate independently.

An opposite situation occurs for the second term in Eq. (2.56), which involves the squared current $J_{\widehat{\text{bb}}}^2$ connecting the two bottom quarks from the top- and antitop-quark decays. This contribution dominates when $\tau_t \lesssim \tau_g$. Here the top-quark life time is very short compared to the gluon-emission time scale and the two bottom quarks are produced nearly instantaneously. In cases where the gluon cannot resolve the top quark, the radiation pattern is similar to the one of a quark–antiquark pair from the decay of a colour singlet. Since, in the case of resonant topologies, the bulk of the radiation comprises gluons such that $E_g \gg \Gamma_t$, the $J_{\widehat{\text{bb}}}^2$ term has only small effects and is thus neglected by PYTHIA8.

Therefore, both for singly- and doubly-resonant topologies, radiation from a bottom/antibottom quark that is part of the decay products of a top/antitop quark is described in PYTHIA8 only by means of the two independent squared currents J_{tb}^2 and $J_{\widehat{\text{tb}}}^2$. Within the splitting process, the recoiling particle cannot be a colour-connected parton in the same dipole, and is therefore chosen by PYTHIA8 to be the W^+/W^- boson. This specific choice of the spectator particle requires to introduce one (two) more PS dipole(s) for a singly-(doubly-)resonant topology to have a proper subtraction of PYTHIA8 first emission. Dipoles with a bottom/antibottom-quark emitter and a W^+/W^- -boson spectator are not part of the list of CS dipoles. We name these $\widehat{\text{bW}}/\widehat{\text{bW}}$ dipoles. The construction of this additional set of dipoles is discussed in Section 2.3.1.

2.3.1 Kinematic mappings for shower decay dipoles

Whenever a bottom/antibottom quark arises from a top/antitop quark, emissions from it are accounted for by PYTHIA8 with a dedicated dipole having a W^+/W^- -boson recoiler (see for instance

Figure 2). As far as the construction of the PS subtraction terms is concerned, these dipoles just differ from the ones discussed in Section 2.2.1 by the kinematics of the splitting, but not by the form of the splitting kernels. Nevertheless, the splitting kinematics plays a crucial role when using the change of variables of Eq. (2.18) that is required to embed the integration of the shower counterterms in the CS-based matching. Since no CS dipole corresponding to the $\widehat{b\bar{W}}$ one exists, one might first try to incorporate the integration of the $\widehat{b\bar{W}}$ counterterm in a CS dipole with the same emitter but a massless bottom/antibottom-quark spectator. For this dipole, we would have a set of radiation variables (z_{CS}, y_{CS}) that must be used to parametrise the shower variables z_{PS} and $p_{T,PS}^2$ of the $\widehat{b\bar{W}}$ dipole. However, a direct calculation shows that the resulting expressions $z_{PS} = z_{PS}(z_{CS}, y_{CS})$ and $p_{T,PS}^2 = p_{T,PS}^2(z_{CS}, y_{CS})$ destroy the correlation between the shower and CS variables, whose importance has already been stressed in Section 2.2.1. This means that for $y_{CS} \rightarrow 0$, one finds $p_{T,PS}^2 \not\rightarrow 0$ and $z_{PS} \not\rightarrow z_{CS}$.

To circumvent this issue, we propose a different definition of PS counterterms with respect to Eq. (2.14), namely:

$$\mathcal{C}_{PS}^{(r',r)} = \mathcal{G}(\Phi'_{rad})\tilde{\mathcal{C}}_{PS}^{(r')}(\Phi'_B, \Phi'_{rad}) + (1 - \mathcal{G}(\Phi_{rad}))\mathcal{C}_{dip}^{(r)}(\Phi_B, \Phi_{rad}). \quad (2.57)$$

In this case, the proper PS counterterm $\tilde{\mathcal{C}}_{PS}^{(r')}$ and the CS correction term $\mathcal{C}_{dip}^{(r)}$ are defined for different CS radiation kinematics constructed with the same emitter–emissus pair, but with different recoilers: a massive one for Φ'_{rad} and a massless (colour-connected to the emitter) one for Φ_{rad} . Even if for a standard-event weight $\Phi_B = \Phi'_B$, Eq. (2.57) also accounts for cases where the underlying-Born kinematics Φ_B and Φ'_B are different, as for hard-event weights.

For a hard event, dipoles are constructed starting from the real kinematics, and both Φ_{rad} and Φ_B are obtained as usual for each of them with a direct CS mapping. If a potential bottom emitter is present, the set of dipoles comprises a dipole r where the massless bottom emitter is colour connected to a massless spectator chosen among the final-state partons of the process. For simple processes with diagonal CKM matrix, the spectator is an antibottom and the dipole a $\widehat{b\bar{b}}$ one. However, whenever this bottom emitter arises from a top resonance, an additional CS dipole r' is added to the list. In this latter case, a massive W boson (reconstructed from the kinematics of its decay products) is used as a spectator, and Φ'_{rad} and Φ'_B are obtained with the CS direct mapping for a massive recoiler [44]. Since this dipole region r' shares the same emitter–emissus pair with the standard dipole r with a massless recoiler, when the pair approaches a singular limit, both $y_{CS} \in \Phi_{rad}$ and $y'_{CS} \in \Phi'_{rad}$ will tend to zero and clearly $\Phi'_B \rightarrow \Phi_B$. The two kinematic regions in Eq. (2.57) are naturally correlated in terms of different CS variables for a hard event. For a standard event, this correlation is enforced by construction, since a set of Born and radiation variables is generated once and used for the evaluation of all terms entering the standard-event cross section.

The remaining step is to determine z_{PS} and $p_{T,PS}^2$ in terms of $\{y_{CS}, z_{CS}\} \in \Phi'_{rad}$. We start from Eq. (5.9) of Ref. [44] for the direct CS mapping. We specialise it to the case of a mapping that brings a massless emitter $p_i^2 = 0$, massless radiated particle (emissus) $p_j^2 = 0$, and massive spectator $p_k^2 = Q_W^2$ into a massless pre-branching emitter $\tilde{p}_i^2 = 0$ and massive pre-branching spectator $\tilde{p}_k^2 = Q_W^2$. Note that Q_W^2 is the invariant mass of the off-shell W boson, which is preserved by the splitting. If we also name the invariant mass of the dipole $m_{b\bar{W}}^2$, our expressions for the direct mapping read,

$$\tilde{p}_k^\mu = r \left(p_k^\mu - \frac{p_k \cdot P}{m_{b\bar{W}}^2} P^\mu \right) + \frac{m_{b\bar{W}}^2 + Q_W^2}{2m_{b\bar{W}}^2} P^\mu, \quad (2.58)$$

$$\tilde{p}_i^\mu = P^\mu - \tilde{p}_k^\mu, \quad (2.59)$$

where

$$P^\mu = \tilde{p}_k^\mu + \tilde{p}_i^\mu = p_i^\mu + p_j^\mu + p_k^\mu, \quad r = \sqrt{\frac{\lambda(m_{\text{bW}}^2, 0, Q_{\text{W}}^2)}{\lambda(m_{\text{bW}}^2, 2p_i \cdot p_j, Q_{\text{W}}^2)}}, \quad (2.60)$$

with the Källén function $\lambda(x, y, z) = x^2 + y^2 + z^2 - 2xy - 2xz - 2yz$. The four-momentum P is the one of the emitter–spectator system having an invariant mass $P^2 = m_{\text{bW}}^2$. The CS radiation variables are constructed as for the standard fully-massless case [see Eq. (2.31)].

To relate the CS parametrisation of the splitting to the shower kinematics, which always increases the multiplicity of an event, we first have to derive formulae for the inverse CS mapping. Looking at the definitions complementary to the ones in Eq. (2.31), namely

$$1 - y_{\text{CS}} = \frac{p_i \cdot p_k + p_j \cdot p_k}{p_i \cdot p_j + p_i \cdot p_k + p_j \cdot p_k} = \frac{2p_i \cdot p_k + 2p_j \cdot p_k}{m_{\text{bW}}^2 - Q_{\text{W}}^2}, \quad 1 - z_{\text{CS}} = \frac{p_j \cdot p_k}{p_i \cdot p_k + p_j \cdot p_k}, \quad (2.61)$$

one immediately obtains an expression for the product $p_j \cdot p_k$ in terms of CS variables, m_{bW}^2 and Q_{W}^2 only,

$$(1 - y_{\text{CS}})(1 - z_{\text{CS}}) = \frac{2p_j \cdot p_k}{m_{\text{bW}}^2 - Q_{\text{W}}^2} \Rightarrow 2p_j \cdot p_k = (m_{\text{bW}}^2 - Q_{\text{W}}^2)(1 - y_{\text{CS}})(1 - z_{\text{CS}}), \quad (2.62)$$

which can be used to express all scalar products needed in the following:

$$2p_i \cdot p_j = (m_{\text{bW}}^2 - Q_{\text{W}}^2)y_{\text{CS}}, \quad (2.63)$$

$$2p_i \cdot p_k = (m_{\text{bW}}^2 - Q_{\text{W}}^2)z_{\text{CS}}(1 - y_{\text{CS}}), \quad (2.64)$$

$$2p_k \cdot P = 2Q_{\text{W}}^2 + (m_{\text{bW}}^2 - Q_{\text{W}}^2)(1 - y_{\text{CS}}), \quad (2.65)$$

$$2p_i \cdot P = (m_{\text{bW}}^2 - Q_{\text{W}}^2)(y_{\text{CS}} + z_{\text{CS}} - y_{\text{CS}}z_{\text{CS}}). \quad (2.66)$$

We parametrise the emitter four-vector p_i first in terms of the post-branching momentum p_k , of P , and of an orthogonal component k_\perp (defined as usual such that $p_k \cdot k_\perp = P \cdot k_\perp = 0$),

$$p_i^\mu = \alpha p_k^\mu + \beta P^\mu + k_\perp^\mu, \quad (2.67)$$

where the unknowns α and β can be derived from the system of equations obtained by contracting Eq. (2.67) with p_k and P :

$$\begin{aligned} p_i \cdot p_k &= \alpha Q_{\text{W}}^2 + \beta p_k \cdot P \\ p_i \cdot P &= \alpha p_k \cdot P + \beta m_{\text{bW}}^2 \end{aligned} \Rightarrow \begin{aligned} \alpha &= \frac{(p_i \cdot P)(p_k \cdot P) - m_{\text{bW}}^2(p_i \cdot p_k)}{(p_k \cdot P)^2 - m_{\text{bW}}^2 Q_{\text{W}}^2} \\ \beta &= \frac{(p_i \cdot p_k)(p_k \cdot P) - Q_{\text{W}}^2(p_i \cdot P)}{(p_k \cdot P)^2 - m_{\text{bW}}^2 Q_{\text{W}}^2}. \end{aligned} \quad (2.68)$$

Using Eqs. (2.63)–(2.66), α and β are fully determined:

$$\alpha = (m_{\text{bW}}^2 - Q_{\text{W}}^2) \frac{(y_{\text{CS}} + z_{\text{CS}} - y_{\text{CS}}z_{\text{CS}})[2Q_{\text{W}}^2 + (m_{\text{bW}}^2 - Q_{\text{W}}^2)(1 - y_{\text{CS}})] - 2m_{\text{bW}}^2 z_{\text{CS}}(1 - y_{\text{CS}})}{[2Q_{\text{W}}^2 + (m_{\text{bW}}^2 - Q_{\text{W}}^2)(1 - y_{\text{CS}})]^2 - 4m_{\text{bW}}^2 Q_{\text{W}}^2}, \quad (2.69)$$

$$\beta = (m_{\text{bW}}^2 - Q_{\text{W}}^2) \frac{[2Q_{\text{W}}^2 + (m_{\text{bW}}^2 - Q_{\text{W}}^2)(1 - y_{\text{CS}})]z_{\text{CS}}(1 - y_{\text{CS}}) - 2Q_{\text{W}}^2(y_{\text{CS}} + z_{\text{CS}} - y_{\text{CS}}z_{\text{CS}})}{[2Q_{\text{W}}^2 + (m_{\text{bW}}^2 - Q_{\text{W}}^2)(1 - y_{\text{CS}})]^2 - 4m_{\text{bW}}^2 Q_{\text{W}}^2}. \quad (2.70)$$

We invert Eq. (2.58),

$$p_k^\mu = \frac{1}{r} \tilde{p}_k^\mu + \underbrace{\left(\frac{2r(p_k \cdot P) - m_{\text{bW}}^2 - Q_{\text{W}}^2}{2r m_{\text{bW}}^2} \right)}_{=\delta} P^\mu, \quad (2.71)$$

where $p_k \cdot P$ can be rewritten using Eq. (2.65), and finally parametrise the real momenta p_i , p_j , and p_k in terms of the pre-branching momenta \tilde{p}_i and \tilde{p}_k starting from Eq. (2.67) and using the definition of P in Eq. (2.60):

$$p_i^\mu = \left(\frac{\alpha}{r} + \alpha \delta + \beta \right) \tilde{p}_k^\mu + \left(\alpha \delta + \beta \right) \tilde{p}_i^\mu + k_\perp^\mu, \quad (2.72)$$

$$p_k^\mu = \left(\frac{2r(p_k \cdot P) + m_{\text{bW}}^2 - Q_{\text{W}}^2}{2r m_{\text{bW}}^2} \right) \tilde{p}_k^\mu + \left(\frac{2r(p_k \cdot P) - m_{\text{bW}}^2 - Q_{\text{W}}^2}{2r m_{\text{bW}}^2} \right) \tilde{p}_i^\mu, \quad (2.73)$$

$$p_j^\mu = P^\mu - p_i^\mu - p_k^\mu. \quad (2.74)$$

Once the expressions for α , β , r , and $p_k \cdot P$ are used, the previous equations provide the inverse mapping in terms of y_{CS} , z_{CS} , m_{bW}^2 , and Q_{W}^2 .

The parametrisation in Eqs. (2.72)–(2.74) can be put into one-to-one correspondence with the one of a PYTHIA8 splitting. Since the latter is usually described in the centre-of-mass frame of the dipole, we choose the four-vectors \tilde{p}_i and \tilde{p}_k as

$$\tilde{p}_i = (\tilde{E}_i, 0, 0, \tilde{E}_i), \quad \tilde{p}_k = \left(\sqrt{Q_{\text{W}}^2 + \tilde{E}_i^2}, 0, 0, -\tilde{E}_i \right), \quad (2.75)$$

where we used $\tilde{p}_i^2 = 0$, $\tilde{p}_k^2 = Q_{\text{W}}^2$, and $\vec{p}_i + \vec{p}_k = \vec{0}$. We obtain \tilde{E}_i from P^2 via

$$m_{\text{bW}}^2 = P^2 = Q_{\text{W}}^2 + 2\tilde{p}_i \cdot \tilde{p}_k = Q_{\text{W}}^2 + 2\tilde{E}_i^2 + 2\tilde{E}_i \sqrt{Q_{\text{W}}^2 + \tilde{E}_i^2} \Rightarrow \tilde{E}_i^2 = \frac{(m_{\text{bW}}^2 - Q_{\text{W}}^2)^2}{4m_{\text{bW}}^2}. \quad (2.76)$$

Compared to Section 2.2.3, the kinematics of the splitting can be adapted by setting $m_{\text{dip}} = m_{\text{bW}}$ and accounting for the non-zero recoiler mass $m_{\text{rec}} = \sqrt{Q_{\text{W}}^2}$. In particular, Eq. (2.33) reads:

$$m_{\text{bW}} = E_a + E_{\text{W}}, \quad E_a^2 = Q^2 + p_{a,z}^2, \quad E_{\text{W}}^2 = p_{\text{W},z}^2 + Q_{\text{W}}^2, \quad (2.77)$$

where we recall that Q^2 denotes the virtuality of the splitting. Going through a similar derivation, one obtains new expressions for E_a and $p_{a,z}$, with an explicit dependence on the new recoiler:

$$E_a = \frac{m_{\text{bW}}^2 + Q^2 - Q_{\text{W}}^2}{2m_{\text{bW}}}, \quad (2.78)$$

$$p_{a,z} = \frac{\sqrt{(m_{\text{bW}}^2 - Q^2 - Q_{\text{W}}^2)^2 - 4Q_{\text{W}}^2 Q^2}}{2m_{\text{bW}}}. \quad (2.79)$$

As for the massless case, we can derive an expression for the virtuality Q^2 in terms of CS variables by equating Eq. (2.79) to the z component of $(p_i + p_j)$ as given in Eqs. (2.72) and (2.74). Again, the longitudinal component of this sum just depends on y_{CS} ,

$$(p_i + p_j)_z = P_z - p_{k,z} \Rightarrow (p_i + p_j)_z = \frac{\tilde{E}_i}{r}, \quad (2.80)$$

where r is a function of y_{CS} only through $p_i \cdot p_j$. If we set $p_{a,z} = (p_i + p_j)_z$, we obtain an equation,

$$\frac{\sqrt{(m_{\text{bW}}^2 - Q^2 - Q_{\text{W}}^2)^2 - 4Q_{\text{W}}^2 Q^2}}{2m_{\text{bW}}} = \frac{\tilde{E}_i}{r}, \quad (2.81)$$

which can be solved for Q^2

$$Q^2 = (m_{\text{bW}}^2 + Q_{\text{W}}^2) \pm \sqrt{4Q_{\text{W}}^2 m_{\text{bW}}^2 + \lambda(m_{\text{bW}}^2, (m_{\text{bW}}^2 - Q_{\text{W}}^2)y_{\text{CS}}, Q_{\text{W}}^2)}. \quad (2.82)$$

We choose the solution with the minus sign, since it allows one to recover the value of the virtuality in the massless-recoiler limit $Q_W^2 \rightarrow 0$:

$$Q^2 = y_{\text{CS}} (m_{\text{bW}}^2 - Q_W^2) \xrightarrow{Q_W^2 \rightarrow 0} m_{\text{bW}}^2 y_{\text{CS}}. \quad (2.83)$$

Following again the derivation in Section 2.2.3, the z component of p_i can be taken from Eq. (2.72) (with \tilde{p}_i and \tilde{p}_k evaluated in the rest frame of the dipole) and equated to the one from the shower parametrisation in Eq. (2.37). Indeed, the latter equation remains valid also in the presence of a massive recoiler, provided that the new expressions for E_a , $p_{a,z}$, and Q are used. Hence, one obtains

$$\frac{2 z_{\text{PS}} E_a^2 - Q^2}{2 p_{a,z}} = \left(\frac{\alpha}{r} + \alpha \delta + \beta \right) (-\tilde{E}_i) + (\alpha \delta + \beta) \tilde{E}_i \Rightarrow z_{\text{PS}} = \frac{z_{\text{CS}} + y_{\text{CS}} - y_{\text{CS}} z_{\text{CS}}}{1 + y_{\text{CS}}}, \quad (2.84)$$

where we recovered Eq. (2.40) for a dipole with massless emitter and a massless spectator. Since Eq. (2.42) still holds, once Q^2 and z_{PS} are known in terms of CS variables, the missing relation $p_{\text{T,PS}}^2 = p_{\text{T,PS}}^2(y_{\text{CS}}, z_{\text{CS}})$ can be found. In the collinear limit, the virtuality Q^2 correctly tends to zero, which ensures $p_{\text{T,PS}}^2 \rightarrow 0$ for $y_{\text{CS}} \rightarrow 0$ as well.

Once all needed relations are known, one can directly compute the Jacobian factor $J_{\text{var}}(z_{\text{CS}}, y_{\text{CS}})$ for the change of integration variables:

$$J_{\text{var}}(z_{\text{CS}}, y_{\text{CS}}) = (m_{\text{bW}}^2 - Q_W^2) \left| \frac{(1 - y_{\text{CS}})(1 - z_{\text{CS}} + y_{\text{CS}} z_{\text{CS}})(y_{\text{CS}} + z_{\text{CS}} - y_{\text{CS}} z_{\text{CS}})}{(1 + y_{\text{CS}})^3} \right|, \quad (2.85)$$

which correctly reproduces Eq. (2.44) in the massless-recoiler limit $Q_W^2 \rightarrow 0$.

The integration ranges of the PS variables in the presence of a massive recoiler also need to be adapted. In PYTHIA8 the range in Eq. (2.47) becomes

$$t_0 \leq p_{\text{T,PS}}^2 \leq \min \left\{ t_{\text{ext}}, \frac{(m_{\text{bW}} - \sqrt{Q_W^2})^2}{4} \right\}. \quad (2.86)$$

As far as z_{PS} is concerned, the first condition on its acceptance range in Eq. (2.48) gets modified as

$$\frac{1}{2} \left(1 - \sqrt{1 - \frac{4 p_{\text{T,PS}}^2}{(m_{\text{bW}} - \sqrt{Q_W^2})^2}} \right) \leq z_{\text{PS}} \leq \frac{1}{2} \left(1 + \sqrt{1 - \frac{4 p_{\text{T,PS}}^2}{(m_{\text{bW}} - \sqrt{Q_W^2})^2}} \right). \quad (2.87)$$

Moreover, the constraint $p_{\perp,ij}^2 > 0$ on the relative transverse momentum of the splitting pair leads to the inequality

$$[z_{\text{PS}} (1 - z_{\text{PS}}) (m_{\text{bW}}^2 - Q_W^2) + p_{\text{T,PS}}^2]^2 - m_{\text{bW}}^2 p_{\text{T,PS}}^2 > 0. \quad (2.88)$$

For the case of a massive recoiler, the integration ranges for z_{CS} and y_{CS} in Eq. (2.26) have a non-trivial form and must be enforced when integrating a standard event. From Ref. [44], one finds

$$0 < y_{\text{CS}} < y_+ = 1 - \frac{2 \sqrt{Q_W^2}}{m_{\text{bW}} + \sqrt{Q_W^2}}, \quad (2.89)$$

so that only the upper integration limit is affected, while the collinear limit $y_{\text{CS}} \rightarrow 0$ remains accessible, as expected. For z_{CS} , one has instead

$$z_- = \frac{1 - v}{2} < z_{\text{CS}} < z_+ = \frac{1 + v}{2}, \quad (2.90)$$

where v is given by

$$v = \frac{\sqrt{[2Q_W^2 + (m_{\text{bW}}^2 - Q_W^2)(1 - y_{\text{CS}})]^2 - 4Q_W^2 m_{\text{bW}}^2}}{(m_{\text{bW}}^2 - Q_W^2)(1 - y_{\text{CS}})}. \quad (2.91)$$

Hence, when $y_{\text{CS}} \rightarrow 0$, both $v \rightarrow 1$ and z_{CS} approach the soft-singular limit $z_{\text{CS}} \rightarrow 0$, since $(z_-, z_+) \rightarrow (0, 1)$. For the integration of the hard event, one needs the correct Jacobian factor J_{CS} to be used in Eq. (2.28). From Ref. [44], one sees that Eq. (2.21) for the massless-recoiler case remains true.

2.3.2 Kinematic mappings for shower production dipoles

Whenever PYTHIA8 reads in an event whose resonance information comprises an intermediate top quark, the selection of the recoiler for a radiating bottom quark arising from the top quark is modified. This must be accounted for by appropriate $\widehat{\text{bW}}/\widehat{\text{bW}}$ dipoles, as discussed above. Moreover, radiation from the top quark is generated by the shower, which gives rise to additional sources of double counting. Either radiation from top quarks is completely switched off in the shower, or new PS counterterms have to be introduced. Even if the first approach removes all double-counting issues, it limits the matching to the decay part of the process, since the shower radiation from the production is entirely disabled. In this section, we illustrate how the remaining counterterms required to reach a complete matching both in the production and the decay can be obtained. In particular, to cover both doubly- and singly-resonant topologies, $\widehat{\text{tt}}/\widehat{\text{tt}}$, $\widehat{\text{tb}}/\widehat{\text{tb}}$, and $\widehat{\text{bt}}/\widehat{\text{bt}}$ dipoles are needed (see examples in Figure 2). To achieve this, we adopt the strategy previously used for the $\widehat{\text{bW}}/\widehat{\text{bW}}$ dipoles. The PS variables are written in terms of CS ones including massive emitters and recoilors (where needed) to allow proper correlations between the shower and the integration variables. Generalised PS counterterms as the one in Eq. (2.57) must be defined. We would like to stress that all counterterms involving a top or antitop quark as radiator need to be introduced with the only purpose of removing double counting, and not to cancel un-subtracted IR singularities. Still, we consider a construction based on variable correlation in the singular limits the natural way of embedding these PS counterterms in our formalism.

As a first step, we summarise how a branching is described in PYTHIA8 when a massive radiator is involved [74]. We consider the general case where a radiator of invariant mass $m_{\text{rad}} \neq 0$ recoils against a spectator of invariant mass $m_{\text{rec}} \neq 0$. Both masses are preserved by the splitting. The definition of the evolution variable $p_{\text{T,PS}}^2$ is formally the same as in Eq. (2.42), i.e. $p_{\text{T,PS}}^2 = z_{\text{PS}}(1 - z_{\text{PS}})Q^2$, but $Q^2 = (m_{\text{rad}}^*)^2 - m_{\text{rad}}^2$, where m_{rad}^* is the virtuality that the radiator acquires in order for the branching to take place. Adjusting the definition of Q^2 to account for the radiator mass makes it possible to catch the correct propagator factor for the branching probability. The z_{PS} variable keeps the same definition of an energy sharing [6], and the splitting kernels $\mathcal{C}_{\text{PS}}^{(r)}$ are still described by the ones with a massless emitter and a massless spectator in Section 2.1.2 [specifically, for a $q \rightarrow qg$ splitting, see Eq. (2.10)]. Since the probability of a branching is computed in PYTHIA8 via the *veto algorithm* [7] applied on the Sudakov form factor $\Delta^{\text{PS}}(p_{\text{T,PS}}^2)$ of Eq. (2.7), for a massive radiator this probability is just corrected by changing the definition of $p_{\text{T,PS}}^2$ as shown above.

We turn to the construction of the kinematics of the branching. First, the splitting of the massive radiator a with four momentum $p_a^\mu = (E_a, \vec{p}_a)$ into a pair of massless particles i and j is considered. If the dipole rest frame (with \vec{p}_a aligned to the z axes) is chosen, one can write

$$\begin{aligned} m_{\text{dip}} &= E_a + E_{\text{rec}}, & E_a^2 &= Q^2 + m_{\text{rad}}^2 + p_{a,z}^2, & E_{\text{rec}}^2 &= p_{a,z}^2 + m_{\text{rec}}^2, \\ p_{z,a} &= p'_{i,z} + p'_{j,z}, & E'_i &= z_{\text{PS}} E_a, & E'_j &= (1 - z_{\text{PS}}) E_a, \\ (E'_i)^2 &= (p'_{i,z})^2 + (p'_{\perp,ij})^2, & (E'_j)^2 &= (p'_{j,z})^2 + (p'_{\perp,ij})^2. \end{aligned} \quad (2.92)$$

From the first line in Eq. (2.92), E_a , E_{rec} , and $p_{z,a}$ can be derived. For our purposes, it is enough to report the expressions of E_a and $p_{z,a}$,

$$E_a = \frac{m_{\text{dip}}^2 + Q^2 + m_{\text{rad}}^2 - m_{\text{rec}}^2}{2m_{\text{dip}}}, \quad (2.93)$$

$$p_{a,z} = \frac{\sqrt{(m_{\text{dip}}^2 - Q^2 - m_{\text{rad}}^2 - m_{\text{rec}}^2)^2 - 4m_{\text{rec}}^2(Q^2 + m_{\text{rad}}^2)}}{2m_{\text{dip}}}. \quad (2.94)$$

Since the last two lines in Eq. (2.92) describe a splitting $a \rightarrow ij$ into massless particles, one can derive expressions for $p'_{i,z}$ and $p'_{j,z}$ as in the case of a massless radiator,

$$p'_{i,z} = \frac{2z_{\text{PS}}E_a^2 - Q^2 - m_{\text{rad}}^2}{2p_{a,z}}, \quad p'_{j,z} = \frac{2(1-z_{\text{PS}})E_a^2 - Q^2 - m_{\text{rad}}^2}{2p_{a,z}}, \quad (2.95)$$

where now $p_{a,z}$ is given by the massive-radiator expression in Eq. (2.94). If a gluon is emitted from an off-shell top quark, i.e. $t_a \rightarrow t_i g_j$, the on-shell condition $(p'_i)^2 = 0$ must be replaced by $(p'_i)^2 = m_{\text{rad}}^2$ in order to restore the correct virtuality of the top quark t_i . For practical reasons, this is done by PYTHIA8 after the branching has been accepted. Indeed, only at this point the nature of the splitting (and thus the daughters of the branching process) is known. Particles i and j are assigned new momenta p_i and p_j defined as (see Ref. [74])

$$p_i = (1 - k_g)p'_i + k_t p'_j, \quad p_j = (1 - k_t)p'_j + k_g p'_i, \quad (2.96)$$

where k_g and k_t can be fixed by enforcing $p_i^2 = m_{\text{rad}}^2$ and $p_j^2 = 0$. This gives $k_g = 0$ and, by noticing that $p_i^2 = 2k_t p'_i \cdot p'_j = k_t(Q^2 + m_{\text{rad}}^2)$, one gets $k_t = m_{\text{rad}}^2/(Q^2 + m_{\text{rad}}^2) < 1$. We can read off from Eq. (2.96) the relevant components for a massive splitting:

$$\begin{aligned} p_{\perp,ij} &= \left(1 - \frac{m_{\text{rad}}^2}{Q^2 + m_{\text{rad}}^2}\right) p'_{\perp,ij}, \\ p_{i,z} &= p'_{i,z} + \frac{m_{\text{rad}}^2}{Q^2 + m_{\text{rad}}^2} p'_{j,z}, \quad p_{j,z} = \left(1 - \frac{m_{\text{rad}}^2}{Q^2 + m_{\text{rad}}^2}\right) p'_{j,z}. \end{aligned} \quad (2.97)$$

Once the kinematics of the splitting has been fully determined, for a massive radiator an additional cut on $p_{\text{T,PS}}^2$ is applied in PYTHIA8 before moving to the next splitting, namely the branching is accepted only if ⁴

$$p_{\text{T,PS}}^2 \cdot \left(1 - \frac{m_{\text{rad}}^2}{Q^2 + m_{\text{rad}}^2}\right)^2 > t_0. \quad (2.98)$$

Before deriving the relations $p_{\text{T,PS}}^2 = p_{\text{T,PS}}^2(z_{\text{CS}}, y_{\text{CS}})$ and $z_{\text{PS}} = z_{\text{PS}}(z_{\text{CS}}, y_{\text{CS}})$ for the different dipoles, a short remark is in order. We notice that z_{PS} is used in PYTHIA8 as an argument of the splitting kernels, meaning that the limit $z_{\text{PS}} \rightarrow 1$ reproduces the soft enhancement of the branching probability. For the massless-radiator case, one sees that, when $z_{\text{PS}} \rightarrow 1$ and $Q^2 \rightarrow 0$, the four-vector components of the emitter particle j vanish as expected, since $E'_j = (1 - z_{\text{PS}})E_a \rightarrow 0$, together with $p_{j,z} \rightarrow 0$ and $p_{\perp,ij} \rightarrow 0$ [see Eqs. (2.37) and (2.50)]. However, for the massive-radiator case, the very same limits only give $E_j \rightarrow 0$, but $p'_{j,z}$ in Eq. (2.95) does not vanish. Only after correcting the branching kinematics in Eq. (2.97), the soft limit can be approached for $Q^2 \rightarrow 0$.

⁴The fact that PYTHIA8 applies a kinematics reduction to the evolution variable as in Eq. (2.98) has been extracted from the code (specifically the release 8.315) by checking the behaviour of the function `bool branch(Event& event, bool isInterleaved)` from the source file `SimpleTimeShower.cc`.

Radiation off the $\widehat{\text{tt}}/\widehat{\text{tt}}$ dipoles As for the case of $\widehat{\text{bW}}/\widehat{\text{bW}}$ dipoles, one can derive explicit expressions for the inverse CS mapping that give the momenta of a massive emitter $p_i^2 = m_{\text{rad}}^2$, a massive spectator $p_k^2 = m_{\text{rec}}^2$, and a massless emissus $p_j^2 = 0$ in terms of the pre-branching momenta of the emitter $\tilde{p}_i^2 = m_{\text{rad}}^2$ and spectator $\tilde{p}_k^2 = m_{\text{rec}}^2$. We set $m_{\text{dip}} = m_{\text{tt}}$. Starting from the direct CS mapping in Eq. (5.9) of Ref. [44],

$$\begin{aligned}\tilde{p}_k^\mu &= r \left(p_k^\mu - \frac{p_k \cdot P}{m_{\text{tt}}^2} P^\mu \right) + \frac{m_{\text{tt}}^2 + m_{\text{rec}}^2 - m_{\text{rad}}^2}{2m_{\text{tt}}^2} P^\mu, \\ \tilde{p}_i^\mu &= P^\mu - \tilde{p}_k^\mu,\end{aligned}\tag{2.99}$$

we obtain the inverse mapping:

$$p_i^\mu = \left(\frac{\alpha}{r} + \alpha \delta + \beta \right) \tilde{p}_k^\mu + (\alpha \delta + \beta) \tilde{p}_i^\mu + k_\perp^\mu,\tag{2.100}$$

$$p_k^\mu = \left(\frac{2r(p_k \cdot P) + m_{\text{tt}}^2 - m_{\text{rec}}^2 + m_{\text{rad}}^2}{2r m_{\text{tt}}^2} \right) \tilde{p}_k^\mu + \left(\frac{2r(p_k \cdot P) - m_{\text{tt}}^2 - m_{\text{rec}}^2 + m_{\text{rad}}^2}{2r m_{\text{tt}}^2} \right) \tilde{p}_i^\mu,\tag{2.101}$$

$$p_j^\mu = P^\mu - p_i^\mu - p_k^\mu,\tag{2.102}$$

where

$$P^\mu = \tilde{p}_k^\mu + \tilde{p}_i^\mu = p_i^\mu + p_j^\mu + p_k^\mu, \quad r = \sqrt{\frac{\lambda(m_{\text{tt}}^2, m_{\text{rad}}^2, m_{\text{rec}}^2)}{\lambda(m_{\text{tt}}^2, m_{\text{rad}}^2 + 2p_i \cdot p_j, m_{\text{rec}}^2)}},\tag{2.103}$$

with

$$2p_i \cdot p_j = (m_{\text{tt}}^2 - m_{\text{rad}}^2 - m_{\text{rec}}^2)y_{\text{CS}}, \quad 2p_k \cdot P = 2m_{\text{rec}}^2 + (m_{\text{tt}}^2 - m_{\text{rec}}^2 - m_{\text{rad}}^2)(1 - y_{\text{CS}}).\tag{2.104}$$

The definitions of the CS variables y_{CS} and z_{CS} are left untouched and can be read off from Eq. (2.31). Expressions for α , β , and δ can be obtained in full generality:

$$\begin{aligned}\alpha &= \frac{(m_{\text{tt}}^2 - m_{\text{rad}}^2 - m_{\text{rec}}^2)[(y_{\text{CS}} + z_{\text{CS}} - y_{\text{CS}}z_{\text{CS}})(2p_k \cdot P) - 2m_{\text{tt}}^2 z_{\text{CS}}(1 - y_{\text{CS}})] + 2m_{\text{rad}}^2(2p_k \cdot P)}{[(2m_{\text{rec}}^2 + (m_{\text{tt}}^2 - m_{\text{rad}}^2 - m_{\text{rec}}^2)(1 - y_{\text{CS}}))^2 - 4m_{\text{tt}}^2 m_{\text{rec}}^2]}, \\ \beta &= \frac{(m_{\text{tt}}^2 - m_{\text{rad}}^2 - m_{\text{rec}}^2)[z_{\text{CS}}(1 - y_{\text{CS}})(2p_k \cdot P) - 2m_{\text{rec}}^2(y_{\text{CS}} + z_{\text{CS}} - y_{\text{CS}}z_{\text{CS}})] - 4m_{\text{rad}}^2 m_{\text{rec}}^2}{[(2m_{\text{rec}}^2 + (m_{\text{tt}}^2 - m_{\text{rad}}^2 - m_{\text{rec}}^2)(1 - y_{\text{CS}}))^2 - 4m_{\text{tt}}^2 m_{\text{rec}}^2]}, \\ \delta &= \frac{(2p_k \cdot P)r - m_{\text{tt}}^2 - m_{\text{rec}}^2 + m_{\text{rad}}^2}{2r m_{\text{tt}}^2}.\end{aligned}\tag{2.105}$$

The CS parametrisation can be related to the shower kinematics by writing the pre-branching momentum formulae for the CS emitter i and spectator k in the dipole rest frame as,

$$\tilde{p}_i = \left(\sqrt{m_{\text{rad}}^2 + \tilde{p}_{i,z}^2}, 0, 0, \tilde{p}_{i,z} \right), \quad \tilde{p}_k = \left(\sqrt{m_{\text{rec}}^2 + \tilde{p}_{k,z}^2}, 0, 0, -\tilde{p}_{k,z} \right),\tag{2.106}$$

where we have set $\tilde{p}_i^2 = m_{\text{rad}}^2$ and $\tilde{p}_k^2 = m_{\text{rec}}^2$. Since the dipole mass m_{tt} is an input parameter, we can extract $\tilde{p}_{i,z}$ from the equality $m_{\text{tt}}^2 = (\tilde{p}_i + \tilde{p}_k)^2$, which leads to

$$\tilde{p}_{i,z} = \frac{\sqrt{(m_{\text{tt}}^2 - m_{\text{rec}}^2 - m_{\text{rad}}^2)^2 - 4m_{\text{rec}}^2 m_{\text{rad}}^2}}{2m_{\text{tt}}}.\tag{2.107}$$

We derive an expression for the shower virtuality in terms of y_{CS} and z_{CS} by solving the equation $p_{a,z} = (p_i + p_j)_z$, with the left-hand side taken from Eq. (2.94) and the right-hand side from the CS parametrisation in Eq. (2.100), leading to

$$(Q^2 + m_{\text{rad}}^2)^2 - 2(m_{\text{tt}}^2 + m_{\text{rec}}^2)(Q^2 + m_{\text{rad}}^2) + (m_{\text{tt}}^2 - m_{\text{rec}}^2)^2 - 4m_{\text{tt}}^2 \frac{p_{i,z}^2}{r^2} = 0,\tag{2.108}$$

which gives

$$Q^2 = y_{\text{CS}} (m_{\text{tt}}^2 - m_{\text{rec}}^2 - m_{\text{rad}}^2). \quad (2.109)$$

Between the two solutions of the quadratic equation in Q^2 , we have chosen the one ensuring the correct correlation in the quasi-collinear limit for a massive radiator. Such limit (see for instance Ref. [44]) corresponds to the case where the magnitude of the transverse component k_{\perp}^{μ} in Eq. (2.100) [and implicitly in Eq. (2.102)] becomes comparable to the masses of the problem. It can be parametrised by λ after performing a uniform positive rescaling $\{\lambda k_{\perp}^{\mu}, \lambda m_{\text{tt}}, \lambda m_{\text{rec}}, \lambda m_{\text{rad}}\}$ and sending $\lambda \rightarrow 0$. This limit corresponds to $y_{\text{CS}} \rightarrow 0$ and thus to $Q^2 \rightarrow 0$ because of Eq. (2.109). Moreover, the collinear limit is restored for $m_{\text{rad}} \rightarrow 0$, where Eq. (2.109) matches Eq. (2.83).

To express z_{PS} in terms of z_{CS} and y_{CS} , one might follow the procedure used for dipoles with massless radiators. This, however, exposes a subtlety in the link between z_{PS} and the soft limit as discussed below Eq. (2.98).⁵ Using $p_{j,z}$ as a starting point to correlate z_{PS} to CS variables does not lead to a correct result. This originates from the shower definition of z_{PS} . Setting $z_{\text{PS}} \rightarrow 1$ is in general not related to the kinematic limit where all components of the emitted momentum tend to zero, i.e. $p_j^{\mu} \rightarrow 0$. The only exception is the energy component, since z_{PS} is defined as an energy share. Therefore, even if for a massless-radiator case no restriction applies, for a dipole with a massive radiator a correlated expression for $z_{\text{PS}} = z_{\text{PS}}(z_{\text{CS}}, y_{\text{CS}})$ must be extracted from the energy components of the radiator daughters.

Therefore, we repeat our derivation using E_i . In terms of shower variables, before enforcing the correct masses via Eq. (2.96), the energy component of the radiating top quark is simply $E_i' = z_{\text{PS}} E_a$, while we can obtain the equivalent CS parametrisation from Eq. (2.100) (note that $k_{\perp}^0 = 0$). We just need to derive a closed-form expression for $\tilde{E}_i = \tilde{p}_i^0$ and $\tilde{E}_k = \tilde{p}_k^0$. We first observe that $\tilde{E}_i + \tilde{E}_k = m_{\text{tt}}$. Moreover, from the conditions $\tilde{E}_i^2 - \tilde{p}_{i,z}^2 = m_{\text{rad}}^2$ and $\tilde{E}_k^2 - \tilde{p}_{k,z}^2 = m_{\text{rec}}^2$, we obtain $\tilde{E}_i^2 - \tilde{E}_k^2 = m_{\text{rad}}^2 - m_{\text{rec}}^2$, which, together with the previous constraint on the energy sum, allows us to write

$$\tilde{E}_i = \frac{m_{\text{tt}}^2 - m_{\text{rec}}^2 + m_{\text{rad}}^2}{2m_{\text{tt}}}, \quad \tilde{E}_k = \frac{m_{\text{tt}}^2 + m_{\text{rec}}^2 - m_{\text{rad}}^2}{2m_{\text{tt}}}. \quad (2.110)$$

By equating the two parametrisations of E_i , we finally obtain an expression for z_{PS} , which can be simplified to

$$\begin{aligned} z_{\text{PS}} &= \left(\frac{\alpha}{r} + \alpha\delta + \beta \right) \frac{\tilde{E}_k}{E_a} + (\alpha\delta + \beta) \frac{\tilde{E}_i}{E_a} \\ &= \frac{(m_{\text{tt}}^2 - m_{\text{rec}}^2)[y_{\text{CS}}(1 - z_{\text{CS}}) + z_{\text{CS}}] + m_{\text{rad}}^2(2 - y_{\text{CS}} - z_{\text{CS}} + y_{\text{CS}}z_{\text{CS}})}{m_{\text{rad}}^2(1 - y_{\text{CS}}) + (m_{\text{tt}}^2 - m_{\text{rec}}^2)(1 + y_{\text{CS}})}. \end{aligned} \quad (2.111)$$

It is straightforward to show that $z_{\text{PS}} \rightarrow 1$ in the soft limit. Had we begun our calculation with the expression for E_i following the kinematical adjustments in Eq. (2.96), we would have had to use

$$E_i = \left(z_{\text{PS}}^* + \frac{m_{\text{rad}}^2}{Q^2 + m_{\text{rad}}^2} (1 - z_{\text{PS}}^*) \right) E_a, \quad (2.112)$$

where z_{PS}^* is the reinterpretation of the shower variable z_{PS} after enforcing the on-shell conditions for particles i and j . In the limits $z_{\text{CS}} \rightarrow 1$ and $y_{\text{CS}} \rightarrow 0$, one still gets

$$z_{\text{PS}}^* = \frac{(Q^2 + m_{\text{rad}}^2)z_{\text{CS}} - m_{\text{rad}}^2}{Q^2} \stackrel{y_{\text{CS}} \rightarrow 0}{\approx} 1. \quad (2.113)$$

⁵Indeed, taking the longitudinal component of Eq. (2.102), i.e. $p_{j,z}$, from the CS parametrisation, and equating it to its shower correspondence in Eq. (2.95), one obtains an equation that can be solved for z_{PS} , but that does not reproduce the desired correlation in the soft limit, meaning that $(y_{\text{CS}}, z_{\text{CS}}) \rightarrow (0, 1)$ does not lead to $z_{\text{PS}} \rightarrow 1$.

Even though both z_{PS} and z_{PS}^* can be correlated to z_{CS} , the correct relation to be used is Eq. (2.111) rather than Eq. (2.113). Indeed, PYTHIA8 generates a branching by sampling $p_{\text{T,PS}}^2$ and z_{PS} . Only after the splitting has occurred, the massless momenta (p'_i, p'_j) are mapped to the correct ones (p_i, p_j) where z_{PS}^* enters.

Now that all ingredients are available, we can evaluate the Jacobian factor J_{var} using expressions for $p_{\text{T,PS}}^2$ [with Q^2 as in Eq. (2.109)] and z_{PS} from Eq. (2.111), which gives

$$J_{\text{var}}(z_{\text{CS}}, y_{\text{CS}}) = \left| \frac{(1 - y_{\text{CS}})(1 - z_{\text{CS}} + y_{\text{CS}}z_{\text{CS}})(m_{\text{tt}}^2 - m_{\text{rad}}^2 - m_{\text{rec}}^2)^3}{\left[2m_{\text{rad}}^2 + (1 + y_{\text{CS}})(m_{\text{tt}}^2 - m_{\text{rad}}^2 - m_{\text{rec}}^2)\right]^3} \right. \\ \left. \times \left[2m_{\text{rad}}^2 + (m_{\text{tt}}^2 - m_{\text{rec}}^2 - m_{\text{rad}}^2)(y_{\text{CS}} + z_{\text{CS}} - y_{\text{CS}}z_{\text{CS}})\right] \right|. \quad (2.114)$$

The reshuffling of the post-branching kinematics in Eqs. (2.96) and (2.97) does not affect the integration ranges of the PS variables. The only way the kinematical suppression due to a massive radiator enters is via the last requirement in Eq. (2.98), which modifies the available phase space for the evolution variable $p_{\text{T,PS}}^2$ as

$$\frac{t_0}{\left(1 - \frac{m_{\text{rad}}^2}{m_{\text{rad}}^2 + Q^2}\right)^2} \leq p_{\text{T,PS}}^2 \leq \min\left\{t_{\text{ext}}, \frac{(m_{\text{tt}} - m_{\text{rec}})^2 - m_{\text{rad}}^2}{4}\right\}. \quad (2.115)$$

The first acceptance range for z_{PS} in Eqs. (2.48) and (2.87) generalises to

$$\frac{1}{2}\left(1 - \sqrt{1 - \frac{4p_{\text{T,PS}}^2}{(m_{\text{tt}} - m_{\text{rec}})^2 - m_{\text{rad}}^2}}\right) \leq z_{\text{PS}} \leq \frac{1}{2}\left(1 + \sqrt{1 - \frac{4p_{\text{T,PS}}^2}{(m_{\text{tt}} - m_{\text{rec}})^2 - m_{\text{rad}}^2}}\right), \quad (2.116)$$

while the positivity condition on the relative transverse momentum of the splitting pair $p_{\perp,ij}^2$ gives a more involved quadratic equation for z_{PS}

$$[z_{\text{PS}}(1 - z_{\text{PS}})(m_{\text{tt}}^2 - m_{\text{rec}}^2 + m_{\text{rad}}^2) + p_{\text{T,PS}}^2]^2 - z_{\text{PS}}(1 - z_{\text{PS}})m_{\text{tt}}^2 m_{\text{rad}}^2 - m_{\text{tt}}^2 p_{\text{T,PS}}^2 > 0. \quad (2.117)$$

For a standard event, the correct ranges for the CS variables in Eq. (2.26) must be set,

$$0 < y_{\text{CS}} < y_+ = 1 - \frac{2m_{\text{rec}}(m_{\text{tt}} - m_{\text{rec}})}{m_{\text{tt}}^2 - m_{\text{rad}}^2 - m_{\text{rec}}^2}, \quad (2.118)$$

$$z_- = q(1 - v) < z_{\text{CS}} < z_+ = q(1 + v), \quad (2.119)$$

where

$$q = \frac{2m_{\text{rad}}^2 + (m_{\text{tt}}^2 - m_{\text{rad}}^2 - m_{\text{rec}}^2)y_{\text{CS}}}{2[m_{\text{rad}}^2 + (m_{\text{tt}}^2 - m_{\text{rad}}^2 - m_{\text{rec}}^2)y_{\text{CS}}]}, \quad (2.120)$$

$$v = \frac{\sqrt{[2m_{\text{rec}}^2 + (m_{\text{tt}}^2 - m_{\text{rad}}^2 - m_{\text{rec}}^2)(1 - y_{\text{CS}})]^2 - 4m_{\text{rec}}^2 m_{\text{tt}}^2}}{(m_{\text{tt}}^2 - m_{\text{rad}}^2 - m_{\text{rec}}^2)y_{\text{CS}} + 2m_{\text{rad}}^2} \frac{y_{\text{CS}}}{1 - y_{\text{CS}}}. \quad (2.121)$$

Enforcing these conditions in the integration of the counterterms for the standard events is crucial to match the same integration as for a hard event, where such ranges are automatically respected by the inverse CS mapping.

A final remark to properly embed PS counterterms with massive emitter–spectator pair in a hard event concerns Eq. (2.28). Our factorised parametrisation $(\Phi_{\text{B}}, \Phi_{\text{rad}})$ of the real phase space Φ_{R} relies on the CS mapping with a massive emitter and a massive spectator, being the only one which can correlate $(z_{\text{CS}}, y_{\text{CS}})$ to $(z_{\text{PS}}, p_{\text{T,PS}}^2)$. Therefore, in Eq. (2.28) one has to replace the

expression of J_{CS} given in Eq. (2.21) (relying on a CS parameterisation with a massless emitter) entering c_J with,

$$J_{\text{CS}} = \frac{2\tilde{p}_i \cdot \tilde{p}_k (1 - y_{\text{CS}})}{16\pi^2} \frac{m_{\text{tt}}^2 - m_{\text{rad}}^2 - m_{\text{rec}}^2}{2\pi \sqrt{\lambda(m_{\text{tt}}^2, m_{\text{rad}}^2, m_{\text{rec}}^2)}}. \quad (2.122)$$

Radiation off the $\widehat{\text{tb}}/\widehat{\text{tb}}$ dipoles For singly-resonant topologies, configurations where a massive top/antitop-quark radiator is directly colour connected to a massless antibottom/bottom quark appear. In this case, the antibottom/bottom quark is in charge of absorbing the recoil of the splitting. Formulae for these dipoles can be directly derived from the ones of the $\widehat{\text{tt}}$ dipole, i.e. Eqs. (2.99)–(2.117) by simply replacing $m_{\text{tt}} \mapsto m_{\text{tb}}$ and $m_{\text{rec}} \mapsto m_{\text{b}} = 0$, with m_{tb} the new dipole mass.

We see that, as long as the recoiler mass vanishes, the CS integration boundaries for y_{CS} boil down to the ones for a dipole with massless emitter and a massless spectator, so that one simply has

$$0 < y_{\text{CS}} < y_+ = 1, \quad (2.123)$$

while for z_{CS} the expressions for q and v in Eq. (2.119) read

$$q = \frac{2m_{\text{rad}}^2 + (m_{\text{tb}}^2 - m_{\text{rad}}^2)y_{\text{CS}}}{2[m_{\text{rad}}^2 + (m_{\text{tb}}^2 - m_{\text{rad}}^2)y_{\text{CS}}]}, \quad v = \frac{(m_{\text{tb}}^2 - m_{\text{rad}}^2)y_{\text{CS}}}{(m_{\text{tb}}^2 - m_{\text{rad}}^2)y_{\text{CS}} + 2m_{\text{rad}}^2}. \quad (2.124)$$

Radiation off the $\widehat{\text{bt}}/\widehat{\text{bt}}$ dipoles For singly-resonant topologies, the $\widehat{\text{tb}}/\widehat{\text{tb}}$ dipoles are always accompanied by $\widehat{\text{bt}}/\widehat{\text{bt}}$ ones, which describe the reversed situation where a radiating bottom/antibottom quark recoils against a massive top/antitop quark. Analytic expressions for this dipoles are identical to the ones derived for the $\widehat{\text{bW}}/\widehat{\text{bW}}$ dipoles, i.e. Eqs. (2.58)–(2.91), upon replacing $\sqrt{Q_{\text{W}}^2} \mapsto m_{\text{rec}}$ and $m_{\text{bW}} \mapsto m_{\text{bt}}$, with m_{bt} the corresponding dipole mass.

2.3.3 Decay phase space of a massive emitter/spectator particle

When evaluating the PS subtraction terms for the hard event in Eq. (2.28), the underlying-Born phase space is constructed from the direct CS mappings for each dipole. When we consider decay or production dipoles (see Sections 2.3.1 and 2.3.2), the kinematic mappings do not provide a prescription to construct the momenta of the decay products of the massive recoiler and/or emitter. Nonetheless, we show in this section that a natural prescription for this arises from the factorisation of the real phase space. For illustrative purpose, we examine the case where only one emitter or one spectator is massive, and we name its momentum p_{M} . Our conclusions also hold when both the emitter and the spectator are massive, as in the $\widehat{\text{tt}}/\widehat{\text{tt}}$ dipoles.

We consider a real process involving $n + 1$ final-state particles in the set \mathcal{F} (labelled by indices running from 1 to $n + 1$). We introduce the four-vector Q_{in}^μ given by the sum of the incoming momenta. Since the massive particle entering the CS mapping can either be a W boson or a top quark, two or three particles can be attributed to its decay products, respectively. Therefore, to keep the discussion general, we consider a massive particle decaying into a set of d particles $\mathcal{D} \subset \mathcal{F}$

labelled by indices running from $n-d+2$ to $n+1$. We rewrite the real phase-space measure Φ_{R} as

$$\begin{aligned}
d\Phi_{\text{R}} &= \prod_{r=1}^{n+1} \left[\frac{d^D p_r}{(2\pi)^{D-1}} \delta_+(p_r^2) \right] (2\pi)^D \delta^{(D)} \left(\sum_{l=1}^{n+1} p_l - Q_{\text{in}} \right) \\
&= \prod_{r=1}^{n-d+1} \left[\frac{d^D p_r}{(2\pi)^{D-1}} \delta_+(p_r^2) \right] \prod_{s=n-d+2}^{n+1} \left[\frac{d^D p_s}{(2\pi)^{D-1}} \delta_+(p_s^2) \right] (2\pi)^D \delta^{(D)} \left(\sum_{l=1}^{n+1} p_l - Q_{\text{in}} \right) \\
&= \prod_{r=1}^{n-d+1} \left[\frac{d^D p_r}{(2\pi)^{D-1}} \delta_+(p_r^2) \right] \underbrace{\left[\frac{d Q_{\text{M}}^2}{2\pi} \frac{d^D p_{\text{M}}}{(2\pi)^{D-1}} \delta_+(p_{\text{M}}^2 - Q_{\text{M}}^2) (2\pi)^D \delta^{(D)} \left(p_{\text{M}} - \sum_{s=n-d+2}^{n+1} p_s \right) \right]}_{=1} \\
&\quad \times \prod_{s=n-d+2}^{n+1} \left[\frac{d^D p_s}{(2\pi)^{D-1}} \delta_+(p_s^2) \right] (2\pi)^D \delta^{(D)} \left(\sum_{l=1}^{n-d+1} p_l + p_{\text{M}} - Q_{\text{in}} \right), \tag{2.125}
\end{aligned}$$

where in the last step we exploited the definition of the Dirac δ function upon integration over p_{M} in D dimensions and over its invariant mass Q_{M}^2 . We rearrange the terms in the previous expression and introduce one more δ -function term that evaluates to one after integration over a four-vector P^μ , defined such that $P^2 = m_{\text{dip}}^2$. Hence, one obtains

$$\begin{aligned}
d\Phi_{\text{R}} &= \prod_{r=1}^{n-d-1} \left[\frac{d^D p_r}{(2\pi)^{D-1}} \delta_+(p_r^2) \right] (2\pi)^D \delta^{(D)} \left(\sum_{l=1}^{n-d-1} p_l + p_i + p_j + p_{\text{M}} - Q_{\text{in}} \right) \frac{d^D P}{(2\pi)^{D-1}} \\
&\quad \times d\phi(p_i, p_j, p_{\text{M}}; P) (2\pi)^D \delta^{(D)} \left(p_{\text{M}} - \sum_{s=n-d+2}^{n+1} p_s \right) \prod_{s=n-d+2}^{n+1} \left[\frac{d^D p_s}{(2\pi)^{D-1}} \delta_+(p_s^2) \right], \tag{2.126}
\end{aligned}$$

with the three-particle phase space

$$\begin{aligned}
d\phi(p_i, p_j, p_{\text{M}}; P) &= (2\pi)^D \delta^{(D)}(p_i + p_j + p_{\text{M}} - P) \\
&\quad \times \frac{d Q_{\text{M}}^2}{2\pi} \frac{d^D p_{\text{M}}}{(2\pi)^{D-1}} \delta_+(p_{\text{M}}^2 - Q_{\text{M}}^2) \frac{d^D p_i}{(2\pi)^{D-1}} \delta_+(p_i^2) \frac{d^D p_j}{(2\pi)^{D-1}} \delta_+(p_j^2) \tag{2.127}
\end{aligned}$$

defined by the emitter/spectator $i = n-d$, emissus $j = n-d+1$, and the massive spectator/emitter M. The direct CS mapping acts on this phase-space volume leading to the known factorisation formula into a two-particle phase space defined by the projected momenta \tilde{p}_i and \tilde{p}_{M} , and the three-dimensional phase space of the radiation kinematics $d\Phi_{\text{rad}}$, which reads

$$d\phi(p_i, p_j, p_{\text{M}}; P) = d\phi(\tilde{p}_i, \tilde{p}_{\text{M}}; P) d\Phi_{\text{rad}}. \tag{2.128}$$

Since $d\phi(\tilde{p}_i, \tilde{p}_{\text{M}}; P)$ contains a Dirac δ function with support on $\tilde{p}_i^\mu + \tilde{p}_{\text{M}}^\mu = P^\mu$, we can plug the factorised phase-space expression above into Eq. (2.126) and get rid of the P^μ integration. Additionally, we combine the phase-space volume $d\phi(\tilde{p}_i, \tilde{p}_{\text{M}}; P)$ with the first line of the same equation to define the phase space $\tilde{\Phi}_{\text{B,M}}$. The latter is given by the $n-d+1$ particle phase space defined by the massive spectator/emitter particle of momentum \tilde{p}_{M}^μ , the massless emitter/spectator particle of mapped momentum \tilde{p}_i , and the set of particles whose momenta are not affected by the CS mapping, $\mathcal{F} - D - \{i, j, k\}$, i.e. particles not chosen among the emitter–emissus–spectator triplet and the decay products of the massive particle. This gives:

$$d\Phi_{\text{R}} = d\tilde{\Phi}_{\text{B,M}} d\Phi_{\text{rad}} (2\pi)^D \delta^{(D)} \left(p_{\text{M}} - \sum_{s=n-d+2}^{n+1} p_s \right) \prod_{s=n-d+2}^{n+1} \left[\frac{d^D p_s}{(2\pi)^{D-1}} \delta_+(p_s^2) \right]. \tag{2.129}$$

We turn to the last part of the previous equation, involving the decay products of the massive spectator/emitter. Since in $d\tilde{\Phi}_{\text{B,M}}$ an integration over the projected momentum \tilde{p}_{M}^μ appears, we

write also the remaining part of the $d\Phi_{\text{R}}$ in terms of this momentum. Though the CS mapping guarantees that $\tilde{p}_{\text{M}}^2 = p_{\text{M}}^2 = Q_{\text{M}}^2$, one has $p_{\text{M}}^\mu \neq \tilde{p}_{\text{M}}^\mu$ away from the soft/collinear limits. Therefore, we define the Lorentz boost Λ_{M} such that $\tilde{p}_{\text{M}}^\mu = (\Lambda_{\text{M}})^\mu{}_\nu p_{\text{M}}^\nu$. Using the property of the Dirac δ function under a change of variables, and given that for a proper Lorentz transformation $\det(\Lambda_{\text{M}}) = 1$ holds, we arrive at

$$d\Phi_{\text{R}} = \underbrace{d\tilde{\Phi}_{\text{B,M}} (2\pi)^D \delta^{(D)}\left(\tilde{p}_{\text{M}} - \sum_{s=n-d+2}^{n+1} \tilde{p}_s\right) \prod_{s=n-d+2}^{n+1} \left[\frac{d^D \tilde{p}_s}{(2\pi)^{D-1}} \delta_+(\tilde{p}_s^2)\right]}_{d\tilde{\Phi}_{\text{B}}} d\Phi_{\text{rad}}, \quad (2.130)$$

where we have defined the mapped momenta arising from the massive-particle decay as $\{\tilde{p}_s\}_{s=n-d+2}^{n+1} = \{\Lambda_{\text{M}} \cdot p_s\}_{s=n-d+2}^{n+1}$. These momenta are the ones that enter the underlying-Born phase space $\tilde{\Phi}_{\text{B}}$, appropriately defined in terms of final-state particles.

One can define an inverse mapping from a Born to a real phase space that connects the set of Born momenta associated to the internal massive resonance to a set of real momenta after the resonance momentum has been modified by the splitting process. Then, the inverse of the above construction can be used to define the momenta $\{p_s\}_{s=n-d+2}^{n+1} = \{\Lambda_{\text{M}}^{-1} \cdot \tilde{p}_s\}_{s=n-d+2}^{n+1}$. Note that this is how PYTHIA8 adjusts the momenta of the decay products (when read from a LHE file) of the massive resonance participating to the branching as an emitter or spectator.

2.3.4 Selection of resonance histories

So far we have seen that in a resonance-aware MC@NLO matching special care must be taken to remove double counting. We have shown in previous sections that, depending on whether an event is *labelled* as doubly, singly, or non-resonant in the top/antitop quark, and as soon as this information is passed to PYTHIA8, different subsets of PS counterterms [like the ones in Eq. (2.57)] must be used. At this point, two interleaved problems arise:

- (a) The definition of an event as resonant is subject to some degree of arbitrariness (see for instance the discussion in Ref. [53], in particular Section 2.2). Therefore, there is no unique way to classify a kinematic configuration as resonant on an event-by-event basis, such that PYTHIA8 is instructed to preserve the invariant mass of a set of momenta originating from a potential intermediate resonance.
- (b) Despite the freedom in the definition of a resonant event, the selection of a resonant configuration must not spoil the MC@NLO construction that is designed to prevent double counting. This is usually true, unless the definition of the shower counterterms is connected to the resonant configuration of the event itself, like for the decay and production dipoles of Sections 2.3.1 and 2.3.2.

The second problem is related to the cancellation discussed in Section 2.1.1 occurring between the hard and the standard events after the shower action [see Eqs. (2.8) and (2.9)]. Let us assume that standard events with Born kinematics are labelled as doubly resonant in the $t\bar{t}$ pair $n_{\bar{t}t}$ percent of the time inside a LHE file. For these events, PYTHIA8 distributes the recoil of the radiation from the top/antitop quark and from its decay products differently than if a non-resonant or singly-resonant topology was read in. When we consider the integration of the standard-event cross section, this fraction $n_{\bar{t}t}$ must be consistently related to a weight $f_{\text{res}}^{t\bar{t}}$ multiplying the PS counterterms associated to a doubly-resonant topology. To get a proper cancellation of spurious $\mathcal{O}(\alpha_s)$ terms, these PS counterterms must come with the very same weight $f_{\text{res}}^{t\bar{t}}$ also when the integration is performed for the hard cross section. However, since the standard and hard contributions are integrated separately, this task is non-trivial. For a hard event, the resonance information of a

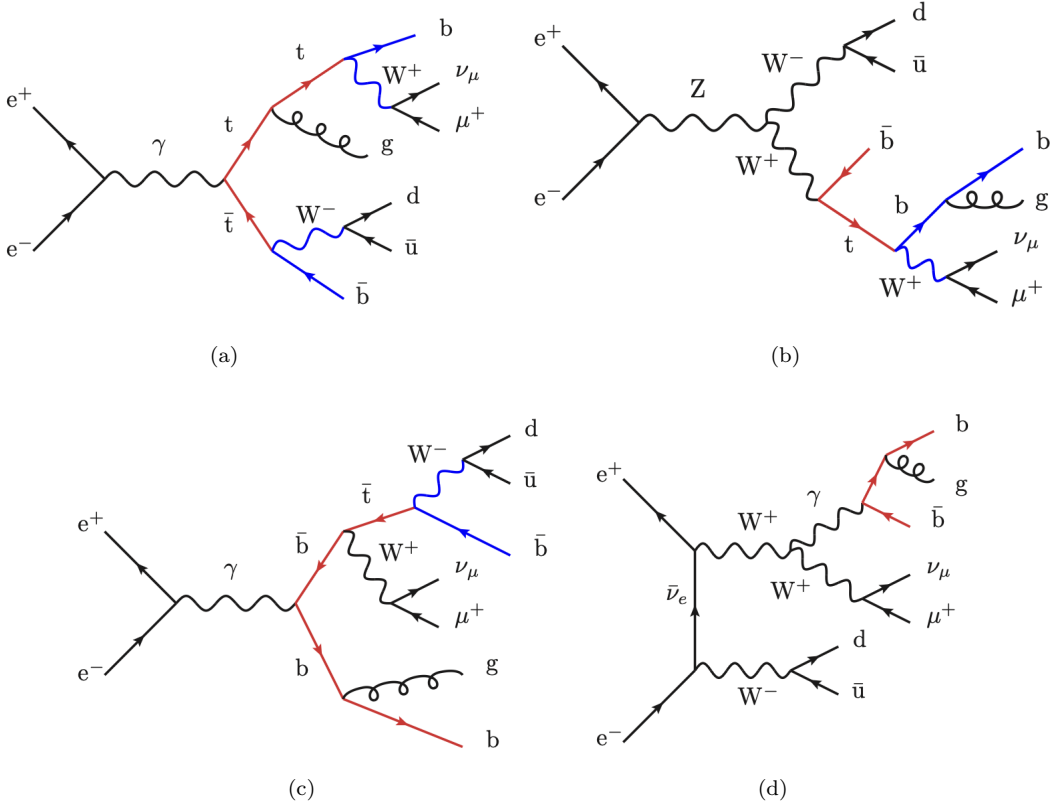


Figure 2. Representative Feynman diagrams for each of the four resonance histories considered for the process $e^+e^- \rightarrow \mu^+\nu_\mu jj_jb$. Specifically, we show a doubly-resonant topology in the top and antitop quark [2(a)], a singly-resonant topology in the top quark [2(b)], a singly-resonant topology in the antitop quark [2(c)], and a non-resonant topology in the top and antitop quark [2(d)]. Red and blue fermion lines mark shower production and decay dipoles, respectively, that are active in the presence of either a bottom- or an antibottom-quark emitter.

LHE affects how PYTHIA8 generates radiation at $\mathcal{O}(\alpha_s^2)$ relative to the Born process, so beyond NLO accuracy. Moreover, the fraction of times an event with real kinematics is classified as doubly resonant in the $\bar{t}t$ pair, namely $\bar{n}_{\bar{t}t}$, does not match in general the fraction of doubly-resonant Born-like events, meaning that $\bar{n}_{\bar{t}t} \neq n_{\bar{t}t}$. Therefore, a criterion based on the underlying-Born kinematics must be used to determine the weight $f_{\text{res}}^{t\bar{t}}$ for the hard contribution.

If the process of interest has at most N_{res} resonances, a set $\mathcal{S}_{\text{R,B}}$ of $2^{N_{\text{res}}}$ resonance histories can be defined, obtained by switching on and off each resonance independently. In this set $\mathcal{S}_{\text{R,B}}$, there are $\binom{N_{\text{res}}}{k}$ k -resonant histories, such that $\sum_{k=0}^{N_{\text{res}}} \binom{N_{\text{res}}}{k} = 2^{N_{\text{res}}}$. To be more concrete and for ease of notation, we specialise our discussion to processes whose final state comprises only one bottom and one antibottom quark, and that can be at most doubly resonant in a $\bar{t}t$ pair, so that $N_{\text{res}} = 2$. The formalism described in this section can be easily extended to more general cases. Moreover, dealing with the specific case mentioned above helps us making contact with the process $e^+e^- \rightarrow \mu^+\nu_\mu jj_jb$, for which we are presenting explicit results in Section 4. In Figure 2 we report some representative Feynman diagrams for each of the four resonance histories. Shower production and decay dipoles, which are used by PYTHIA8 whenever either a bottom- or an antibottom-quark emitter is present, are marked in red and blue, respectively.

Consider the construction of a dipole where a bottom quark is an emitter (a similar discussion

holds for an antibottom-quark emitter). Two scenarios are possible, where either the bottom quark arises from a resonant top quark or not. Within these two situations, additional subcases appear, which require dedicated choices of PS counterterms.

- The bottom-quark emitter originates from a resonant top quark.
 - If this top quark is colour-connected to a resonant antitop quark, PS counterterms accounting for radiation from the top quark itself (production stage) and from the bottom quark (decay stage) must be included by means of a $\widehat{t\bar{t}}$ and a $\widehat{b\bar{W}}$ dipole, respectively. For our case of interest, this situation appears for doubly-resonant $\bar{t}t$ topologies [see Figure 2(a)]. Note that both the production and the decay contributions must be corrected by PS subtraction counterterms. Indeed, by default PYTHIA8 showers the production and the decay part of the process independently [70] using two non-interleaved parton showers with two different starting scales (which guarantees that the invariant mass of the top-quark resonance is preserved).
 - If this top quark is colour-connected to a antibottom quark, again radiation from the production and the decay must be accounted for, but now a $\widehat{t\bar{b}}$ and a $\widehat{b\bar{W}}$ dipole must be used. This case can only occur for resonance histories with a single top quark, as in Figure 2(b).
- The bottom-quark emitter comes from the production stage, meaning that it is not part of the decay products of a resonant top quark.
 - If it is colour connected to a resonant antitop quark, the shower allows the bottom quark to radiate and recoil against that antitop quark. Therefore, PS counterterms must be constructed using a $\widehat{b\bar{t}}$ dipole. These configurations arise for resonance histories with a single antitop quark, as in Figure 2(c).
 - If it is not colour connected to a resonance, but to another massless antiquark (in our case an antibottom quark), the standard $\widehat{b\bar{b}}$ dipole can be used for the PS counterterms. An exemplary topology for this case is shown in Figure 2(d).

The four scenarios above correspond to four resonance histories in the set $\mathcal{S}_{R,B} = \{\bar{t}t, \bar{t}b, b\bar{t}, b\bar{b}\}$. Each of these scenarios must be weighted by a function that parametrises their probabilities to occur, which we named $f_{\text{res}}^{t\bar{t}}$, $f_{\text{res}}^{t\bar{b}}$, $f_{\text{nr}}^{b\bar{t}}$, and $f_{\text{nr}}^{b\bar{b}}$, respectively. As clear from issue (a), their choice is to some extent arbitrary. Moreover, as motivated above, in order to address issue (b) these functions must be defined on a Born-like kinematics. Given their probabilistic interpretation, they must respect the constraints

$$0 \leq f_{\text{res}}^{t\bar{t}}(\Phi_B), f_{\text{res}}^{t\bar{b}}(\Phi_B), f_{\text{nr}}^{b\bar{t}}(\Phi_B), f_{\text{nr}}^{b\bar{b}}(\Phi_B) \leq 1, \quad (2.131)$$

$$f_{\text{res}}^{t\bar{t}}(\Phi_B) + f_{\text{res}}^{t\bar{b}}(\Phi_B) + f_{\text{nr}}^{b\bar{t}}(\Phi_B) + f_{\text{nr}}^{b\bar{b}}(\Phi_B) = 1, \quad (2.132)$$

over the entire Born phase space. Note that the second condition requires all functions to be evaluated on the same Born kinematics Φ_B .

For the construction of the individual functions, we adopt the following approach. We first introduce the factors P_i , which are given by products of N_{res} terms chosen among resonant and non-resonant factors. One has a resonant factor P_a^{res} for each resonance present in the resonant history i , and a non-resonant factor P_a^{nr} for each missing one. For the resonant factor P_a^{res} , we use an expression inspired by the s -channel resonance propagator,

$$P_a^{\text{res}}(s_a) = \frac{(s_a + M_a^2)^2 + \Gamma_a^2 M_a^2}{(s_a - M_a^2)^2 + \Gamma_a^2 M_a^2}, \quad (2.133)$$

where M_a and Γ_a are the mass and the width of the resonance a in the resonance history i , respectively, and s_a the invariant mass of its decay products computed in the Born kinematics Φ_B . Note that P_a^{res} has a maximum at $s_a = M_a^2$, and tends to one when moving away from the resonant peak, i.e. $P_a^{\text{res}} \rightarrow 1$ for $s_a \gg M_a^2$ and $s_a \rightarrow 0$. A non-resonant factor P_a^{nr} accounts for the absence of a resonance in a given history and can be safely set to a constant c_a , i.e. $P_a^{\text{nr}} = c_a$, possibly different for the different resonances. With this choice, for a given resonance a we guarantee that the probability to select a resonant over a non-resonant contribution tends to a constant c_a and does not bear any spurious energy dependence away from the resonant peak. In these regions the value of c_a can be used to favour or disfavour non-resonant configurations. With $c_a = 1$, resonant and non-resonant configurations are equally likely. On the other hand, on the resonant peak, one obtains

$$\frac{P_a^{\text{res}}(M_a^2)}{P_a^{\text{nr}}(M_a^2)} = \frac{1}{c_a} \left(1 + 4 \frac{M_a^2}{\Gamma_a^2} \right) \quad \text{with roughly} \quad \frac{M_W}{\Gamma_W} \approx 39, \quad \frac{M_Z}{\Gamma_Z} \approx 37, \quad \frac{m_t}{\Gamma_t} \approx 129, \quad (2.134)$$

which gives the desired enhancement of resonant configuration. With all this in mind, one can finally write,

$$P_i(\Phi_B) = \prod_{a \in \mathcal{T}_i^{\text{res}}} \frac{(s_a + M_a^2)^2 + \Gamma_a^2 M_a^2}{(s_a - M_a^2)^2 + \Gamma_a^2 M_a^2} \prod_{b \in \mathcal{T}_i^{\text{nr}}} c_b, \quad (2.135)$$

where $\mathcal{T}_i^{\text{res}}$ and $\mathcal{T}_i^{\text{nr}}$ are the sets of resonances and missing resonances, respectively, for the resonance history i . From the P_i factor in Eq. (2.135), we can then build the weight functions for our case of interest,

$$\begin{aligned} f_{\text{res}}^{\text{t}\bar{\text{t}}}(\Phi_B) &= \frac{P_{\text{t}\bar{\text{t}}}(\Phi_B)}{\sum_{j \in \mathcal{S}_{\text{R,B}}} P_j(\Phi_B)}, & f_{\text{res}}^{\text{t}\bar{\text{b}}}(\Phi_B) &= \frac{P_{\text{t}\bar{\text{b}}}(\Phi_B)}{\sum_{j \in \mathcal{S}_{\text{R,B}}} P_j(\Phi_B)}, \\ f_{\text{nr}}^{\text{b}\bar{\text{t}}}(\Phi_B) &= \frac{P_{\text{b}\bar{\text{t}}}(\Phi_B)}{\sum_{j \in \mathcal{S}_{\text{R,B}}} P_j(\Phi_B)}, & f_{\text{nr}}^{\text{b}\bar{\text{b}}}(\Phi_B) &= \frac{P_{\text{b}\bar{\text{b}}}(\Phi_B)}{\sum_{j \in \mathcal{S}_{\text{R,B}}} P_j(\Phi_B)}, \end{aligned} \quad (2.136)$$

which clearly satisfy Eqs. (2.131) and (2.132). We use these functions to combine all relevant PS counterterms for a bottom/antibottom-quark emitter in one single term.

Standard event In the integration of the PS counterterms for a standard-event contribution, one starts generating a phase-space point with Born kinematics in Φ_B , together with different sets of radiation variables for each dipole. For a bottom-quark emitter, we introduce a vector labelling all dipole regions $\vec{r} = \{\text{bW}, \text{t}\bar{\text{t}}, \text{t}\bar{\text{b}}, \text{b}\bar{\text{t}}, \text{b}\bar{\text{b}}\}$, together with a vector of radiation phase spaces obtained with the respective CS mappings $\vec{\Phi}_{\text{rad}} = \{\Phi_{\text{rad}}^{\text{bW}}, \Phi_{\text{rad}}^{\text{t}\bar{\text{t}}}, \Phi_{\text{rad}}^{\text{t}\bar{\text{b}}}, \Phi_{\text{rad}}^{\text{b}\bar{\text{t}}}, \Phi_{\text{rad}}^{\text{b}\bar{\text{b}}}\}$. Then we can define a general resonance-aware PS counterterm for the standard-event contribution as

$$\begin{aligned} \widehat{\mathcal{C}}_{\text{PS}}^{\vec{r}}(\Phi_B; \vec{\Phi}_{\text{rad}}) &= f_{\text{res}}^{\text{t}\bar{\text{t}}}(\Phi_B) \left[\mathcal{G}(\Phi_{\text{rad}}^{\text{bW}}) \tilde{\mathcal{C}}_{\text{PS}}^{(\text{bW})}(\Phi_B, \Phi_{\text{rad}}^{\text{bW}}) + \mathcal{G}(\Phi_{\text{rad}}^{\text{t}\bar{\text{t}}}) \tilde{\mathcal{C}}_{\text{PS}}^{(\text{t}\bar{\text{t}})}(\Phi_B, \Phi_{\text{rad}}^{\text{t}\bar{\text{t}}}) \right] \\ &+ f_{\text{res}}^{\text{t}\bar{\text{b}}}(\Phi_B) \left[\mathcal{G}(\Phi_{\text{rad}}^{\text{bW}}) \tilde{\mathcal{C}}_{\text{PS}}^{(\text{bW})}(\Phi_B, \Phi_{\text{rad}}^{\text{bW}}) + \mathcal{G}(\Phi_{\text{rad}}^{\text{t}\bar{\text{b}}}) \tilde{\mathcal{C}}_{\text{PS}}^{(\text{t}\bar{\text{b}})}(\Phi_B, \Phi_{\text{rad}}^{\text{t}\bar{\text{b}}}) \right] \\ &+ f_{\text{nr}}^{\text{b}\bar{\text{t}}}(\Phi_B) \left[\mathcal{G}(\Phi_{\text{rad}}^{\text{b}\bar{\text{t}}}) \tilde{\mathcal{C}}_{\text{PS}}^{(\text{b}\bar{\text{t}})}(\Phi_B, \Phi_{\text{rad}}^{\text{b}\bar{\text{t}}}) \right] + f_{\text{nr}}^{\text{b}\bar{\text{b}}}(\Phi_B) \left[\mathcal{G}(\Phi_{\text{rad}}^{\text{b}\bar{\text{b}}}) \tilde{\mathcal{C}}_{\text{PS}}^{(\text{b}\bar{\text{b}})}(\Phi_B, \Phi_{\text{rad}}^{\text{b}\bar{\text{b}}}) \right] \\ &+ (1 - \mathcal{G}(\Phi_{\text{rad}})) \mathcal{C}_{\text{dip}}^{(\text{b}\bar{\text{b}})}(\Phi_B, \Phi_{\text{rad}}^{\text{b}\bar{\text{b}}}). \end{aligned} \quad (2.137)$$

We first notice that in the two categories weighted by $f_{\text{res}}^{\text{t}\bar{\text{t}}}$ and $f_{\text{res}}^{\text{t}\bar{\text{b}}}$ the singularity of the real matrix elements is taken care of by the counterterm $\tilde{\mathcal{C}}_{\text{PS}}^{(\text{bW})}$, which is included in both. The two PS counterterms $\tilde{\mathcal{C}}_{\text{PS}}^{(\text{t}\bar{\text{t}})}$ and $\tilde{\mathcal{C}}_{\text{PS}}^{(\text{t}\bar{\text{b}})}$ are only required to remove double counting of top-quark radiation, but do not cause singularities to be subtracted twice inside the two categories.

Moreover, the damping functions \mathcal{G} guarantee that the correct IR subtraction is restored close to singularities, which reside anyway outside the PS validity regime. Were the PS counterterms capable of correctly reproducing the IR structure of the real amplitude, one could set $\mathcal{G} = 1$. In this ideal scenario, since in the singular limits all radiation phase spaces tend to the same kinematics, and owing to Eq. (2.132), the singularities would be exactly subtracted once for each singular region.

Hard event When integrating the hard-event contribution, the real kinematics Φ_R is generated first, and, starting therefrom, sets of underlying-Born and radiation kinematics are derived using direct CS mappings that are different for each dipole. As for the standard event, we stick to the case of a bottom-quark emitter. If we introduce a vector of underlying-Born phase spaces $\vec{\Phi}_B = \{\Phi_B^{\text{bW}}, \Phi_B^{\text{t}\bar{\text{t}}}, \Phi_B^{\text{t}\bar{\text{b}}}, \Phi_B^{\text{b}\bar{\text{t}}}, \Phi_B^{\text{b}\bar{\text{b}}}\}$, a general resonance-aware PS counterterm for the hard-event contribution is defined via

$$\begin{aligned} \widehat{\mathcal{C}}_{\text{PS}}^{\vec{r}}(\vec{\Phi}_B; \vec{\Phi}_{\text{rad}}) &= f_{\text{res}}^{\text{t}\bar{\text{t}}}(\Phi_B^{\text{bW}}) \mathcal{G}(\Phi_{\text{rad}}^{\text{bW}}) \tilde{\mathcal{C}}_{\text{PS}}^{(\text{bW})}(\Phi_B^{\text{bW}}, \Phi_{\text{rad}}^{\text{bW}}) + f_{\text{res}}^{\text{t}\bar{\text{t}}}(\Phi_B^{\text{t}\bar{\text{t}}}) \mathcal{G}(\Phi_{\text{rad}}^{\text{t}\bar{\text{t}}}) \tilde{\mathcal{C}}_{\text{PS}}^{(\text{t}\bar{\text{t}})}(\Phi_B^{\text{t}\bar{\text{t}}}, \Phi_{\text{rad}}^{\text{t}\bar{\text{t}}}) \\ &+ f_{\text{res}}^{\text{t}\bar{\text{b}}}(\Phi_B^{\text{bW}}) \mathcal{G}(\Phi_{\text{rad}}^{\text{bW}}) \tilde{\mathcal{C}}_{\text{PS}}^{(\text{bW})}(\Phi_B^{\text{bW}}, \Phi_{\text{rad}}^{\text{bW}}) + f_{\text{res}}^{\text{t}\bar{\text{b}}}(\Phi_B^{\text{t}\bar{\text{b}}}) \mathcal{G}(\Phi_{\text{rad}}^{\text{t}\bar{\text{b}}}) \tilde{\mathcal{C}}_{\text{PS}}^{(\text{t}\bar{\text{b}})}(\Phi_B^{\text{t}\bar{\text{b}}}, \Phi_{\text{rad}}^{\text{t}\bar{\text{b}}}) \\ &+ f_{\text{nr}}^{\text{b}\bar{\text{t}}}(\Phi_B^{\text{b}\bar{\text{t}}}) \mathcal{G}(\Phi_{\text{rad}}^{\text{b}\bar{\text{t}}}) \tilde{\mathcal{C}}_{\text{PS}}^{(\text{b}\bar{\text{t}})}(\Phi_B^{\text{b}\bar{\text{t}}}, \Phi_{\text{rad}}^{\text{b}\bar{\text{t}}}) + f_{\text{nr}}^{\text{b}\bar{\text{b}}}(\Phi_B^{\text{b}\bar{\text{b}}}) \mathcal{G}(\Phi_{\text{rad}}^{\text{b}\bar{\text{b}}}) \tilde{\mathcal{C}}_{\text{PS}}^{(\text{b}\bar{\text{b}})}(\Phi_B^{\text{b}\bar{\text{b}}}, \Phi_{\text{rad}}^{\text{b}\bar{\text{b}}}) \\ &+ (1 - \mathcal{G}(\Phi_{\text{rad}})) \mathcal{C}_{\text{dip}}^{(\text{b}\bar{\text{b}})}(\Phi_B^{\text{b}\bar{\text{b}}}, \Phi_{\text{rad}}^{\text{b}\bar{\text{b}}}). \end{aligned} \quad (2.138)$$

Since for a given real kinematics, different underlying-Born kinematics are constructed, and since Eq. (2.132) only holds at fixed Born kinematics, for a hard event the weight functions will not sum up to one locally. This can only be problematic in the singular limits, where the PS counterterms can fail in subtracting singularities correctly by under/overcounting them (at least in the ideal case where one can set $\mathcal{G} = 1$). However, since in those limits all underlying-Born kinematics match, the probabilistic constraint in Eq. (2.132) is restored.

The last requirement to be fulfilled is that the cancellation between the PS counterterms in the hard and standard contribution after the shower action, namely between Eqs. (2.8) and (2.9), is not spoiled. Since the two event types are generated independently, such cancellation is only taking place once the sets are combined, i.e. at the integrated level. We notice that a prerequisite for the CS subtraction to work is that the same function defined on different mapped kinematics (i.e. kinematics factorised into radiation and underlying-Born phase spaces) must integrate to the same value. This is how the cancellation among the subtraction counterterms of a real event and the integrated dipoles occurs. This must also apply to the PS counterterms, even after the introduction of the weight functions. Therefore, once the integration over the real phase space is performed, their values at the integrated level will match the corresponding ones obtained from a standard event.

Resonance information The previous discussion gives us a simple criterion to probabilistically assign a resonance history at event-generation level. This must be provided as an additional information to the LHEs to be processed by PYTHIA8. The algorithm simply works as follows.

Once a set of momenta has been generated, $2^{N_{\text{res}}}$ possible resonance histories in the set $\mathcal{S}_{R,B}$ can be chosen for a standard-event sample. Each history $i \in \mathcal{S}_{R,B}$ comes with a weight ω_i , defined as

$$\omega_i(\Phi_B) = \frac{P_i(\Phi_B)}{\sum_{j \in \mathcal{S}_{R,B}} P_j(\Phi_B)}, \quad \text{with} \quad \sum_{i \in \mathcal{S}_{R,B}} \omega_i = 1. \quad (2.139)$$

Note that, for our construction to be consistent, the expressions for the weights ω_i must match the weight functions in Eq. (2.136). Once the categories in $\mathcal{S}_{R,B}$ are given an arbitrary (but fixed) ordering, a random number x is generated such that for each event the resonance history k is

selected if

$$\sum_{i=1}^{k-1} \omega_i < x < \sum_{j=k+1}^{2^{N_{\text{res}}}} \omega_j. \quad (2.140)$$

Conversely, the assignment of a resonance history to a hard event is not bound to respect the same consistency criterion as for standard events. Nonetheless, we have pursued a strategy similar to the one outlined above. The main difference resides in the fact that the weights ω_l must be evaluated on the real kinematics Φ_R of the event, with l running on an enlarged set $\mathcal{S}_{R,\text{rad}}$ that accounts for the attribution of the gluon radiation to the production stage or to the decays of the top(antitop) quark. In the latter case, if the W^+ (W^-) boson from the top(antitop) quark decays hadronically, different weights are given to configurations where the radiation arises from the bottom(antibottom) quark or from the decays of the W^+ (W^-) boson. To be more concrete, if we consider the case where the top quark decays leptonically and the antitop one hadronically, $\mathcal{S}_{R,\text{rad}}$ comprises nine different categories that we label $\mathcal{S}_{R,\text{rad}} = \{t_g \bar{t}, t \bar{t}_g, t \bar{t}_g^W, t \bar{b}, t_g \bar{b}, b \bar{t}, b \bar{t}_g, b \bar{t}_g^W, b \bar{b}\}$. For doubly-resonant topologies, three categories can be chosen, depending on whether the gluon radiation is attributed to the leptonically decaying top quark ($t_g \bar{t}$), or to either the antibottom quark ($t \bar{t}_g$) or the hadronically decaying W^- boson ($t \bar{t}_g^W$), both originating from the antitop quark. For singly-resonant topologies in the leptonically decaying top quark, we consistently distinguish between categories where the radiation comes from the top quark ($t_g \bar{b}$), or the colour-connected antibottom quark, which does not originate from a resonant antitop quark ($t \bar{b}$). With the same logic, three categories are found for singly-resonant topologies in the hadronically decaying antitop quark ($b \bar{t}, b \bar{t}_g, b \bar{t}_g^W$), and only one category for non-resonant configurations ($b \bar{b}$).

Similarly to Eq. (2.139), we can write the weights ω_l as

$$\omega_l(\Phi_R) = \frac{P_l(\Phi_R)}{\sum_{m \in \mathcal{S}_{R,\text{rad}}} P_m(\Phi_R)}. \quad (2.141)$$

The functions $P_m(\Phi_R)$ are still constructed according to Eq. (2.135) up to some minor changes in the definition of the resonant factors P_t^{res} and $P_{\bar{t}}^{\text{res}}$. For P_t^{res} , we use [see Eq. (2.133)],

$$P_t^{\text{res}}(s_t) = \frac{(s_t + m_t^2)^2 + \Gamma_t^2 m_t^2}{(s_t - m_t^2)^2 + \Gamma_t^2 m_t^2}, \quad \text{with} \quad s_t = \begin{cases} (p_b + p_{W^+})^2 & \text{for } i \in \{t \bar{t}_g, t \bar{t}_g^W, t \bar{b}\} \\ (p_b + p_{W^+} + p_g)^2 & \text{for } i \in \{t_g \bar{t}, t_g \bar{b}\} \end{cases}, \quad (2.142)$$

with p_b^μ , $p_{W^+}^\mu$, and p_g^μ , the four momenta of the bottom quark, the W^+ boson, and the gluon possibly arising from the leptonically decaying top quark. Furthermore, whenever the gluon is assigned to the hadronically decaying antitop quark, i.e. $s_{\bar{t}} = (p_{\bar{b}} + p_{W^-} + p_g)^2$, we apply a resonant factor,

$$P_{\bar{t}}^{\bar{b},\text{res}}(s_{\bar{t}}) = \frac{(s_{\bar{t}} + m_t^2)^2 + \Gamma_t^2 m_t^2}{(s_{\bar{t}} - m_t^2)^2 + \Gamma_t^2 m_t^2} \frac{\beta_h P_{W^-}^{\text{res}}(s_W)}{\beta_h P_{W^-}^{\text{res}}(s_W) + (1 - \beta_h) P_{W^-}^{\text{res}}(s_{Wg})}, \quad (2.143)$$

if the gluon is radiated off the antibottom quark, and

$$P_{\bar{t}}^{W,\text{res}}(s_{\bar{t}}) = \frac{(s_{\bar{t}} + m_t^2)^2 + \Gamma_t^2 m_t^2}{(s_{\bar{t}} - m_t^2)^2 + \Gamma_t^2 m_t^2} \frac{(1 - \beta_h) P_{W^-}^{\text{res}}(s_{Wg})}{\beta_h P_{W^-}^{\text{res}}(s_W) + (1 - \beta_h) P_{W^-}^{\text{res}}(s_{Wg})}, \quad (2.144)$$

if the gluon comes from the W^- -boson decay. In Eqs. (2.143)–(2.144), the resonant factor $P_{W^-}^{\text{res}}$ for the hadronically decaying W^- boson is defined as in Eq. (2.133), with $M_a = M_W$ and $\Gamma_a = \Gamma_W$, and where $s_W = (p_{q_1} + p_{q_2})^2$ and $s_{Wg} = (p_{q_1} + p_{q_2} + p_g)^2$, with $p_{q_1}^\mu$ and $p_{q_2}^\mu$ the four momenta of the partons arising from the W^- boson. Note that by definition:

$$P_{\bar{t}}^{\bar{b},\text{res}}(s_{\bar{t}}) + P_{\bar{t}}^{W,\text{res}}(s_{\bar{t}}) = P_{\bar{t}}^{\text{res}}(s_{\bar{t}}) = \frac{(s_{\bar{t}} + m_t^2)^2 + \Gamma_t^2 m_t^2}{(s_{\bar{t}} - m_t^2)^2 + \Gamma_t^2 m_t^2}. \quad (2.145)$$

The additional real variable $\beta_h \in [0, 1]$ can be used to at least partly parametrise the freedom in the assignment of a resonance history to a hard event as far as the hadronically decaying antitop-quark is concerned: for $\beta_h > 0.5$, configurations with a gluon arising from the decay products of the W^- boson are favoured. If no radiation is assigned to the hadronically decaying antitop quark, we use the definition of $P_{\bar{t}}^{\text{res}}(s_{\bar{t}})$ with $s_{\bar{t}} = (p_{\bar{b}} + p_{W^-})^2$. Once the ω_i weights have been defined, an equation similar to Eq. (2.140) is used to select a resonance history within $\mathcal{S}_{\text{R,rad}}$.

3 Details of the calculation

The method outlined in the previous section is applied to the production of a top–antitop pair in e^+e^- collisions in the semi-leptonic decay channel,

$$e^+e^- \rightarrow \mu^+\nu_\mu j j j_b j_b. \quad (3.1)$$

In particular, NLO QCD corrections of order $\mathcal{O}(\alpha_s\alpha^6)$ to the full off-shell process are matched to the PYTHIA8 PS. The fixed-order part of our results closely follows the calculation of Ref. [46]. We consider final-state particles (quarks and leptons) as massless, and we do not take into account any quark-generation mixing (unit CKM matrix).

Over the years, the theoretical predictions for the production of a top-quark pair in e^+e^- collisions have seen significant developments, with precise predictions using non-relativistic QCD and resummation techniques at threshold [75–78]. At the differential level, predictions including the transition to the continuum described by fixed-order QCD have been obtained in Ref. [79]. Above threshold and for on-shell top quarks, several computations became available up to next-to-next-to-next-to-leading-order (N³LO) accuracy at the level of the inclusive cross section [80–82] and up to NNLO accuracy for differential distributions [83–86]. Considering off-shell top quarks and leptonic decays, NLO QCD accuracy has been established by several groups [87–89]. NLO EW precision has been reached for inclusive cross sections many years ago [90–92] and supplemented by $\mathcal{O}(\alpha^2)$ ISR effects few years ago [93]. Finally, for on-shell production, QED ISR effects at NLL in collinear factorisation have been matched to NLO EW corrections [94], while further investigations of EW effects have been carried out for polarised initial and final states [95]. The semi-leptonic decay has only been studied very recently at NLO QCD [46] and regarding factorisation properties in boosted topologies [96].

In Section 3.1 we discuss some aspects of the event generation relevant to obtain our results. We continue with a summary of the input parameters that we employ in Section 3.2.1, together with an explanation of the setup used for the NLO matching and for running PYTHIA8 in Section 3.2.2. Finally, we report in Section 3.2.3 the definition of the fiducial phase space.

3.1 Technical aspects of the event generation

MOCANLO [37] is a Monte Carlo integrator that can deal with general collider processes at LO and NLO in the QCD and EW coupling. Integrated cross sections and distributions are evaluated on weighted-event samples, as standard in many fixed-order codes. Final results are obtained by combining a posteriori individual runs for each contribution entering a standard NLO calculation [see Eq. (2.1)]. In order to match the predictions of MOCANLO to PSs, many significant changes and adaptations have been implemented.

Since for the process of interest the momenta of the initial-state particles are fixed (no lepton PDF is considered), all events with a Born-like kinematics are correlated and therefore have to be integrated together as part of a standard-event contribution, in line with the discussion in Section 2.1.1. Only events with a resolved QCD radiation enter a separate sample of hard events,

to be combined a posteriori with the former sample to obtain results with the correct NLO normalisation. On top of this first substantial modification to the usual code workflow, unweighted events for the two event sets had to be made available.

Events in MoCANLO are stored in LHE files including all information needed by the PS to correctly dress the event with additional soft and collinear radiation: flavour, kinematics, colour flow in the large N_c limit, and resonance history (see Section 2.3). LHE files for both standard and hard contributions contain unweighted events in the form of *equal-weight-event samples*, i.e. all events have the same weight (up to the sign), which is, however, not necessarily equal to one.⁶ The weight w_i of each event i is defined in the same way for all elements of the sample. It is given by the sum of the positive part σ_+ and the absolute value of the negative part σ_- of the cross section σ (see Ref. [98]). Weights of events within the standard or the hard sample can only differ by an overall sign, which keeps track of the sign of the individual event. Thus, one has $w_i = w_\pm \forall i$, with $w_\pm = \pm(\sigma_+ + |\sigma_-|)$. This makes it possible to recover the total cross section with the correct event-sample normalisation as the average over the event weights w_i . Note that the fraction of positive f_+ and negative f_- events of a sample is proportional to σ_+/σ and $|\sigma_-|/\sigma$, respectively.

The unweighting of events is achieved both for standard and hard events using the customary rejection sampling algorithms [99], which makes use of the maximum weight w_{\max} (found during a dedicated integration stage) to accept or reject events. Note that the maximum here is taken over the absolute values of the event weights. Given a random number r , an event is included in the sample with a weight w_\pm only if $r \cdot w_{\max} < |d\sigma_i|$, where $d\sigma_i$ is the fully-differential weight of the event i evaluated on the current kinematics. However, as discussed in Ref. [100], w_{\max} might often arise from rare outliers, which can potentially spoil the acceptance–rejection efficiency due to a spuriously small ratio $|d\sigma_i|/w_{\max}$ for most of the events. In Ref. [100], using an estimate \tilde{w}_{\max} of the maximum weight was pointed out as a reasonable compromise between the need of finding the most-faithful maximum weight and a practically-usable acceptance–rejection efficiency. This strategy is also used in MoCANLO, at the price of working with *partially-unweighted-event* samples. Indeed, the event unweighting is carried out using \tilde{w}_{\max} , but also allowing for events with $|d\sigma_i| > \tilde{w}_{\max}$. When these events occur, they are always accepted and given a weight $w_i = w_\pm \cdot |d\sigma_i|/\tilde{w}_{\max}$. Clearly, the fraction of these *upper-bound violating* events must be monitored and remain small.

To determine a reasonable estimate \tilde{w}_{\max} of w_{\max} we considered two different *maximum-reduction approaches*, which have been discussed and used for instance in Refs. [100, 101]. In the first one, during a *warm-up integration stage*, where the integration-channel optimisation takes place, a maximum weight is stored for each batch of integrand evaluations, whose number should be statistically significant. The estimate \tilde{w}_{\max} is then obtained as the *median* of these maximum weights. In the second approach, the p -quantile is computed for each of these batches and \tilde{w}_{\max} just provides the geometric average of the different p -quantiles. After testing the two approaches, also using different values of $p = 0.9$ or higher, and without observing any significant difference in terms of performances between the two for our process of interested, we decided to use the median approach for all of our results.

While the median approach speeds up the event generation of hard events, the standard-event generation is still significantly slowed down by the evaluations of the virtual contribution. In order to partially circumvent this issue, MoCANLO performs the unweighting for standard events in two steps. First, the acceptance–rejection procedure is performed using a *surrogate* maximum weight \tilde{w}_{\max}^B , given by the maximum over the absolute values of the Born weights, estimated with the median approach discussed above. At this stage, only the Born contribution $d\sigma_i^B$ to the event weight is computed. Only if $r \cdot \tilde{w}_{\max}^B < |d\sigma_i^B|$, a second acceptance–rejection step is carried out,

⁶This event-weight definition corresponds to the option `IDWTUP=-4` for the *master switch* according to the Les Houches strategy [97].

which requires the evaluation of the full standard-event weight. Specifically, the ratio $R_i = d\sigma_i/d\sigma_i^{\text{B}}$ is computed, and the event finally accepted if $r' \cdot \tilde{R}_{\text{max}} < |R_i|$ for a second random number r' . Here \tilde{R}_{max} denotes the estimate of the maximum of the absolute values of the ratios R_i , where the maximum is still determined using the median approach.

Although the overall cross section, recovered by summing together the standard and hard contributions, must be positive, events with negative weights contaminate the sample in most cases. It is well established [18] that a large fraction of negative-weight events can visibly reduce the speed of the integration convergence, with longer run time and storage space required. The MC@NLO method [8, 16–18], which was the first NLO-matching strategy to be formulated, is known to be deeply affected by the problem of negative weights by construction. Nonetheless, even the POWHEG-matching approach [20–22], which was devised with the main purpose of reducing the amount of negative weights, is not entirely free of them. Trying to reduce this fraction f_- is a very active research field on its own, which received much attention in the last years. Very recently a new method was proposed that, for sufficiently simple processes, can completely eliminate negative weights in multiplicative-matching schemes [102]. For additive schemes like MC@NLO, a lot of effort was invested to decrease f_- both for the standard [103] and the hard [18] samples. New methods [104, 105] have also explored the possibility to reduce the fraction of negative events through a-posteriori resampling of events.

With our matching strategy based on the MC@NLO method, it is not surprising that our event generation is plagued by a significant amount of negative weights. For the process in Eq. (3.1) that we are considering, their fraction is around 40% for hard samples and approximately 30–35% for the standard ones depending on the way the exact CS counterterms are switched on in the vicinity of the IR poles (as shown in Section 2.2.2). We point out that, in absence of any additional prescription to reduce sources of negative weights, our generation efficiency is in line with expectations and known results from the literature (see for instance Table 1 of Ref. [18]). Both proposals in Ref. [103] and in Ref. [18] could potentially be applied also in MOCANLO to reduce f_- . Further improvements of our program in this direction are left for future work.

3.2 Input parameters and kinematic selections

We consider the process in Eq. (3.1) at a centre-of-mass energy of 365 GeV, which is the highest collision energy envisioned for the FCC-ee [4]. We make use of the same physical input parameters as defined in Ref. [46], which we shortly recap here.

3.2.1 Physical input parameters

We employ the five-flavour scheme, therefore assuming $m_b = 0$ for the bottom-quark mass. The on-shell weak-boson masses and decay widths are fixed as [106]

$$\begin{aligned} M_W^{\text{OS}} &= 80.379 \text{ GeV}, & \Gamma_W^{\text{OS}} &= 2.085 \text{ GeV}, \\ M_Z^{\text{OS}} &= 91.1876 \text{ GeV}, & \Gamma_Z^{\text{OS}} &= 2.4952 \text{ GeV}, \end{aligned} \quad (3.2)$$

and then converted into the pole values [107], which are the ones used in the numerical program. The Higgs-boson and top-quark pole masses are chosen as [106]

$$\begin{aligned} M_H &= 125 \text{ GeV}, & \Gamma_H &= 4.07 \times 10^{-3} \text{ GeV}, \\ m_t &= 173 \text{ GeV}, & \Gamma_t &= 1.3448 \text{ GeV}. \end{aligned} \quad (3.3)$$

While the Higgs-boson width is taken from Ref. [108], the numerical value of the top-quark width is obtained by applying relative QCD corrections from Ref. [109] to the LO top-quark width according to Ref. [110]. All unstable particles are treated within the complex-mass scheme [39, 111–113].

The EW coupling constant α is computed within the G_μ scheme [114] with the Fermi constant set to

$$G_\mu = 1.16638 \cdot 10^{-5} \text{ GeV}^{-2}. \quad (3.4)$$

The running of the strong coupling α_s is carried out at two loops using the RECOLA program [66], assuming $\alpha_s(M_Z) = 0.118$. Finally, the renormalisation scale is set to $\mu_R = m_t$, and the scale uncertainty is obtained by varying μ_R by a factor 2 up and down (3-point scale variation). No factorisation scale enters the calculation, as lepton beams are considered at fixed energy, and no lepton PDF is used.

This setup has been applied to two separate calculations. First, NLO predictions have been recalculated with the fixed-order version of MOCANLO, reproducing the results of Ref. [46]. This calculation results from the sum of four different contributions, namely the Born, virtual, subtracted-real, and integrated-dipole ones. The very same input setting has also been employed in the generation of the standard- and hard-event samples.

3.2.2 Matching and PYTHIA8 settings

The formalism described in Section 2 has been used to generate standard- and hard-event samples with a dedicated version of MOCANLO. All classes of PS counterterms both of production (see Section 2.3.2) and decay (see Section 2.3.1) type have been included in our predictions. This allows us to have a complete matching that preserves the invariant masses of all relevant resonances when showering events with PYTHIA8. To correct the IR behaviour of the PS counterterms, we make use of the strategy outlined in Section 2.2.2, using a damping function as in Eq. (2.29) with a value of α equal to 2. Different values of α have been used for testing our framework, as discussed in Section 4.1. Moreover, regarding the resonance-history selection detailed in Section 2.3.4, we choose for all resonances $c_a = 1$ [see for instance Eq. (2.134)], independently of the resonance history to which they belong. For the parameter β_h in Eqs. (2.143)–(2.144) we take $\beta_h = 0.5$ as a default, even though different values were used to further validate our resonance-assignment criteria presented in Section 2.3.4.

The results have been matched to PYTHIA8 [6, 7] (specifically PYTHIA8.315), using the default Simple-Shower approach. Only radiation from the final-state shower (or time-like shower in the PYTHIA8 jargon) is included, meaning that the initial-state (or space-like) shower has been completely disabled. Moreover, since we aim at NLO-matched predictions in QCD, we completely switch off QED radiation for the time-like shower, i.e. we prevent charged final-state particles and intermediate resonances from radiating photons as well as virtual-photon branchings into lepton or quark pairs. Consistently with our fixed-order choice, we set $\alpha_s = 0.118$ in the PS generation, but we keep the default first-order running for technical reasons.⁷ Both for leptons and quarks (except for the top quark) zero masses are employed and kept untouched at event-generation level when writing the LHE file. For simplicity, we ask PYTHIA8 not to internally reset any of the masses read from the LHE files.⁸

⁷Using a two-loop running for α_s , together with the Catani–Marchesini–Webber (CMW) scheme [115], while necessary (though not sufficient) to achieve NLL accuracy in the PS [68], induces effects beyond NLO and therefore does not affect our matching prescription. Nonetheless, choosing the default PYTHIA8 settings for α_s allows us to test the dependence of the results on the regulator $\sqrt{t_0}$ of the PS counterterms for values of $\sqrt{t_0}$ deep in the IR region, as discussed later. Indeed, in our setup, selecting "TimeShower:alphaSorder = 2", and possibly "TimeShower:alphaSuseCMW = on", freezes the shower cut-off to values $\sqrt{t_0} \gtrsim 0.6 \text{ GeV}$ and $\sqrt{t_0} \gtrsim 1 \text{ GeV}$, respectively.

⁸For quarks, this is done by setting "LesHouches:setQuarkMass = 0", which uses zero quark masses for the first shower branching, but it does not imply that quarks are treated as massless throughout the shower evolution. This can be enforced via "i:m0 = 0.0", with $i = \{1, 2, 3, 4, 5\}$ for the different quarks. We verified that this can have an impact (in absence of hadronisation) of roughly 3.5% on the integrated cross section. Since this option is anyway not allowed in the presence of hadronisation, we excluded it from our default settings.

As for the PS starting scale, we prevent the PS from producing radiation harder than the `scale` value attached to an event in the LHE file. At variance with POWHEG matching, in MC@NLO this scale can be tuned and is not constrained by the algorithm. Refined scale choices in this matching approach have been explored for instance in Ref. [18]. For our simulations, the scale is set to the centre-of-mass energy, allowing PYTHIA8 to start the shower evolution in each dipole from half of the corresponding dipole invariant mass (see Section 2.2.3). As needed for MC@NLO-like matching, we switch off matrix-element corrections from the shower to avoid double counting. At variance with FKS-based MC@NLO matching, we do not have to enforce a global-recoil scheme for the first shower branching, owing to the close similarity between the CS mappings for the counterterm construction and PYTHIA8 handling of the splitting kinematics for final-state radiation, both based on a dipole picture.

Our baseline predictions rely on the default choice for the QCD-shower cut-off $\sqrt{t_0}$ (see Section 2.2.3) of 0.5 GeV. In order to test the dependence of our results on the IR regulator of the PS counterterms of Section 2.2.2, and to probe the sensitivity of some observables to the hadronisation scale, we modify the cut-off scale by a factor of two up and down. This requires a correlated variation of the cut-off scale, which enters both the integration range of the standard and hard PS counterterms (requiring to generate two new event samples for both contributions), and the PS evolution (to be run separately with the QCD-shower cut-off set to 1 GeV and 0.25 GeV).

Finally, some observables have been obtained both with and without hadronisation effects. When hadronisation is active, hadron decays have been disabled in order to simplify the analysis and the identification of leptons from the hard-scattering event.

All discussed settings, which have been used to generate our baseline matched predictions, have been passed to the PS using its `readstring` method in a tailored PYTHIA8 interface:

```
pythia.readstring("PartonLevel:ISR = off");
pythia.readstring("TimeShower:QEDshowerByQ = off");
pythia.readstring("TimeShower:QEDshowerByL = off");
pythia.readstring("TimeShower:QEDshowerByOther = off");
pythia.readstring("TimeShower:QEDshowerByGamma = off");
pythia.readstring("TimeShower:alphaSvalue = 0.118");
pythia.readstring("LesHouches:setQuarkMass = 0 ");
pythia.readstring("LesHouches:setLeptonMass = 0 ");
pythia.readstring("TimeShower:pTmaxMatch = 1");
pythia.readstring("TimeShower:MEcorrections = off");
pythia.readstring("TimeShower:globalRecoil = off");
pythia.readstring("TimeShower:pTmin = 0.5");
pythia.readstring("HadronLevel:All = on/off");
```

3.2.3 Event selection

We present here the kinematic selection used for our results, which closely follows that of Ref. [46]. Note that the generation of the standard- and hard-event samples has been performed on a fully inclusive phase space and cuts have been applied only at the level of the showered event. Thus, no events are removed in the vicinity of cut boundaries that might enter the fiducial volume after showering due recoil effects.

In our setup, the jet-clustering is applied only to partons (quarks and gluons) or hadrons with a rapidity η within the range $|\eta| < 5$ using the the k_T algorithm [116] with resolution radius $R = 0.4$ [117, 118]. As part of the jet clustering, we recombine a b jet and a light jet into a b jet, and two b jets into a light jet. Our selection cuts are inspired by studies carried out for CLIC and FCC-ee colliders [117–119]. Specifically, we impose:

- a missing transverse-momentum cut $p_{T,\text{miss}} > 20 \text{ GeV}$, applied on the neutrino;
- a transverse momentum cut of $p_T > 20 \text{ GeV}$ on the antimuon, the light jets, and the two b-tagged jets;
- a rapidity cut of $|\eta| < 2.44$ (matching the angular selection of Refs. [117–119]) on the antimuon, the light jets, and the two b-tagged jets;
- a minimum rapidity–azimuthal-angle distance between the antimuon and the jets, $\Delta R_{\ell_j}, \Delta R_{\ell_{j_b}} > 0.4$;
- an invariant-mass cut on the system formed by the two hardest visible light jets, the charged lepton, and the neutrino of $M_{jj\mu^+\nu_\mu} > 130 \text{ GeV}$.

Events are accepted only if at least two light jets and two b jets are found satisfying all requirements on the transverse momentum, the angular acceptance, and the rapidity–azimuthal-angle distance to leptons.

Since hadrons are not allowed to decay and the QED shower is disabled, leptons from the hard scattering can still be unambiguously identified for showered events both with and without hadronisation. Moreover, at hadron level, b jets are associated to hadron clusters containing a bottom meson/baryon. Some observables that we considered in our results require to distinguish a b jet arising from bottom and antibottom quarks. At fixed-order level, this identification is done based on the Monte Carlo truth, where only one bottom and one antibottom quark can be present. The event truth is also considered for showered events by examining the flavour of the bottom quark entering the b jet. In configurations where the PS evolution generates multiple jets containing bottom or antibottom quarks, the leading jet of each flavour is identified with the corresponding quark from the hard process. The same is done when hadrons are involved: a b jet is associated to a bottom quark if the bottom meson/baryon has bottomness -1 , and to an antibottom quark for bottomness $+1$. Jets containing a $b\bar{b}$ resonance (bottomness 0) are consistently excluded from b jet candidates.

We also considered observables related to the leptonically decaying top quark (t_{lep}) and the hadronically decaying antitop quark (t_{had}). Their momenta are reconstructed finding the two combinations of momenta $p_{abc} = p_a + p_b + p_c$ that maximise the likelihood function [54]

$$\mathcal{L}_{ij} = \frac{1}{\left(p_{\mu^+\nu_\mu j_b, i}^2 - m_t^2\right)^2 + (m_t \Gamma_t)^2} \frac{1}{\left(p_{j_1 j_2 j_b, j}^2 - m_t^2\right)^2 + (m_t \Gamma_t)^2}, \quad (3.5)$$

given by the product of two Breit–Wigner distributions (of the top and antitop quark). This function mimics the top- and antitop-quark propagators, assuming three-body decays after recombination (both at LO and at NLO QCD). For the reconstruction, only particles passing the event selection are used. Moreover, the definition of t_{had} makes use of the leading and subleading light jets, only. Finally, the combination of bottom jets $\{j_{b,i}, j_{b,j}\}$ that maximises \mathcal{L}_{ij} defines the two bottom jets originating from the leptonic and hadronic top quark, respectively.

4 Results

In this section we present results for the process in Eq. (3.1) in the setup described in Section 3.2. In Section 4.1, events with the sole inclusion of QCD-shower radiation are considered. For these event samples, we show few observables for different values of some technical parameters that enter our matching procedure. In Section 4.2, more results are reported, including also hadronisation effects.

4.1 Matching and shower effects

As a first test of our implementation, we have reproduced the NLO results from Ref. [46]. We recall that, in the CS-based MOCANLO program, fixed-order predictions result from the combination of four different contributions, namely the Born, the virtual, the integrated-dipole, and the subtracted-real terms. We denote by $\sigma_{\text{NLO}}^{(\text{CS})}$ the integrated cross section computed in this manner, in order to distinguish it from $\sigma_{\text{NLO}}^{(\text{MC@NLO})}$, which is obtained from the sum of standard and hard contributions prior to PS matching. As discussed in Section 2.1.1, fixed-order predictions must be recovered when combining standard and hard events whose PS counterterms have been cut on the same phase space, i.e. on Born kinematics. This consistency check gives us the following result:

$$\sigma_{\text{NLO}}^{(\text{MC@NLO})} = 21.56(1)_{-1.9\%}^{+2.3\%} \text{ fb}. \quad (4.1)$$

Despite the independent integration approaches, the central values of $\sigma_{\text{NLO}}^{(\text{CS})}$ from Ref. [46] and $\sigma_{\text{NLO}}^{(\text{MC@NLO})}$ are in good agreement. The correct cancellation of the PS counterterms between standard and hard events has been verified both at the level of the full NLO prediction and individually for each of the PS counterterms discussed in Sections 2.2 and 2.3. Moreover, the agreement of CS- and MC@NLO-based predictions has been corroborated by comparing differential distributions.

Additional tests have been performed after matching our results to the PYTHIA8 QCD Simple Shower, excluding hadronisation effects. Using a damping function with $\alpha = 2$, and the default QCD-shower cut-off of "TimeShower:pTmin = 0.5", we obtain the following value for the integrated cross section:

$$\sigma_{\text{NLO}}^{(\text{PS})} = 17.98(6)_{-2.7\%}^{+3.2\%} \text{ fb}. \quad (4.2)$$

When comparing the above result with $\sigma_{\text{NLO}}^{(\text{MC@NLO})}$ in Eq. (4.1), we see a reduction of the cross section by more than 16% after the inclusion of QCD-shower radiation. This effect is expected and due to the larger efficiency of cuts acting on jet-related quantities.

Even more pronounced and interesting effects emerge when considering differential distributions. Both in this and in the following subsection, differential results are organised as follows. In a main frame, we report NLO results prior to PS matching with a black solid line (simply dubbed NLO), together with PS-matched predictions for $\alpha = 2$ and "TimeShower:pTmin = 0.5" with a red solid line. In some plots, for PS-matched curves we present separately their standard and hard contributions using the same colour as for the corresponding curve for their sum, but with dotted and dashed lines, respectively. Independently of the used parameters, these additional curves are labelled merely with S and H for simplicity. For all plots in this section, two more panels are added, showing ratios of all PS-matched curves in the main frame to the NLO one, and ratios of the different PS-matched predictions to our baseline one, i.e. $\alpha = 2$ and "TimeShower:pTmin = 0.5". Whenever present, uncertainty bands are obtained using 3-point scale variations, where the renormalisation scale is changed only in the fixed-order calculation and kept fixed in the shower.

In Figure 3, we report two exemplary plots where we tested the independence of our predictions with respect to the form of the damping function. In particular, we consider different values for the power α entering Eq. (2.29). On top of the curve for $\alpha = 2$, results for $\alpha = 1$ and $\alpha = 4$ are included in green and limegreen colour, respectively. As expected, no dependence on the analytic expression of the interpolating function \mathcal{G} is observed at the differential level for a fixed value of the shower cut-off. We have checked that the same conclusions hold for all distributions we considered.

In Figure 4, we estimate the impact of the different assignments of the gluon radiation to a certain resonance history for hard events. Despite inducing effects that are formally beyond NLO accuracy, the different choices can be phenomenologically relevant. We restrict these tests to the variation of the β_h parameter in Eqs. (2.143)–(2.144), which modifies the frequency with which a

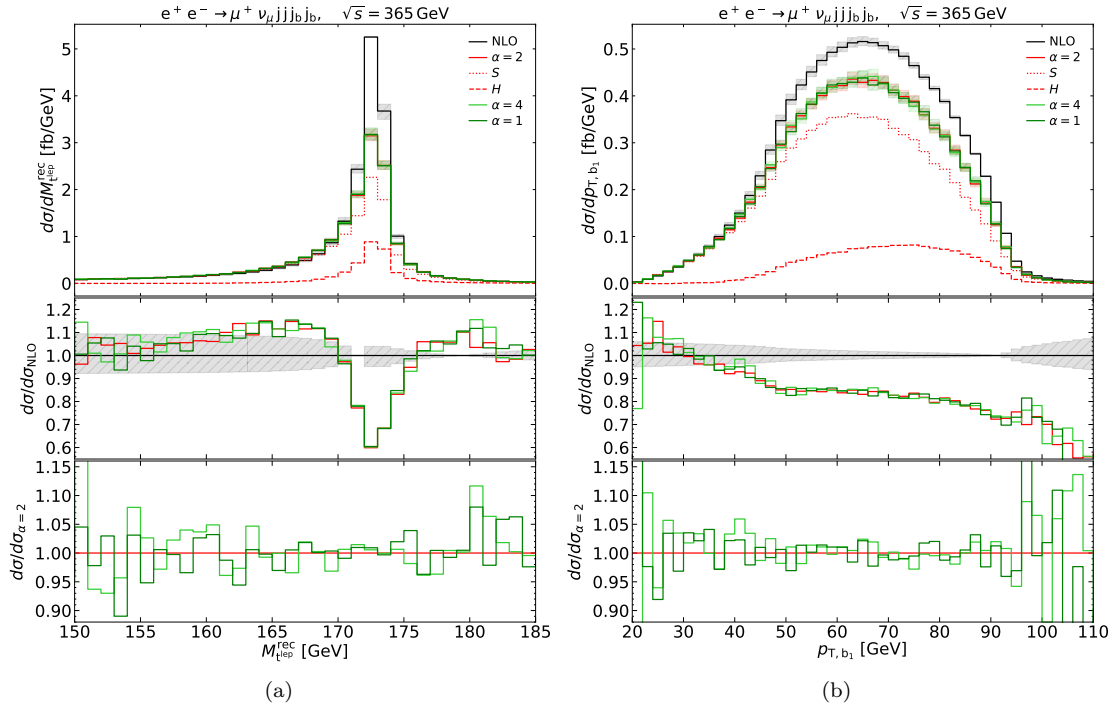


Figure 3. Distributions in the transverse momentum of the leading b jet [3(a)] and in the invariant mass of the reconstructed leptonically decaying top quark [3(b)]. Results for different choices of α in Eq. (2.29) are presented: $\alpha = 2$ (in red), $\alpha = 1$ (in green), and $\alpha = 4$ (in limegreen).

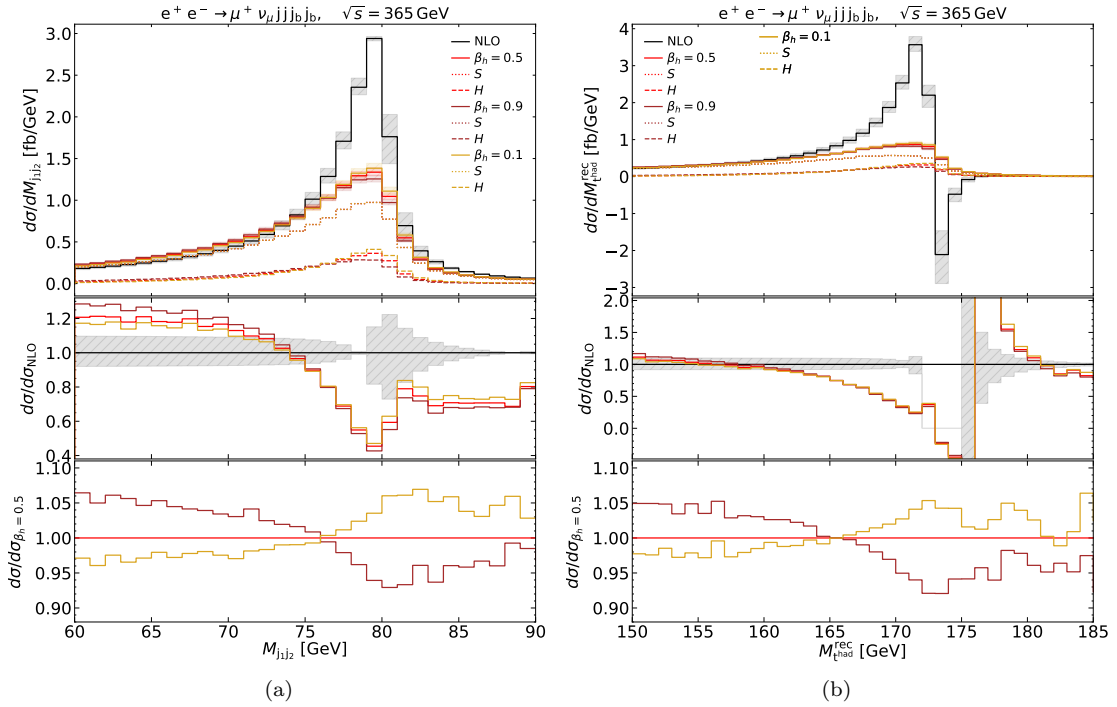


Figure 4. Distributions in the invariant mass of the two light jets [4(a)] and of the reconstructed hadronically decaying top quark [4(b)]. Results for different choices of β_h in Eqs. (2.143)–(2.144) are presented: $\beta_h = 0.5$ (in red), $\beta_h = 0.9$ (in brown), and $\beta_h = 0.1$ (in goldenrod).

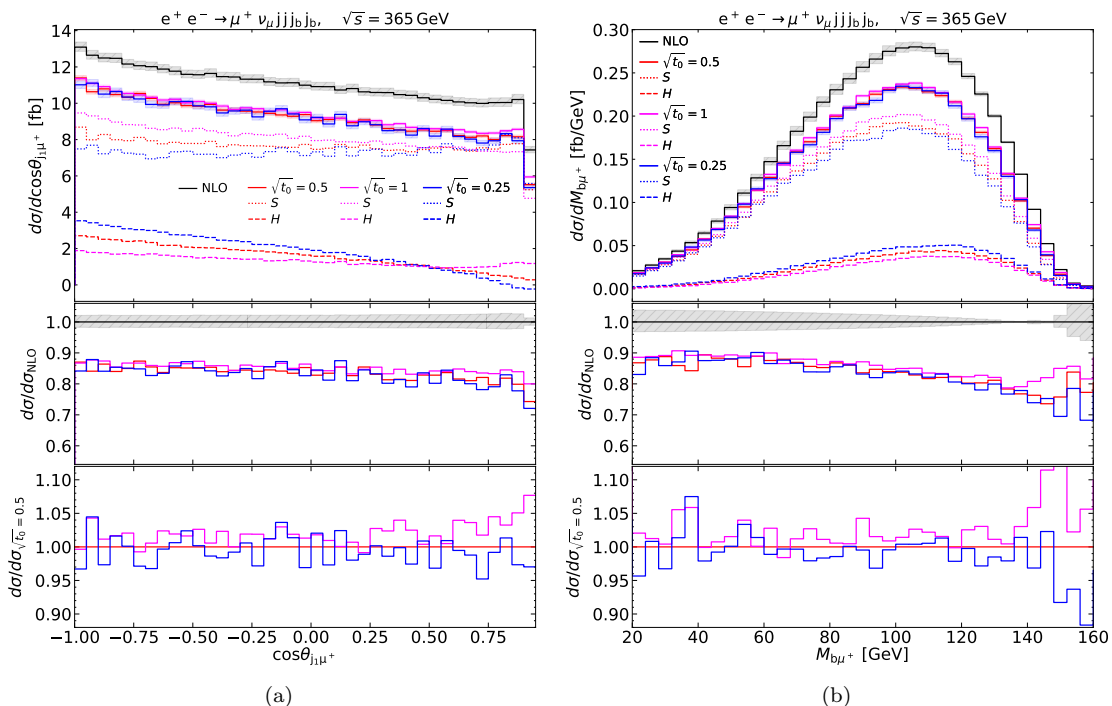


Figure 5. Distributions in the cosine of the polar angle between the leading jet and the antimuon [5(a)] and in the invariant mass of the b-jet–antimuon system [5(b)]. Results for different choices of $\sqrt{t_0}$ are presented: $\sqrt{t_0} = 0.5$ GeV (in red), $\sqrt{t_0} = 0.25$ GeV (in blue), and $\sqrt{t_0} = 1$ GeV (in magenta).

gluon from a hadronically decaying top quark is assigned to an antibottom quark or to the decay products of the W^- boson. Therefore, differences for separate choices of β_h can only be expected for observables related to the hadronic decay of the top quark and of the W^- boson, as the ones in Figure 4. Here, we show, together with the baseline choice of $\beta_h = 0.5$ (in red), results for $\beta_h = 0.9$ in brown and $\beta_h = 0.1$ in goldenrod. Similar effects up to $\pm 8\%$ are observed in both distributions: the invariant mass of the two light jets arising from the hadronically decaying W^- boson in Figure 4(a) and the invariant mass of the reconstructed hadronically decaying top quark in Figure 4(b). The fixed-order corrections to the latter are ill behaved, and the NLO cross section even becomes negative above the resonance peak, where a Sudakov-like shoulder [120] develops. However, the inclusion of PS corrections restores a physically sensible behaviour.

In Figure 5, we finally assess the sensitivity of the predictions to the shower cut-off scale $\sqrt{t_0}$, which enters both the integration of the PS counterterms and the PYTHIA8 evolution. The red curve corresponds to a choice of $\sqrt{t_0} = 0.5$ GeV and "TimeShower:pTmin = 0.5". Predictions for $\sqrt{t_0} = 0.25$ GeV and "TimeShower:pTmin = 0.25" as well as for $\sqrt{t_0} = 1$ GeV and "TimeShower:pTmin = 1" are reported with a blue and a magenta line, respectively. For the two distributions in Figure 5, namely in the cosine of the polar angle between the leading jet and the antimuon in Figure 5(a) and in the invariant mass of the b-jet–antimuon system in Figure 5(b), different values of $\sqrt{t_0}$ affect the standard- and hard-event distributions separately, but any dependence on $\sqrt{t_0}$ disappears at the level of the combined prediction. While this holds for most distributions, in the following section we encounter cases where this is not true, i.e. we present observables with a strong dependence on the shower cut-off scale prior to the inclusion of hadronisation.

4.2 Hadron-level events

In this section we consider PS-matched predictions with the inclusion of hadronisation effects. Even though the normalisation of the event sample is not affected by hadronisation, i.e. the result for the integrated cross section in Eq. (4.2) does not change, important shape distortions are visible in some distributions. All plots in this section still present a main frame, where the NLO curve is accompanied by PS-matched predictions before hadronisation for different values of $\sqrt{t_0}$ as in Figure 5. Additionally, the corresponding hadron-level results are reported in orange for $\sqrt{t_0} = 0.5$ GeV, in violet for $\sqrt{t_0} = 1$ GeV, and in deep sky blue for $\sqrt{t_0} = 0.25$ GeV. In the middle panel, ratios of all PS-matched predictions to the NLO results are shown, while the bottom panel presents the ratio of the different PS-matched curves at hadron level to the one for $\sqrt{t_0} = 0.5$ GeV.

We start in Figure 6 from transverse-momentum distributions, specifically in the transverse momentum of the bottom–antibottom-quark system in Figure 6(a), of the leading b jet in Figure 6(b), and of the leading and next-to-leading light jet in Figures 6(c) and 6(d), respectively. In all cases, predictions for different values of the QCD cut-off scale agree with each other, signalling essentially no sensitivity to IR physics for these quantities. Moreover, no visible effect is found when including hadronisation.

The situation is substantially different for the invariant-mass distributions reported in Figure 7. For this kind of observables, the sizeable effects of hadronisation are not new and were already studied in the literature, as in Refs. [121, 122]. In the distribution in the invariant mass of the b-jet–antimuon system in Figure 7(a), results are independent of the choice of $\sqrt{t_0}$ both without hadronisation and at hadron level. When moving to the other three distributions in the same figure, namely the invariant mass of two light jets in Figure 7(b), of the reconstructed hadronically decaying antitop quark in Figure 7(c), and of the reconstructed leptonically decaying top quark in Figure 7(d), we see a strong dependence on the QCD cut-off scale of the results before hadronisation near the resonance peaks. For instance, the PS radiation cures the perturbative instability in the invariant mass of the reconstructed hadronically decaying antitop at $M_{t_{\text{had}}}^{\text{rec}} = m_t$ for all values of $\sqrt{t_0}$, but with very different shapes. It is worth emphasising that any unphysical dependence of the cut-off scale is removed upon the inclusion of hadronisation for all these observables.

5 Conclusions

In this work we have proposed a method to match NLO corrections in QCD to parton shower (PS) for off-shell collider processes using the MC@NLO approach in a resonance-aware fashion. These results represent an important contribution to the treatment of resonances in the context of NLO matching to PS, which, despite the attention received in the past, still remains a delicate and often problematic task.

We performed the fixed-order part of the simulation using MOCANLO, a Monte Carlo integrator that was already employed in many calculations of NLO corrections in the QCD and EW coupling for processes with a high multiplicity of the final state and a non-trivial resonance structure. The capability of MOCANLO to deal with this kind of processes relies on an advanced multichannel integration. Performing the PS matching with the MC@NLO method allowed us to fully benefit from this feature by keeping the integration of the Born-like and real contributions separate in standard- and hard-event contributions, respectively, and targeting them with dedicated integration channels.

We matched our results to the PYTHIA8 QCD Simple Shower, which, at least for the generation of final-state radiation, implements a dipole shower, where each emission is characterised by an emitter, a radiated parton, and a spectator. This feature closely resembles the way a dipole subtraction identifies singular regions. Therefore, making use of the Catani–Seymour-based imple-

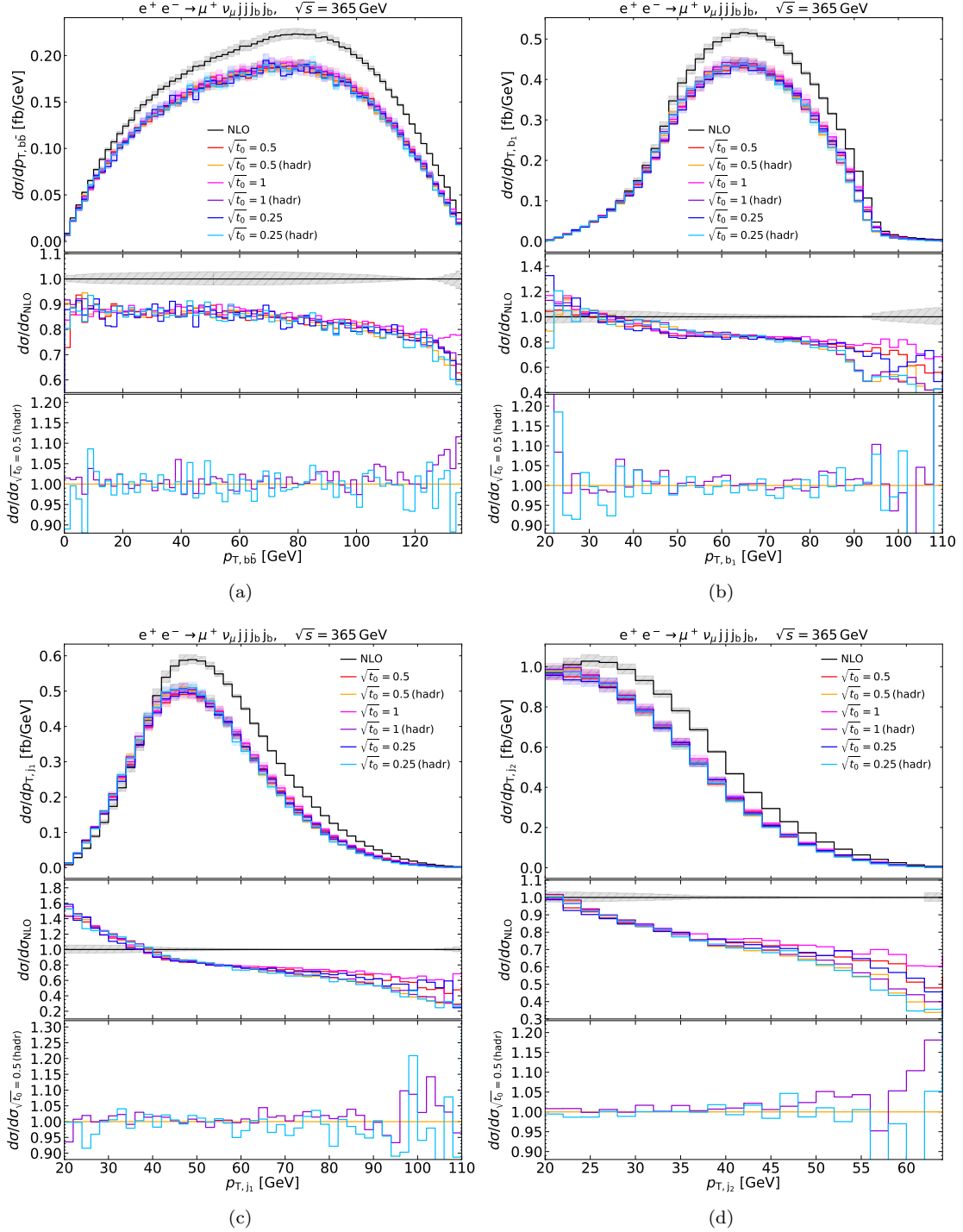


Figure 6. Distributions in the transverse momentum of the bottom–antibottom-quark system [6(a)], of the leading b jet [6(b)], and of the leading [6(c)] and next-to-leading [6(d)] light jet. Results for different choices of $\sqrt{t_0}$ are presented both with and without hadronisation.

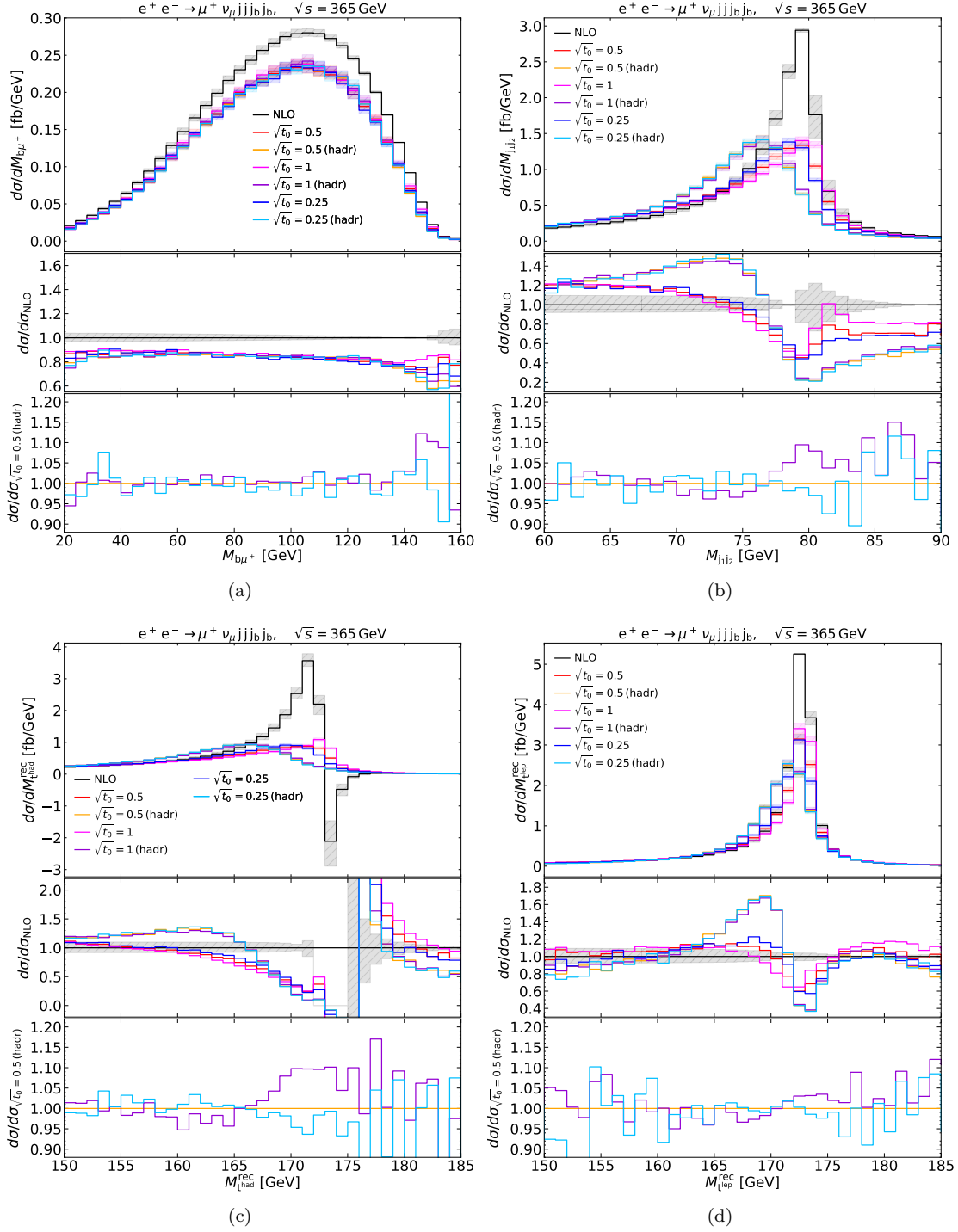


Figure 7. Distributions in the invariant mass of the b-jet-antimuon system [7(a)], of the two light jets [7(b)], the reconstructed hadronically decaying antitop quark [7(c)], and the reconstructed leptonically decaying top quark [7(d)]. Results for different choices of $\sqrt{t_0}$ are presented both with and without hadronisation.

mentation of MOCANLO significantly simplified the matching with MC@NLO, where a thorough knowledge of the shower is needed for the construction of the PS counterterms.

To preserve the invariant masses of the resonances and to avoid distortions of line shapes, information on the resonance-cascade chain of the event must be passed to the shower. This affects the way PYTHIA8 treats the event and showers it with QCD emissions when colourful resonances like the top quark are present. Since the MC@NLO method must remove any source of double counting by subtracting the exact terms used by the shower to generate the first emission, implementing a resonance-aware matching requires a new set of PS-subtraction terms that could not be described in terms of Catani–Seymour dipoles with a massless emitter and a massless spectator. In particular, to achieve a complete matching both at production and decay level for processes involving off-shell top quarks, we constructed additional PS counterterms based on the PYTHIA8 shower, having massive top quarks as emitters and/or spectators, and massive W bosons as recoilers.

In order to generate events and store them in a LHE file with all information required by a shower to further process them, we promoted the MOCANLO program to a generator of unweighted events, using a standard rejection sampling algorithm. To improve the efficiency of the event generation, we approximated the maximum weight with the median approach. Moreover, to further boost the generation of standard events, suffering from the time-consuming evaluation of the virtual corrections, we employed a two-step rejection, where a surrogate maximum weight is used for the first acceptance–rejection step. Only if the event passes through this first step, the computation of the full contribution is carried out.

As a first application of our machinery, we considered the process $e^+e^- \rightarrow \mu^+\nu_\mu jjj_b j_b$, which offers an ideal environment to test our method. Indeed, on the one hand, restricting to electron–positron collisions significantly simplifies the treatment of the QCD-singular regions. On the other hand, the above reaction already exhibits a quite elaborated resonance structure with top quarks and weak bosons, therefore providing a stringent test of the devised resonance-aware matching. For validation, we presented differential results for different values of some technical parameters entering our MC@NLO-matching approach. For some observables, we considered event samples both with and without hadronisation. As expected, the matched predictions improve the description of phase-space regions where the fixed-order calculation suffers from perturbative instabilities. The impact of hadronisation on our results is in line with the findings reported in the literature.

All in all, this manuscript provides an alternative way to match NLO results to PS that could serve as a basis for further studies and developments. This framework was implemented in a significantly extended and adapted version of the MOCANLO integrator that we dub MOCANLO_{PS}. Our method covers QCD predictions for processes at electron–positron colliders, which only require the inclusion of final-state radiation. In this case, PYTHIA8 behaves like a dipole shower, rendering NLO matching to MOCANLO, which is using Catani–Seymour subtraction, much simpler. Conversely, for initial-state radiation, PYTHIA8 intrinsically differs from a dipole shower, so that our approach would have to be carefully adapted in order to be extended to proton–proton collisions. Moreover, our strategy for handling resonance awareness prepares the stage for the matching of NLO EW calculations to QED/EW showers. In this respect, an interesting future direction would be to interface our generator with alternative showers that offer an improved treatment of resonances, such as VINCIA. All that will be part of future work and investigation.

Acknowledgements

We thank Stephen Mrenna, Paolo Nason, Christian T. Preuss, Silvia Ferrario Ravasio, Emanuele Re, Marek Schönherr, Peter Skands, and Paolo Torrielli for useful discussions. We are particularly grateful to Christian T. Preuss for his careful reading of the manuscript and his very useful comments. This work is supported by the German Federal Ministry for Research, Technology and Space

(BMFTR) under contracts Nr. 05H21WWCAA and 05H24WWA and the German Research Foundation (DFG) under reference Nr. DE 623/8-1 and through the Research Training Group RTG2044. The research of DL has also been supported by the Italian Ministry of Universities and Research (MUR) under the FIS grant (CUP: D53C24005480001, FLAME). GP acknowledges support from the EU Horizon Europe research and innovation programme under the Marie-Sklodowska Curie Action (MSCA) “POEBLITA - Polarised Electroweak Bosons at the LHC with Improved Theoretical Accuracy” - grant agreement Nr. 101149251 (CUP H45E2300129000) and from the Italian Ministry of University and Research (MUR), with EU funds (NextGenerationEU), through the PRIN2022 grant agreement Nr. 20229KEFAM (CUP H53D23000980006).

References

- [1] H. Baer et al., eds., *The International Linear Collider Technical Design Report - Volume 2: Physics*, 2013.
- [2] T. Behnke, J.E. Brau, P.N. Burrows, J. Fuster, M. Peskin, M. Stanitzki et al., eds., *The International Linear Collider Technical Design Report - Volume 4: Detectors*, 2013.
- [3] P. Bambade et al., *The International Linear Collider: A Global Project*, [1903.01629](#).
- [4] FCC collaboration, *FCC-ee: The Lepton Collider: Future Circular Collider Conceptual Design Report Volume 2*, *Eur. Phys. J. ST* **228** (2019) 261.
- [5] L. Linssen, A. Miyamoto, M. Stanitzki and H. Weerts, eds., *Physics and Detectors at CLIC: CLIC Conceptual Design Report*, 2012. 10.5170/CERN-2012-003.
- [6] T. Sjöstrand and P.Z. Skands, *Transverse-momentum-ordered showers and interleaved multiple interactions*, *Eur. Phys. J. C* **39** (2005) 129 [[hep-ph/0408302](#)].
- [7] C. Bierlich et al., *A comprehensive guide to the physics and usage of PYTHIA 8.3*, *SciPost Phys. Codeb.* **2022** (2022) 8 [[2203.11601](#)].
- [8] S. Frixione, F. Stoeckli, P. Torrielli and B.R. Webber, *NLO QCD corrections in Herwig++ with MC@NLO*, *JHEP* **01** (2011) 053 [[1010.0568](#)].
- [9] J. Bellm et al., *The Physics of Herwig 7*, [2512.16645](#).
- [10] SHERPA collaboration, *Event Generation with Sherpa 2.2*, *SciPost Phys.* **7** (2019) 034 [[1905.09127](#)].
- [11] T. Gleisberg, S. Höche, F. Krauss, M. Schönherr, S. Schumann, F. Siegert et al., *Event generation with SHERPA 1.1*, *JHEP* **02** (2009) 007 [[0811.4622](#)].
- [12] S. Höche and S. Prestel, *The midpoint between dipole and parton showers*, *Eur. Phys. J. C* **75** (2015) 461 [[1506.05057](#)].
- [13] W.T. Giele, D.A. Kosower and P.Z. Skands, *A simple shower and matching algorithm*, *Phys. Rev. D* **78** (2008) 014026 [[0707.3652](#)].
- [14] N. Fischer, S. Prestel, M. Ritzmann and P. Skands, *Vincia for Hadron Colliders*, *Eur. Phys. J. C* **76** (2016) 589 [[1605.06142](#)].
- [15] H. Brooks, C.T. Preuss and P. Skands, *Sector Showers for Hadron Collisions*, *JHEP* **07** (2020) 032 [[2003.00702](#)].
- [16] S. Frixione and B.R. Webber, *Matching NLO QCD computations and parton shower simulations*, *JHEP* **06** (2002) 029 [[hep-ph/0204244](#)].
- [17] P. Torrielli and S. Frixione, *Matching NLO QCD computations with PYTHIA using MC@NLO*, *JHEP* **04** (2010) 110 [[1002.4293](#)].
- [18] R. Frederix, S. Frixione, S. Prestel and P. Torrielli, *On the reduction of negative weights in MC@NLO-type matching procedures*, *JHEP* **07** (2020) 238 [[2002.12716](#)].

- [19] S.E. Farkh, R. Frederix and M. Gouighri, *MC@NLO event generation by reweighting unweighted Born events*, [2602.18124](#).
- [20] P. Nason, *A new method for combining NLO QCD with shower Monte Carlo algorithms*, *JHEP* **11** (2004) 040 [[hep-ph/0409146](#)].
- [21] S. Frixione, P. Nason and C. Oleari, *Matching NLO QCD computations with Parton Shower simulations: the POWHEG method*, *JHEP* **11** (2007) 070 [[0709.2092](#)].
- [22] S. Alioli, P. Nason, C. Oleari and E. Re, *A general framework for implementing NLO calculations in shower Monte Carlo programs: the POWHEG BOX*, *JHEP* **06** (2010) 043 [[1002.2581](#)].
- [23] S. Jadach, W. Płaczek, S. Sapeta, A. Siódmok and M. Skrzypek, *Matching NLO QCD with parton shower in Monte Carlo scheme — the KrkNLO method*, *JHEP* **10** (2015) 052 [[1503.06849](#)].
- [24] P. Sarmah, A. Siódmok and J. Whitehead, *KrkNLO matching and phenomenology for vector boson processes*, [2511.16605](#).
- [25] P. Nason and G.P. Salam, *Multiplicative-accumulative matching of NLO calculations with parton showers*, *JHEP* **01** (2022) 067 [[2111.03553](#)].
- [26] S. Alioli, C.W. Bauer, C. Berggren, F.J. Tackmann, J.R. Walsh and S. Zuberi, *Matching Fully Differential NNLO Calculations and Parton Showers*, *JHEP* **06** (2014) 089 [[1311.0286](#)].
- [27] K. Hamilton, P. Nason, E. Re and G. Zanderighi, *NNLOPS simulation of Higgs boson production*, *JHEP* **10** (2013) 222 [[1309.0017](#)].
- [28] S. Höche, Y. Li and S. Prestel, *Drell-Yan lepton pair production at NNLO QCD with parton showers*, *Phys. Rev. D* **91** (2015) 074015 [[1405.3607](#)].
- [29] P.F. Monni, P. Nason, E. Re, M. Wiesemann and G. Zanderighi, *MiNNLO_{PS}: a new method to match NNLO QCD to parton showers*, *JHEP* **05** (2020) 143 [[1908.06987](#)].
- [30] J.M. Campbell, S. Höche, H.T. Li, C.T. Preuss and P. Skands, *Towards NNLO+PS matching with sector showers*, *Phys. Lett. B* **836** (2023) 137614 [[2108.07133](#)].
- [31] M. van Beekveld, S. Ferrario Ravasio, K. Hamilton, G.P. Salam, A. Soto-Ontoso, G. Soyez et al., *PanScales showers for hadron collisions: all-order validation*, *JHEP* **11** (2022) 020 [[2207.09467](#)].
- [32] M. van Beekveld, S. Ferrario Ravasio, G.P. Salam, A. Soto-Ontoso, G. Soyez and R. Verheyen, *PanScales parton showers for hadron collisions: formulation and fixed-order studies*, *JHEP* **11** (2022) 019 [[2205.02237](#)].
- [33] J.R. Forshaw, J. Holguin and S. Plätzer, *Building a consistent parton shower*, *JHEP* **09** (2020) 014 [[2003.06400](#)].
- [34] Z. Nagy and D.E. Soper, *Summations of large logarithms by parton showers*, *Phys. Rev. D* **104** (2021) 054049 [[2011.04773](#)].
- [35] F. Herren, S. Höche, F. Krauss, D. Reichelt and M. Schönherr, *A new approach to color-coherent parton evolution*, *JHEP* **10** (2023) 091 [[2208.06057](#)].
- [36] C.T. Preuss, *A partitioned dipole-antenna shower with improved transverse recoil*, *JHEP* **07** (2024) 161 [[2403.19452](#)].
- [37] A. Denner, D. Lombardi, S. Lopez Portillo Chavez, M. Pellen and G. Pelliccioli, *MoCaNLO: a Monte Carlo integrator for NLO calculations*, [2602.19842](#).
- [38] F.A. Berends, R. Pittau and R. Kleiss, *All electroweak four fermion processes in electron-positron collisions*, *Nucl. Phys.* **B424** (1994) 308 [[hep-ph/9404313](#)].
- [39] A. Denner, S. Dittmaier, M. Roth and D. Wackerroth, *Predictions for all processes $e^+e^- \rightarrow 4 \text{ fermions} + \gamma$* , *Nucl. Phys.* **B560** (1999) 33 [[hep-ph/9904472](#)].
- [40] S. Dittmaier and M. Roth, *LUSIFER: A LUCid approach to six FERMion production*, *Nucl. Phys.* **B642** (2002) 307 [[hep-ph/0206070](#)].

- [41] S. Frixione, Z. Kunszt and A. Signer, *Three jet cross-sections to next-to-leading order*, *Nucl. Phys. B* **467** (1996) 399 [[hep-ph/9512328](#)].
- [42] S. Catani and M.H. Seymour, *A general algorithm for calculating jet cross-sections in NLO QCD*, *Nucl. Phys. B* **485** (1997) 291 [[hep-ph/9605323](#)].
- [43] S. Dittmaier, *A general approach to photon radiation off fermions*, *Nucl. Phys. B* **565** (2000) 69 [[hep-ph/9904440](#)].
- [44] S. Catani, S. Dittmaier, M.H. Seymour and Z. Trócsányi, *The dipole formalism for next-to-leading order QCD calculations with massive partons*, *Nucl. Phys. B* **627** (2002) 189 [[hep-ph/0201036](#)].
- [45] S. Alioli, P. Nason, C. Oleari and E. Re, *NLO vector-boson production matched with shower in POWHEG*, *JHEP* **07** (2008) 060 [[0805.4802](#)].
- [46] A. Denner, M. Pellen and G. Pelliccioli, *NLO QCD corrections to off-shell top-antitop production with semi-leptonic decays at lepton colliders*, *Eur. Phys. J. C* **83** (2023) 353 [[2302.04188](#)].
- [47] T. Ježo, J.M. Lindert, P. Nason, C. Oleari and S. Pozzorini, *An NLO+PS generator for $t\bar{t}$ and Wt production and decay including non-resonant and interference effects*, *Eur. Phys. J. C* **76** (2016) 691 [[1607.04538](#)].
- [48] T. Ježo, J.M. Lindert and S. Pozzorini, *Resonance-aware NLOPS matching for off-shell $t\bar{t} + tW$ production with semileptonic decays*, *JHEP* **10** (2023) 008 [[2307.15653](#)].
- [49] C.M. Carloni Calame, M. Chiesa, H. Martinez, G. Montagna, O. Nicrosini, F. Piccinini et al., *Precision Measurement of the W-Boson Mass: Theoretical Contributions and Uncertainties*, *Phys. Rev. D* **96** (2017) 093005 [[1612.02841](#)].
- [50] A. Mück and L. Oymanns, *Resonance-improved parton-shower matching for the Drell-Yan process including electroweak corrections*, *JHEP* **05** (2017) 090 [[1612.04292](#)].
- [51] M. Chiesa, A. Denner, J.-N. Lang and M. Pellen, *An event generator for same-sign W-boson scattering at the LHC including electroweak corrections*, *Eur. Phys. J. C* **79** (2019) 788 [[1906.01863](#)].
- [52] M. Chiesa, C. Oleari and E. Re, *NLO QCD+NLO EW corrections to diboson production matched to parton shower*, *Eur. Phys. J. C* **80** (2020) 849 [[2005.12146](#)].
- [53] R. Frederix, S. Frixione, A.S. Papanastasiou, S. Prestel and P. Torrielli, *Off-shell single-top production at NLO matched to parton showers*, *JHEP* **06** (2016) 027 [[1603.01178](#)].
- [54] A. Denner, J.-N. Lang and M. Pellen, *Full NLO QCD corrections to off-shell $t\bar{t}b\bar{b}$ production*, *Phys. Rev. D* **104** (2021) 056018 [[2008.00918](#)].
- [55] A. Denner, R. Franken, M. Pellen and T. Schmidt, *Full NLO predictions for vector-boson scattering into Z bosons and its irreducible background at the LHC*, *JHEP* **10** (2021) 228 [[2107.10688](#)].
- [56] A. Denner, D. Lombardi and G. Pelliccioli, *Complete NLO corrections to off-shell $t\bar{t}Z$ production at the LHC*, *JHEP* **09** (2023) 072 [[2306.13535](#)].
- [57] A. Denner, M. Pellen, M. Schönherr and S. Schumann, *Tri-boson and WH production in the W^+W^+jj channel: predictions at full NLO accuracy and beyond*, *JHEP* **08** (2024) 043 [[2406.11516](#)].
- [58] S. Höche, F. Krauss, M. Schönherr and F. Siegert, *A critical appraisal of NLO+PS matching methods*, *JHEP* **09** (2012) 049 [[1111.1220](#)].
- [59] V.N. Gribov and L.N. Lipatov, *Deep inelastic e p scattering in perturbation theory*, *Sov. J. Nucl. Phys.* **15** (1972) 438.
- [60] G. Altarelli and G. Parisi, *Asymptotic Freedom in Parton Language*, *Nucl. Phys. B* **126** (1977) 298.
- [61] Y.L. Dokshitzer, *Calculation of the Structure Functions for Deep Inelastic Scattering and e^+e^- Annihilation by Perturbation Theory in Quantum Chromodynamics.*, *Sov. Phys. JETP* **46** (1977) 641.

- [62] G. Gustafson and U. Pettersson, *Dipole Formulation of QCD Cascades*, *Nucl. Phys. B* **306** (1988) 746.
- [63] B. Cabouat and T. Sjöstrand, *Some Dipole Shower Studies*, *Eur. Phys. J. C* **78** (2018) 226 [1710.00391].
- [64] D. Amati, A. Bassetto, M. Ciafaloni, G. Marchesini and G. Veneziano, *A Treatment of Hard Processes Sensitive to the Infrared Structure of QCD*, *Nucl. Phys. B* **173** (1980) 429.
- [65] K. Odagiri, *Color connection structure of supersymmetric QCD ($2 \rightarrow 2$) processes*, *JHEP* **10** (1998) 006 [hep-ph/9806531].
- [66] S. Actis, A. Denner, L. Hofer, J.-N. Lang, A. Scharf and S. Uccirati, *RECOLA: REcursive Computation of One-Loop Amplitudes*, *Comput. Phys. Commun.* **214** (2017) 140 [1605.01090].
- [67] J. Alwall, R. Frederix, S. Frixione, V. Hirschi, F. Maltoni, O. Mattelaer et al., *The automated computation of tree-level and next-to-leading order differential cross sections, and their matching to parton shower simulations*, *JHEP* **07** (2014) 079 [1405.0301].
- [68] M. Dasgupta, F.A. Dreyer, K. Hamilton, P.F. Monni and G.P. Salam, *Logarithmic accuracy of parton showers: a fixed-order study*, *JHEP* **09** (2018) 033 [1805.09327].
- [69] S. Alioli et al., *Update of the Binoth Les Houches Accord for a standard interface between Monte Carlo tools and one-loop programs*, *Comput. Phys. Commun.* **185** (2014) 560 [1308.3462].
- [70] “Pythia8, online html manual.” <https://pythia.org/latest-manual/Welcome.html>.
- [71] H. Brooks, P. Skands and R. Verheyen, *Interleaved resonance decays and electroweak radiation in the Vincia parton shower*, *SciPost Phys.* **12** (2022) 101 [2108.10786].
- [72] V.A. Khoze, W.J. Stirling and L.H. Orr, *Soft gluon radiation in $e^+e^- \rightarrow t\bar{t}$* , *Nucl. Phys. B* **378** (1992) 413.
- [73] Y.L. Dokshitzer, V.A. Khoze, L.H. Orr and W.J. Stirling, *Properties of soft radiation near $t\bar{t}$ and W^-W^- threshold*, *Nucl. Phys. B* **403** (1993) 65 [hep-ph/9302250].
- [74] E. Norrbin and T. Sjöstrand, *QCD radiation off heavy particles*, *Nucl. Phys. B* **603** (2001) 297 [hep-ph/0010012].
- [75] A.H. Hoang, C.J. Reisser and P. Ruiz-Femenia, *Phase Space Matching and Finite Lifetime Effects for Top-Pair Production Close to Threshold*, *Phys. Rev. D* **82** (2010) 014005 [1002.3223].
- [76] A.H. Hoang and M. Stahlhofen, *The Top-Antitop Threshold at the ILC: NNLL QCD Uncertainties*, *JHEP* **05** (2014) 121 [1309.6323].
- [77] M. Beneke, Y. Kiyo, P. Marquard, A. Penin, J. Piclum and M. Steinhauser, *Next-to-Next-to-Next-to-Leading Order QCD Prediction for the Top Antitop S-Wave Pair Production Cross Section Near Threshold in e^+e^- Annihilation*, *Phys. Rev. Lett.* **115** (2015) 192001 [1506.06864].
- [78] M. Beneke, A. Maier, T. Rauh and P. Ruiz-Femenia, *Non-resonant and electroweak NNLO correction to the e^+e^- top anti-top threshold*, *JHEP* **02** (2018) 125 [1711.10429].
- [79] F. Bach, B.C. Nejad, A. Hoang, W. Kilian, J. Reuter, M. Stahlhofen et al., *Fully-differential Top-Pair Production at a Lepton Collider: From Threshold to Continuum*, *JHEP* **03** (2018) 184 [1712.02220].
- [80] A.H. Hoang, V. Mateu and S. Mohammad Zebarjad, *Heavy Quark Vacuum Polarization Function at $\mathcal{O}(\alpha_s^2)$ and $\mathcal{O}(\alpha_s^3)$* , *Nucl. Phys. B* **813** (2009) 349 [0807.4173].
- [81] Y. Kiyo, A. Maier, P. Maierhöfer and P. Marquard, *Reconstruction of heavy quark current correlators at $\mathcal{O}(\alpha_s^3)$* , *Nucl. Phys. B* **823** (2009) 269 [0907.2120].
- [82] X. Chen, X. Guan, C.-Q. He, X. Liu and Y.-Q. Ma, *Heavy-Quark Pair Production at Lepton Colliders at NNNLO in QCD*, *Phys. Rev. Lett.* **132** (2024) 101901 [2209.14259].

- [83] J. Gao and H.X. Zhu, *Top Quark Forward-Backward Asymmetry in e^+e^- Annihilation at Next-to-Next-to-Leading Order in QCD*, *Phys. Rev. D* **90** (2014) 114022 [[1408.5150](#)].
- [84] J. Gao and H.X. Zhu, *Top Quark Forward-Backward Asymmetry in e^+e^- Annihilation at Next-to-Next-to-Leading Order in QCD*, *Phys. Rev. Lett.* **113** (2014) 262001 [[1410.3165](#)].
- [85] L. Chen, O. Dekkers, D. Heisler, W. Bernreuther and Z.-G. Si, *Top-quark pair production at next-to-next-to-leading order QCD in electron positron collisions*, *JHEP* **12** (2016) 098 [[1610.07897](#)].
- [86] W. Bernreuther, L. Chen, P.-C. Lu and Z.-G. Si, *Top and bottom quark forward-backward asymmetries at next-to-next-to-leading order QCD in (un)polarized electron positron collisions*, *JHEP* **05** (2023) 094 [[2301.12632](#)].
- [87] L. Guo, W.-G. Ma, R.-Y. Zhang and S.-M. Wang, *One-loop QCD corrections to the $e^+e^- \rightarrow W^+W^-b\bar{b}$ process at the ILC*, *Phys. Lett. B* **662** (2008) 150 [[0802.4124](#)].
- [88] S. Liebler, G. Moortgat-Pick and A.S. Papanastasiou, *Probing the top-quark width through ratios of resonance contributions of $e^+e^- \rightarrow W^+W^-b\bar{b}$* , *JHEP* **03** (2016) 099 [[1511.02350](#)].
- [89] B. Chokouf e Nejad, W. Kilian, J.M. Lindert, S. Pozzorini, J. Reuter and C. Weiss, *NLO QCD predictions for off-shell $t\bar{t}$ and $t\bar{t}H$ production and decay at a linear collider*, *JHEP* **12** (2016) 075 [[1609.03390](#)].
- [90] J. Fujimoto and Y. Shimizu, *Radiative Corrections to $e^+e^- \rightarrow t\bar{t}$ in Electroweak Theory*, *Mod. Phys. Lett. A* **3** (1988) 581.
- [91] W. Beenakker, S.C. van der Marck and W. Hollik, *e^+e^- annihilation into heavy fermion pairs at high-energy colliders*, *Nucl. Phys. B* **365** (1991) 24.
- [92] J. Fleischer, A. Leike, T. Riemann and A. Werthenbach, *Electroweak one loop corrections for e^+e^- annihilation into $t\bar{t}$ including hard bremsstrahlung*, *Eur. Phys. J. C* **31** (2003) 37 [[hep-ph/0302259](#)].
- [93] N.M.U. Quach and Y. Kurihara, *ISR effects on loop corrections of a top pair-production at the ILC*, *J. Phys. Conf. Ser.* **920** (2017) 012012 [[1706.07042](#)].
- [94] V. Bertone, M. Cacciari, S. Frixione, G. Stagnitto, M. Zaro and X. Zhao, *Improving methods and predictions at high-energy e^+e^- colliders within collinear factorisation*, *JHEP* **10** (2022) 089 [[2207.03265](#)].
- [95] A. Arbuzov, S. Bondarenko, L. Kalinovskaya, R. Sadykov and V. Yermolchyk, *Electroweak radiative corrections to polarized top quark pair production*, *Phys. Rev. D* **107** (2023) 113006 [[2305.09569](#)].
- [96] A.H. Hoang and C. Regner, *Endpoint Factorization for Semileptonic Decays of Boosted and Resonant Off-Shell Top Quarks with a Fat Bottom Jet*, *JHEP* **02** (2026) 132 [[2507.17872](#)].
- [97] E. Boos et al., *Generic User Process Interface for Event Generators*, in *2nd Les Houches Workshop on Physics at TeV Colliders*, 9, 2001 [[hep-ph/0109068](#)].
- [98] S. Alioli, P. Nason, C. Oleari and E. Re, *Vector boson plus one jet production in POWHEG*, *JHEP* **01** (2011) 095 [[1009.5594](#)].
- [99] J. von Neumann, *Various techniques used in connection with random digits*, in *Monte Carlo Method*, A.S. Householder, G.E. Forsythe and H.H. Germond, eds., vol. 12 of *National Bureau of Standards Applied Mathematics Series*, (Washington, DC), pp. 36–38, US Government Printing Office (1951).
- [100] K. Danziger, T. Jan en, S. Schumann and F. Siegert, *Accelerating Monte Carlo event generation – rejection sampling using neural network event-weight estimates*, *SciPost Phys.* **12** (2022) 164 [[2109.11964](#)].
- [101] C. Gao, S. H oche, J. Isaacson, C. Krause and H. Schulz, *Event Generation with Normalizing Flows*, *Phys. Rev. D* **101** (2020) 076002 [[2001.10028](#)].
- [102] M. van Beekveld, S. Ferrario Ravasio, J. Helliwell, A. Karlberg, G.P. Salam, L. Scyboz et al.,

- Logarithmically-accurate and positive-definite NLO shower matching*, *JHEP* **10** (2025) 038 [[2504.05377](#)].
- [103] R. Frederix and P. Torrielli, *A new way of reducing negative weights in MC@NLO*, *Eur. Phys. J. C* **83** (2023) 1051 [[2310.04160](#)].
- [104] J.R. Andersen, A. Maier and D. Maître, *Efficient negative-weight elimination in large high-multiplicity Monte Carlo event samples*, *Eur. Phys. J. C* **83** (2023) 835 [[2303.15246](#)].
- [105] J.R. Andersen, A. Cueto, S.P. Jones and A. Maier, *A Cell Resampler study of Negative Weights in Multi-jet Merged Samples*, [2411.11651](#).
- [106] PARTICLE DATA GROUP collaboration, *Review of Particle Physics*, *PTEP* **2020** (2020) 083C01.
- [107] D. Bardin, A. Leike, T. Riemann and M. Sachwitz, *Energy-dependent width effects in e^+e^- -annihilation near the Z-boson pole*, *Physics Letters B* **206** (1988) 539.
- [108] LHC HIGGS CROSS SECTION WORKING GROUP collaboration, *Handbook of LHC Higgs Cross Sections: 3. Higgs Properties*, [1307.1347](#).
- [109] L. Basso, S. Dittmaier, A. Huss and L. Oggero, *Techniques for the treatment of IR divergences in decay processes at NLO and application to the top-quark decay*, *Eur. Phys. J. C* **76** (2016) 56 [[1507.04676](#)].
- [110] M. Jezabek and J.H. Kühn, *QCD corrections to semileptonic decays of heavy quarks*, *Nucl. Phys.* **B314** (1989) 1.
- [111] A. Denner, S. Dittmaier, M. Roth and L.H. Wieders, *Electroweak corrections to charged-current $e^+e^- \rightarrow 4$ fermion processes: Technical details and further results*, *Nucl. Phys.* **B724** (2005) 247 [[hep-ph/0505042](#)].
- [112] A. Denner and S. Dittmaier, *The complex-mass scheme for perturbative calculations with unstable particles*, *Nucl. Phys. Proc. Suppl.* **160** (2006) 22 [[hep-ph/0605312](#)].
- [113] A. Denner and S. Dittmaier, *Electroweak Radiative Corrections for Collider Physics*, *Phys. Rept.* **864** (2020) 1 [[1912.06823](#)].
- [114] A. Denner, S. Dittmaier, M. Roth and D. Wackerroth, *Electroweak radiative corrections to $e^+e^- \rightarrow WW \rightarrow 4$ fermions in double pole approximation: The RACONWW approach*, *Nucl. Phys.* **B587** (2000) 67 [[hep-ph/0006307](#)].
- [115] S. Catani, B.R. Webber and G. Marchesini, *QCD coherent branching and semiinclusive processes at large x* , *Nucl. Phys. B* **349** (1991) 635.
- [116] S. Catani, Y.L. Dokshitzer, M.H. Seymour and B.R. Webber, *Longitudinally invariant K_t clustering algorithms for hadron hadron collisions*, *Nucl. Phys. B* **406** (1993) 187.
- [117] M. Boronat, J. Fuster, I. Garcia, P. Roloff, R. Simoniello and M. Vos, *Jet reconstruction at high-energy electron-positron colliders*, *Eur. Phys. J. C* **78** (2018) 144 [[1607.05039](#)].
- [118] CLICDP collaboration, *Top-Quark Physics at the CLIC Electron-Positron Linear Collider*, *JHEP* **11** (2019) 003 [[1807.02441](#)].
- [119] D. Dannheim, K. Krüger, A. Levy, A. Nürnberg and E. Sicking, eds., *Detector Technologies for CLIC*, 2019. [10.23731/CYRM-2019-001](#).
- [120] S. Catani and B.R. Webber, *Infrared safe but infinite: Soft gluon divergences inside the physical region*, *JHEP* **10** (1997) 005 [[hep-ph/9710333](#)].
- [121] S. Ferrario Ravasio, T. Ježo, P. Nason and C. Oleari, *A theoretical study of top-mass measurements at the LHC using NLO+PS generators of increasing accuracy*, *Eur. Phys. J. C* **78** (2018) 458 [[1906.09166](#)].
- [122] S. Ferrario Ravasio, *Top-mass observables: all-orders behaviour, renormalons and NLO + Parton Shower effects*, Ph.D. thesis, Milan Bicocca U., 2018. [1902.05035](#).